Clinicians' Guides to Radionuclide Hybrid Imaging · PET/CT
Series Editors: Jamshed B. Bomanji · Gopinath Gnanasegaran
Stefano Fanti · Homer A. Macapinlac

Kanhaiyalal Agrawal ·
Annah Skillen · Abdulredha Esmail ·
Sharjeel Usmani *Editors*

PET/CT Imaging

Basics and Practice

BNMS
BRITISH NUCLEAR MEDICINE SOCIETY

Springer

Clinicians' Guides to Radionuclide Hybrid Imaging

PET/CT

Series Editors
Jamshed B. Bomanji
London, UK

Gopinath Gnanasegaran
London, UK

Stefano Fanti
Bologna, Italy

Homer A. Macapinlac
Houston, TX, USA

Hybrid imaging with PET/CT and SPECT/CT provides high-quality information on function and structure, thereby permitting accurate localization, characterization, and diagnosis. There is extensive evidence to support the value of PET/CT, which has made a significant impact on oncological imaging and the management of patients with cancer. The evidence in favor of SPECT/CT, especially for orthopaedic indications, is evolving and increasing. This pocket book series on hybrid imaging (PET/CT and SPECT/CT) is specifically aimed at referring clinicians, nuclear medicine/radiology physicians, radiographers/technologists, and nurses who routinely work in nuclear medicine and participate in multidisciplinary meetings. The series will include 18 pocket books on PET/CT and 3 on SPECT/CT. Compiled under the auspices of the British Nuclear Medicine Society, the series is the joint work of many colleagues and professionals worldwide who share a common vision and purpose in promoting and supporting nuclear medicine as an important imaging specialty for the diagnosis and management of oncological and non-oncological conditions.

The PET/CT pocket book series will be dedicated to some of the Society's recently departed peers, including Prof Ignac Fogelman, Dr Muriel Buxton-Thomas and Prof Ajit K Padhy.

More information about this series at http://www.springer.com/series/13803

Kanhaiyalal Agrawal • Annah Skillen
Abdulredha Esmail • Sharjeel Usmani
Editors

PET/CT Imaging

Basics and Practice

Springer

BNMS
BRITISH NUCLEAR MEDICINE SOCIETY

Editors
Kanhaiyalal Agrawal
Department of Nuclear Medicine
All India Institute of Medical
Sciences (AIIMS)
Bhubaneswar
India

Abdulredha Esmail
Department of Nuclear Medicine
Jaber Al-Ahmad Molecular Imaging Center
Kuwait City
Kuwait

Annah Skillen
Nuclear Medicine and Therapy Centre
John Flynn Private Hospital
Tugun, QLD
Australia

Sharjeel Usmani
Department of Nuclear Medicine
Kuwait Cancer Control Center (KCCC)
Shuwaikh
Kuwait

PET/CT

ISSN 2367-2439 ISSN 2367-2447 (electronic)
Clinicians' Guides to Radionuclide Hybrid Imaging
ISBN 978-3-030-75475-4 ISBN 978-3-030-75476-1 (eBook)
https://doi.org/10.1007/978-3-030-75476-1

This Springer imprint is published by the registered company Springer Nature Switzerland AG
The registered company address is: Gewerbestrasse 11, 6330 Cham, Switzerland

Foreword

Clear and concise clinical indications for PET/CT in the management of the oncology patient are presented in this series of 15 separate booklets.

The impact on better staging, tailored management and specific treatment of the patient with cancer has been achieved with the advent of this multimodality imaging technology. Early and accurate diagnosis will always pay, and clear information can be gathered with PET/CT on treatment responses. Prognostic information is gathered and can forward guide additional therapeutic options.

It is a fortunate coincidence that PET/CT was able to derive great benefit from radionuclide-labelled probes, which deliver good and often excellent target to non-target signals. Whilst labelled glucose remains the cornerstone for the clinical benefit achieved, a number of recent probes are definitely adding benefit. PET/CT is hence an evolving technology, extending its applications and indications. Significant advances in the instrumentation and data processing available have also contributed to this technology, which delivers high-throughput and a wealth of data, with good patient tolerance and indeed patient and public acceptance. As an example, the role of PET/CT in the evaluation of cardiac disease is also covered, with emphasis on labelled rubidium and labelled glucose studies.

The novel probes of labelled choline, labelled peptides, such as DOTATATE, and, most recently, labelled PSMA (prostate-specific membrane antigen) have gained rapid clinical utility and acceptance, as significant PET/CT tools for the management of neuroendocrine disease and prostate cancer patients, notwithstanding all the advances achieved with other imaging modalities, such as MRI. Hence a chapter reviewing novel PET tracers forms part of this series.

The oncological community has recognised the value of PET/CT and has delivered advanced diagnostic criteria for some of the most important indications for PET/CT. This includes the recent Deauville criteria for the classification of PET/CT patients with lymphoma—similar criteria are expected to develop for other malignancies, such as head and neck cancer, melanoma and pelvic malignancies. For completion, a separate section covers the role of PET/CT in radiotherapy planning, discussing the indications for planning biological tumour volumes in relevant cancers.

These booklets offer simple, rapid and concise guidelines on the utility of PET/CT in a range of oncological indications. They also deliver a rapid aide memoire on the merits and appropriate indications for PET/CT in oncology.

Peter J. Ell
Professor Emeritus University College
London Hospitals Charity
London, UK

Preface

Hybrid Imaging with PET/CT and SPECT/CT combines best of function and structure to provide accurate localisation, characterisation and diagnosis. There is extensive literature and evidence to support PET/CT, which has made a significant impact on oncological imaging and management of patients with cancer. The evidence in favour of SPECT/CT especially in orthopaedic indications is evolving and increasing.

The *Hybrid Imaging* (PET/CT and SPECT/CT) pocketbook series is specifically aimed at our referring clinicians, nuclear medicine/radiology doctors, radiographers/technologists and nurses who are routinely working in nuclear medicine and participate in multidisciplinary meetings. This series is the joint work of many friends and professionals from different nations who share a common dream and vision towards promoting and supporting nuclear medicine as a useful and important imaging speciality.

We want to thank all those people who have contributed to this work as advisors, authors and reviewers, without whom the book would not have been possible. We want to thank our members from the BNMS (British Nuclear Medicine Society, UK) for their encouragement and support, and we are extremely grateful to Dr. Brian Nielly, Charlotte Weston, the BNMS Education Committee and the BNMS council members for their enthusiasm and trust.

Finally, we wish to extend particular gratitude to the industry for their continuous support towards education and training.

London, UK — Gopinath Gnanasegaran
London, UK — Jamshed B. Bomanji

Acknowledgements

The series co-ordinators and editors would like to express sincere gratitude to the members of the British Nuclear Medicine Society, patients, teachers, colleagues, students, the industry and the BNMS Education Committee Members, for their continued support and inspiration:

Andy Bradley
Brent Drake
Francis Sundram
James Ballinger
Parthiban Arumugam
Rizwan Syed
Sai Han
Vineet Prakash

Contents

List of Contributors

Kanhaiyalal Agrawal Department of Nuclear Medicine, All India Institute of Medical Sciences (AIIMS), Bhubaneswar, India

Matt Aldridge University College London Hospitals NHS Foundation Trust, London, UK

Ashik Amlani Department of Radiology, Guy's and St Thomas' NHS Foundation Trust, London, UK

James Ballinger Guy's and St Thomas' Hospital, London, UK

School of Biomedical Engineering and Imaging Sciences, King's College London, London, UK

Jamshed B. Bomanji Institute of Nuclear Medicine, University College London, London, UK

Andy Bradley Manchester Royal Infirmary, Manchester, UK

Alexis Corrigan Maidstone and Tunbridge Wells NHS Trust, Tunbridge Wells, UK

John Dickson University College London Hospitals NHS Foundation Trust, London, UK

Abdulredha Esmail Department of Nuclear Medicine, Jaber Al-Ahmad Molecular Imaging Center, Kuwait City, Kuwait

Gopinath Gnanasegaran Department of Nuclear Medicine, Royal Free NHS Foundation Trust, London, UK

Arun Kumar Reddy Gorla Department of Nuclear Medicine, American Oncology Institute, Hyderabad, Telangana, India

Richard Manber University College London Hospitals NHS Foundation Trust, London, UK

Fahad Marafi Department of Nuclear Medicine, Jaber Al-Ahmad Molecular Imaging Center, Kuwait City, Kuwait

Bhagwant Rai Mittal Department of Nuclear Medicine, Postgraduate Institute of Medical Education and Research (PGIMER), Chandigarh, India

Keerthini Muthuswamy Department of Radiology, Guy's and St Thomas' NHS Foundation Trust, London, UK

Shaunak Navalkissoor Department of Nuclear Medicine, Royal Free NHS Foundation Trust, London, UK

Ashwin Singh Parihar Department of Nuclear Medicine, Postgraduate Institute of Medical Education and Research (PGIMER), Chandigarh, India

Evangelia Skoura Department of Nuclear Medicine, Royal Free NHS Foundation Trust, London, UK

April-Louise Smith University College London Hospitals NHS Foundation Trust, London, UK

Teresa Szyszko Department of Nuclear Medicine, Royal Free NHS Foundation Trust, London, UK

Deborah Carrick Gold Coast University Hospital, Southport, QLD, Australia

Sharjeel Usmani Department of Nuclear Medicine, Kuwait Cancer Control Center (KCCC), Shuwaikh, Kuwait

Thomas Wagner Department of Nuclear Medicine, Royal Free NHS Foundation Trust, London, UK

Basic Principles of PET/CT Imaging

1

Deborah Carrick, John Dickson, and Andy Bradley

Contents

The content of this chapter has originally been published in: Szyszko (Ed.) PET/CT in Esophageal and Gastric Cancer © Springer 2016.

D. Carrick (✉)
Gold Coast University Hospital, Southport, QLD, Australia
e-mail: deborah.carrick@health.qld.gov.uk

J. Dickson
University College London Hospitals NHS Foundation Trust, London, UK

A. Bradley
Manchester Royal Infirmary, Manchester, UK

K. Agrawal et al. (eds.), *PET/CT Imaging*, Clinicians' Guides to Radionuclide Hybrid Imaging, https://doi.org/10.1007/978-3-030-75476-1_1

1.1 Introduction

PET/CT imaging has become a very powerful tool in cancer imaging. It utilises the detection of the radiation emitted from radionuclides that decay by positron (β^+) emission. This chapter looks into the physical principles of this technique, factors that affect the quality of the images produced and some of the artefacts and problems that may be encountered.

1.2 Positron Emission Tomography (PET)

Positron emission tomography (PET) is the imaging of radiopharmaceuticals labelled with positron-emitting radionuclides. Positrons are the positively charged anti-matter version of the electron and are ejected during the radioactive decay of a proton rich nucleus; during this decay process a proton in the nucleus is converted into a neutron. The positron is ejected from the nucleus carrying a lot of kinetic energy; it then travels a short distance and undergoes a number of interactions with the surrounding atoms. In each interaction the positron loses some kinetic energy and changes its direction of travel, following a 'random walk' through the surrounding matter. When the positron is almost at rest, it and a nearby electron annihilate; their mass is released as energy as described by the famous eq. $E = mc^2$. This energy appears in the form of two photons (gamma rays) each with energy of 511 keV. Conservation of energy and momentum dictate that the two photons are emitted from the point of annihilation travelling in opposite directions (Fig. 1.1). These properties, the instantaneous production of two photons of the same energy with them travelling in exactly opposite directions are the basis of the PET technique to determine the site within the patient they were created.

A PET scanner is composed of several rings of small crystal scintillation detectors. Each individual detector is a few mm in size and in modern scanners is made from a lutetium based scintillator. In traditional 'analogue' scanners, a group of these detectors are formed into a block that is typically connected to a group of four

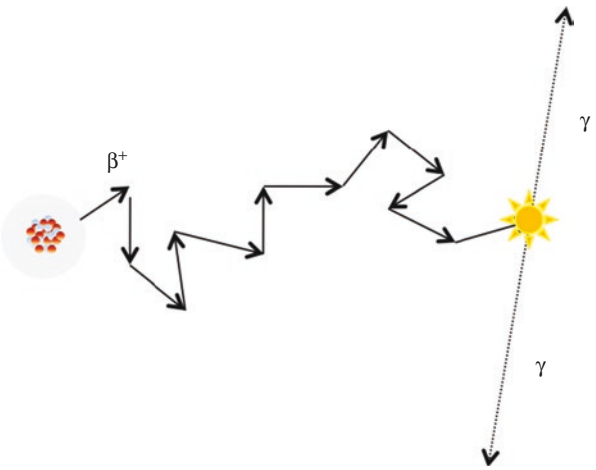

Fig. 1.1 During a nuclear decay, a positron is emitted from a nucleus and undergoes a series of interactions with atoms in the surrounding tissue. When its kinetic energy is almost zero, positron and a neighbouring electron annihilate turning the mass of the two particles into energy in the form of two 511 keV photons (nucleus and random walk are not to scale)

photomultiplier tubes. Modern 'digital' scanners use silicon photo-multipliers (SiPM) that are made up of an array of hundreds or thousands of integrated single-photon avalanche-diodes (SPADs), with the advantage of more sensitive photon detection. This improved sensitivity allows for smaller crystal design and, along with the potential for one-to-one coupling between SPADs and crystals, gives improved spatial resolution. SiPMs are also faster, enabling improved temporal resolution and greater count rate capability. An additional advantage is that SiPM can operate in magnetic fields. The scintillator detectors convert incoming photons into light before amplifying the signal using the SiPM or photomultiplier tubes. When there is a positron emission within the ring of detectors, the two 511 keV photons, travelling at the speed of light will be detected almost instantaneously (within approximately 10 ns). The scanner's electronics look for photons arriving in different detectors within this 'coincidence' time window; this is called a 'coincidence event'. The line between the two detectors that detected the coincidence event is where the annihilation occurred and is called the 'line of response'. When performing PET imaging, it is normal to collect data over several minutes. The coincidences collected over this time can be grouped into parallel lines of response to form the projections that are used for iterative reconstruction. The great advantage of this type of localisation is that, unlike a gamma camera, it does not require collimators to provide positional information and therefore offers much higher sensitivity that single photon emission computed tomography (SPECT).

The type of coincidence event described above is called a 'true' coincidence, and it is these signals that create the useful image. There are, however, other unwanted coincidence events that can occur (Fig. 1.2). A 'random' coincidence event is where multiple positron emissions and annihilations occurring in quick succession lead to a number of photons arriving at the detectors within the coincidence time window. If the wrong pair of detected photons is seen as the coincidence event, this will lead to an incorrect line of response. This process is called a random event as the line of response is not associated with a true annihilation event. The number of random events increases with higher activity concentrations and larger coincidence acceptance time windows, e.g. by moving from 10 ns to 15 ns. A 'scattered' event is where one or both photons coming from a positron-electron annihilation are scattered during their path to the detectors, the line of response will again be incorrect. The number of scattered events increases with increasing activity concentration and

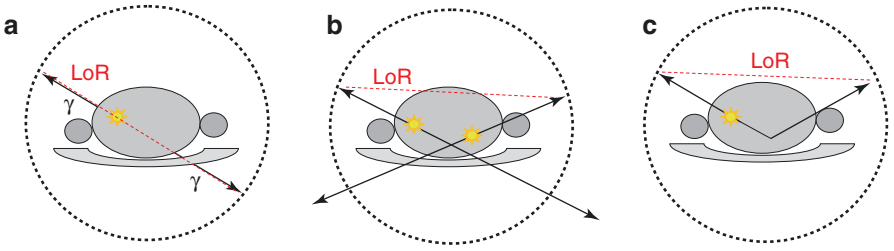

Fig. 1.2 Coincidence events in PET. (**a**) A true event with correct line of response (LoR), (**b**) a random event with two unrelated annihilations registering an incorrect line of response, (**c**) a scattered event where one photon has been scattered leading to an incorrectly positioned line of response

larger or denser tissue. Although unwanted coincidences can degrade image quality, all modern image reconstruction techniques use correction algorithms, which limit the effect of these types of event.

Along with adjustments for scattered and random events there are other corrections that need to be applied during the reconstruction process to increase the accuracy of the final image. These include dead-time corrections to deal with the high count rates found in PET, and a normalisation correction to correct for the difference in measured signal across pairs of detectors used to give the lines of response. However, the most dramatic of the corrections applied in PET is that to correct for photon attenuation within the patient. Although the photons in PET are more energetic than those in single photon tomography, both photons need to be detected for a signal to be registered; this means that the full thickness of patient tissue traversed by both photons affects the relative attenuation of signal from different parts of the patient. The effects of photon attenuation are therefore more dramatic in PET than in SPECT and lead to the classic 'hot' skin and lungs on uncorrected images (Fig. 1.3).

Exact attenuation correction (AC) is relatively straightforward so long as an accurate attenuation map is known. With the advent of PET/CT, the CT scan, which effectively is a map of attenuation at X-ray energies, can, with appropriate conversion factors, provide attenuation correction maps in a matter of seconds. The CT is mounted in the same gantry as the PET and the bed moves the patient between the two scanners for sequential imaging. There are issues to be considered when using attenuation maps derived from CT, such as accurate translation of attenuation coefficients from lower energy X-ray photons to 511 keV; potential misregistration due to patient and respiratory motion; use of contrast agents leading to incorrect attenuation maps owing to their enhanced attenuation only at the lower X-ray energies; the presence of metal artefacts and the additional radiation dose to the patient. Despite these limitations, the use of CT for AC is still the method of choice for most commercial systems because of the low statistical noise in the attenuation maps and the addition of registered anatomical information; the fusion of CT with PET greatly enhances the interpretation of the functional information as will be seen through most of this book.

Most modern scanners include resolution (point spread function) modelling in PET image reconstruction to account for off-axis resolution loss, resulting in

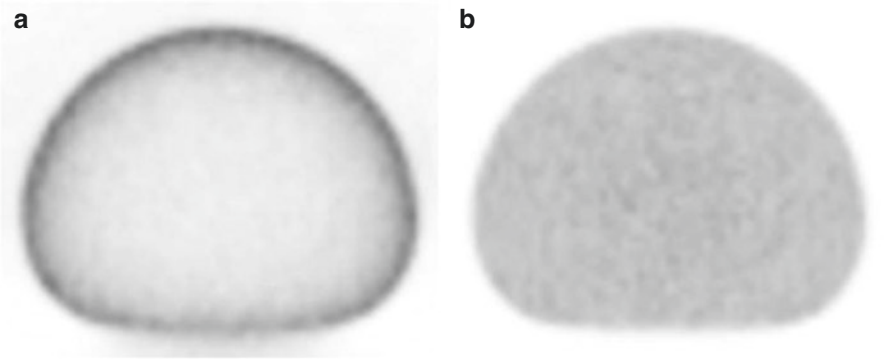

Fig. 1.3 Images of a transaxial slice through a phantom filled with a uniform solution of fluorine-18: (**a**) without correction for photon attenuation and (**b**) with attenuation correction

significant improvements in image resolution and contrast. Also, modern fast crystal scintillators (e.g. lutetium based) are able to more precisely record the difference in the arrival times of the coincidence photons, known as time-of-flight (TOF) imaging. TOF helps localise the point of origin of the annihilation event along the line of response. The reduction in noise offered by TOF can be equated to a gain in image signal to noise ratio. In addition, SiPM are faster than PMT so digital scanners have improved timing resolution and more efficient TOF reconstructions.

An advantage of applying a comprehensive set of corrections in PET/CT is that, with the inclusion of a sensitivity calibration, there is the possibility to calculate voxel values in terms of activity concentration per unit volume (kBq/ml). This activity concentration will change with patient size or administered activity so it becomes more useful if this uptake is represented as a value normalised by the available activity concentration in the body. This is achieved by normalising for injected activity and body size (weight or lean body mass), and this leads to the semiquantitative index known as standardised uptake values (SUV). The SUV in each voxel will equal 1 for a uniform distribution. SUV is defined as.

$$\mathrm{SUV}\left(\mathrm{g/ml}\right) = \frac{\text{activity concentration}\left(\mathrm{kBq/ml}\right)}{\text{administered activity}\ \left(\mathrm{MBq}\right) \Big/ \text{weight}\ \left(\mathrm{kg}\right)}$$

SUV was defined for use in PET whole body oncology imaging with fluorine-18-fluorodeoxyglucose (usually abbreviated as ^{18}F-FDG or just FDG). Most PET display workstations will display PET images in SUV. Although use of SUV is widespread, there are many factors that can affect its accuracy. It requires accurate measurement of administered activity, injection time, scan time and patient weight and is affected by the performance characteristics of the PET scanner and image reconstruction factors. SUV also has a strong positive correlation with body weight. Heavy patients have a higher percentage of body fat that contributes to body weight but accumulates little FDG in the fasting state, so SUVs in non-fatty tissues are increased in larger patients. SUVs normalised to lean body mass or body surface area have been shown to have a lesser dependence on body weight, although SUV normalised to body weight is still the most clinically used parameter. Many physiological factors can affect SUV, including scan delay time (accumulation of FDG continues to increase over time), patient resting state, temperature, blood glucose level, insulin levels and renal clearance. In addition, FDG is not a specific tumour marker, and uptake will be high in areas affected by infective or inflammatory processes that are often seen immediately post-chemotherapy.

Several values of SUV can be quoted, the most common being $\mathrm{SUV}_{\mathrm{max}}$ which is robust and relatively independent of the observer, but as it refers to a single voxel value it is strongly affected by image noise and can change significantly depending on count statistics and reconstruction parameters. It may also not be representative of the overall uptake in a heterogeneous tumour. $\mathrm{SUV}_{\mathrm{mean}}$ is more representative of the average tumour uptake and is less affected by image noise, but can be prone to observer variability if freely drawn regions are used. Although the SUV formula has been criticised, the simplicity of the calculation makes it extremely attractive for routine clinical use.

Table 1.1 Properties of some radionuclides used in clinical PET imaging [1, 2]

Radionuclide	Half-life (min)	Average range (mm)	Positron fraction	Generator produced
Carbon-11	20.4	1.1	100	No
Nitrogen-13	9.96	1.5	100	No
Oxygen-15	2.03	2.5	100	No
Fluorine-18	110	0.6	97	No
Copper-64	762	0.6	18	No
Gallium-68	68	2.9	88	Yes
Rubidium-82	1.25	5.9	95	Yes

Positron-emitting radiotracers:

There is a wide range of positron-emitting radionuclides used in PET (Table 1.1). Many have a short half-life, which requires an expensive cyclotron production facility on the same site as the PET/CT scanner. Fluorine-18 has a slightly longer half-life allowing it to be transported from the production facility to other imaging sites. This explains the popularity of fluorinated PET radiopharmaceuticals such as FDG. There are also longer half-life radionuclides such as copper-64 which allows imaging of pharmaceuticals with slower uptake kinetics. However, not all PET radionuclides require a cyclotron. Generators also exist, similar to the molydenum-99/technetium-99m generator, which can produce PET radionuclides repeatedly on site. Gallium-68 and Rubidium-82 are popular, short-lived, generator produced PET radionuclides; Gallium-68 comes from Germanium-68 parent and Rubidium-82 from Strontium-82 parent.

Not all radioactive decays result in the emission of a positron; for example, with Copper-64, only 18% of decays produce positrons. This means that the sensitivity of the PET scanner to copper-64 labelled compounds is less than a fifth of that possible with fluorine-18. There may also be additional radiations resulting from the other decay routes or contaminants which can affect patient and staff radiation exposure and image quality.

The average range of the positron is important as it determines the distance the positron travels before the creation of the annihilation photons; this range is dependent on the initial energy of the positron following the radioactive decay. Because the positron moves through tissue in a random walk it is not possible to know the exact point in the tissue where the original decay took place. Spatial resolution in the images depends, to some extent, on the average range of the positron in that tissue. As a result, the spatial resolution of Gallium-68 and Rubidium-82 imaging will be worse than that from fluorine-18 tracers. The average positron ranges given in Table 1.1 are for tissue, the range of a positron will be much greater in air.

By far the most common radiopharmaceutical currently used in PET imaging is ^{18}F-FDG. Although FDG is a glucose analogue it does not enter the glycolytic pathway after phosphorylation, but becomes trapped in the cell allowing imaging of FDG concentration, which infers glycolytic rate. Both glucose and FDG are filtered by the glomeruli, but unlike glucose, FDG is not reabsorbed by tubuli and therefore appears in urine. ^{18}F-FDG PET has become an important tool in oncology imaging for diagnosis, staging and to evaluate metabolic changes in tumours at the cellular level. Although very sensitive for imaging many cancer types, it is also non-specific.

Its uptake is seen in many other physiological processes such as inflammation and infection.

1.3 PET Scanning

PET/CT imaging usually starts with a localising scan projection radiograph where the extent of PET scanning is defined. The patient then has a CT scan of this defined length that will be used for attenuation correction and anatomical localisation, before moving through the scanner bore for the PET scan. The axial PET field of view which defines the amount of body that can be scanned at any time is normally around 20–30 cm, although systems are now available with axial fields of view up to 2 m enabling total body imaging. For brain scanning or cardiac scanning, only one field of view is required, however in oncology imaging where the extent of disease is often of interest, whole body imaging can be performed. This can be done by acquiring the image while slowly moving the bed through the detector ring similarly to a whole body acquisition on a gamma camera or by acquiring several fields of view with a slight overlap to allow for the detector sensitivity losses at the edges of the field of view (Fig. 1.4). Each of

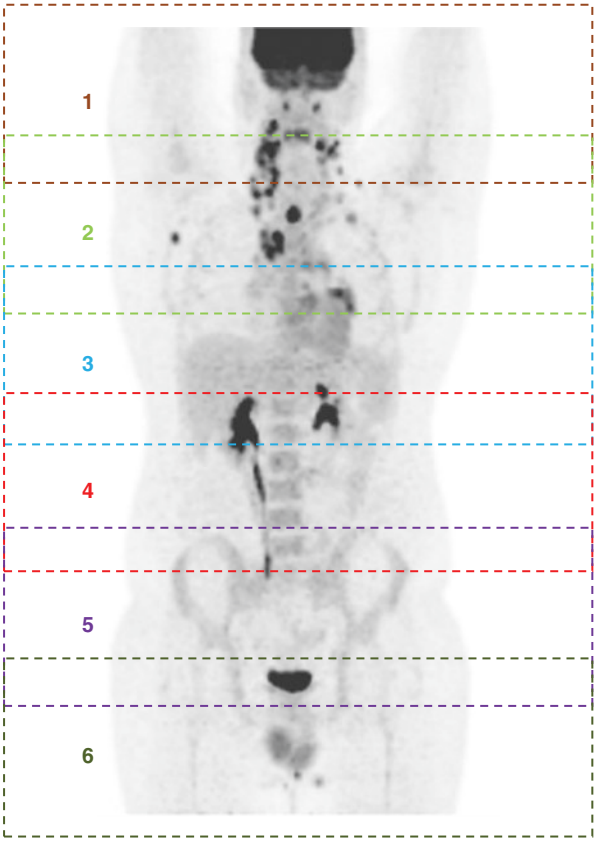

Fig. 1.4 A whole body image may be made up of multiple bed positions that are stitched together; in this example, six acquisitions are required to cover the desired length of the patient

these fields of view is called ‘bed positions’ and the time of each scan at these bed positions can be between 1.5 and 5 min in duration depending on the affinity of the radiopharmaceutical and the sensitivity of the scanner. Patients should be made comfortable and immobilised when necessary to keep the patient in the same position to maintain registration between the PET and the CT used for attenuation correction and localisation and limit movement artefacts.

For some applications, dynamic PET imaging over a single bed position can be useful to understand patient physiology. However, it is more typical to start PET imaging after a fixed period of time; this uptake or resting time is determined by the physiological uptake and excretion of the administered tracer with the aim to scan at the optimum time to have a good uptake in the target tissue with a low background circulation of the tracer in the rest of the body. For repeat imaging to assess disease progression it is important to keep this uptake time duration similar for successive imaging, typically within ±5 min.

1.4 Imaging with [Fluorine-18] FDG PET

The patient must arrive well hydrated and have fasted for between 4 and 6 h to ensure blood glucose level is low prior to injection with FDG. This is to ensure that there is limited competition between FDG and existing blood glucose, so that uptake of FDG is maximised in order to give the best possible image quality. Care needs to be taken with diabetic patients. A patient history should be taken to determine when the patient last had radiotherapy or chemotherapy. FDG uptake can be elevated as a reactive response to these treatments. It is also important to remember that FDG can be sensitive to inflammation/infection, so a general understanding of the patients’ well-being and history of recent physical trauma (including biopsy) is necessary. For SUV calculations, patients’ height and weight should be taken with reliable calibrated instruments to ensure accurate quantification of uptake. Injection of FDG should be intravenous through an indwelling cannula. All PET tracers are beta emitters, so particular care should be taken to reduce the likelihood of extravasation and local radiation burden. To assist in the quantification of FDG uptake, the exact injected activity of FDG should be recorded.

Imaging typically starts at 60 min’ post-injection and the patients must rest and be kept warm during this uptake period to avoid unwanted muscle or brown fat uptake. Patients are asked to void prior to imaging to reduce the activity in the bladder; full bladders containing high activity of FDG can cause difficulties in interpreting the images around this region and also increases the radiation dose to staff while the patient is positioned on the scanner bed. A whole body scan is normally performed from the mid-thigh up to the base of the skull. FDG is processed via renal excretion, so it is important where possible to scan in this direction to avoid scanning a bladder that has refilled with FDG during the scan. With the patient lying supine, whole body imaging is performed with the arms raised above the patient’s head to avoid CT beam hardening artefacts and to ensure that the patient’s body fits within the transaxial field of view. If head and neck imaging is required, an

additional arms down scan over the head and neck area can be helpful to reduce attenuation in this area.

1.5 Artefacts

There are several artefacts that can occur in PET imaging even when all reasonable precautions are taken. One of the hardest artefacts to control is due to respiratory motion that can occur if the patient takes a large breath hold prior to or during the CT. As can be seen in Fig. 1.5a, the result can be a banana artefact caused by mismatch of PET and CT used for attenuation correction at the base of lung and dome of liver. The easiest way to avoid these artefacts is to ensure that the patient is relaxed prior to imaging and asking them not to take any deep intakes of breath—particularly during the CT. Other motion related artefacts are standard patient movement such as that seen in Fig. 1.5b. Relatively common in head and neck imaging, the mismatch of CT and PET can lead to incorrect attenuation correction and difficulty in localising features. Making the patient feel relaxed, helping them understand the need to remain still and appropriate immobilisation can help reduce the likelihood of these artefacts.

An artefact that cannot be easily controlled is the CT X-ray beam hardening effects of metal prosthesis typically in the hip, or where the patient has metal dental work (Fig. 1.6). Many modern systems have algorithms that can help minimise these effects. Nevertheless, care must be taken when quantifying uptake in affected areas because inaccuracies in attenuation correction can lead to inaccuracies in PET

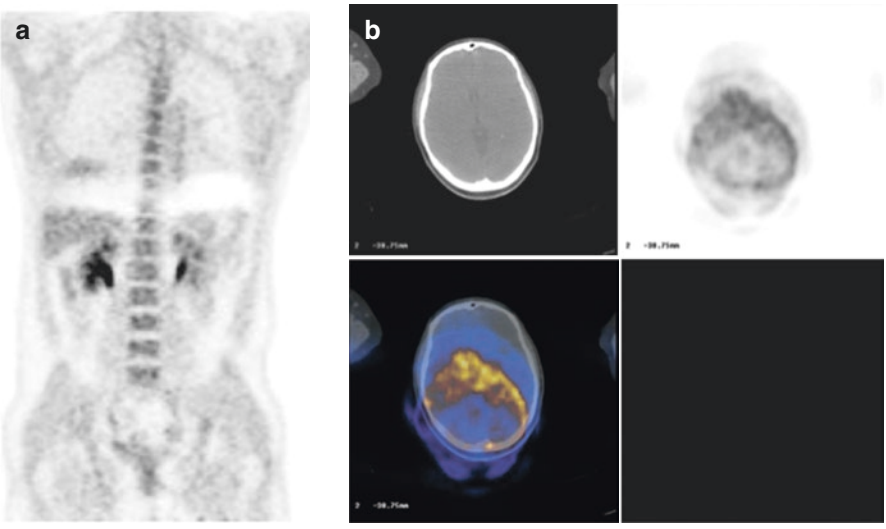

Fig. 1.5 (**a**) Respiratory motion artefact seen at the dome of liver caused by mismatch of PET and CT for attenuation correction. (**b**) Patient motion between CT for attenuation correction and PET leading to poor correction for attenuation and localisation of tracer uptake

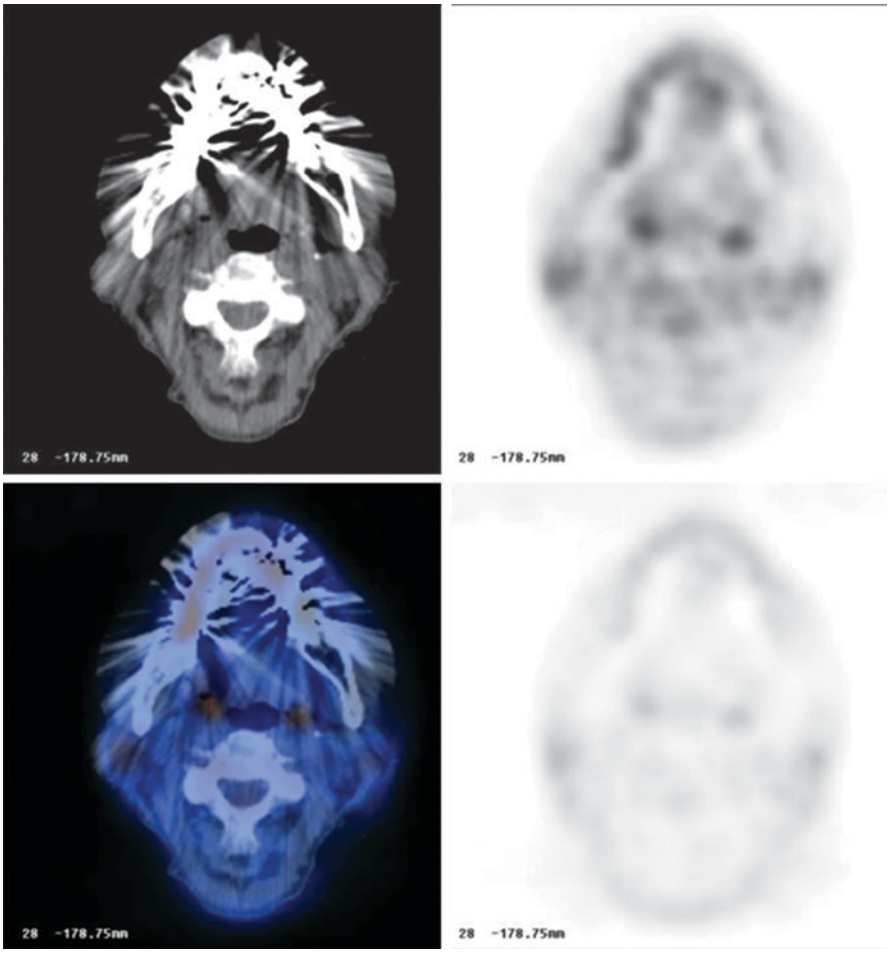

Fig. 1.6 Beam hardening artefacts on CT caused by dental amalgam. PET quantification and localisation can be difficult although non-attenuation corrected data (bottom right panel) may help with identifying artefacts in the attenuation corrected images (top right panel)

quantification. Another area where attenuation correction can fail is when CT contrast has been used. The conversion of the attenuation map at CT X-ray energies to values at PET photon energies can fail in areas of CT contrast accumulation. This is due to the elevated attenuation of contrast media, such as iodine and barium, at the lower X-ray energies due to the k-edge absorption peak; this peak does not affect the absorption of the 511 keV PET photons. As the reconstruction algorithm cannot distinguish between tissue that has a high density and less dense tissue containing CT contrast, the attenuation correction overcorrects areas containing contrast. This again can lead to errors in PET quantification. If quantification is particularly important, e.g. in a trial setting, the contrast CT should be performed last after the PET

data is acquired and the attenuation correction should be performed using a low dose CT acquired before the contrast administration.

A work around for many artefacts is the reading of PET images without attenuation correction. Although these images are then not quantitative, they can be useful to highlight areas of artefact and to assess disease within the patient.

Careful consideration of radiation protection is important due to the high-energy gamma photons. Over ten times the thickness of lead is required to shield PET photons compared to 140 keV photons and the dose rate from a patient administered with fluorine-18 is ten times that of a patient administered with the same activity of Technetium-99 m. Extremity dose can be high when handling PET tracers due to the positron radiations.

The short physical half-lives of PET tracers result in a lower patient dose than might be expected. A typical administered activity of 3 to 4 MBq/kg ^{18}F-FDG corresponds to an effective dose of approximately 6 mSv, and with ongoing improvements in PET detector technology and reconstruction methods, both imaging times and typical administered activities are decreasing. The required level of CT image quality (and therefore effective dose) depends on the use of the CT data. When the CT data are used solely for AC, patient doses can be extremely low (<1 mSv). A notable improvement in image quality (and dose increase) is required if the CT data are to be used for AC and anatomical localisation (typically 3–8 mSv), and a further increase in both image quality and dose is required if the CT images are to be used for diagnostic purposes, usually with the addition of contrast agents (typically >15 mSv).

Key Points

- Positron emission tomography (PET) is the imaging of radiopharmaceuticals labelled with positron-emitting radionuclides.
- Positron decay leads to two 511 keV photons following annihilation of the positron.
- $E = mc^2$. Positron mass = 9.109×10^{-31}g, speed of light = 2.9979×10^{8}m/s, 1 eV = 1.6×10^{-19}J. You know you want to do the calculation….
- A PET scanner is composed of a several rings of scintillation detectors.
- Coincident detection of the two photons in different detectors allows an image to be formed from information gleaned by tracking ‘lines of response’ between these detectors.
- TOF helps localise the point of origin of the annihilation event along the line of response. This helps to decrease noise.
- The sensitivity of the scanner drops towards the edges of the width of the detectors. Adjacent scan lengths need to be overlapped to correct for this.
- Semiquantitative index, standardised uptake values (SUV) are commonly used in clinical PET.
- Several values of SUV can be quoted, the most common being SUV_{max} which is relatively robust, as it is less affected by the observer than SUV_{mean}, but it is strongly affected by image noise.

- SUV_{mean} is more representative of the average tumour uptake and is less affected by image noise, but can be prone to observer variability.
- To assist in the quantification of FDG uptake, the exact injected activity of FDG should be recorded.
- For SUV calculations, patients' height and weight should be taken with reliable calibrated instruments to ensure accurate quantification of uptake.
- SUV values are affected by changes in reconstruction techniques and can vary between scanners; it is only semiquantitative.
- Careful patient preparation is important to obtain good quality PET images.
- All PET tracers are beta emitters, so particular care should be taken to reduce the likelihood of extravasation and local radiation burden.
- There are several artefacts that can occur in PET imaging even when all reasonable precautions are taken, knowledge of these is important when interpreting images.
- The effects of photon attenuation are more dramatic in PET and attenuation correction is very important.
- A typical administered activity of 300 MBq ^{18}F-FDG corresponds to an effective dose of approximately 6 mSv.
- Radiation doses to staff are much higher when exposed to PET tracers than from similar activities of other Technetium based nuclear medicine tracers.

References

1. NUDAT, National Nuclear Data Centre, Brookhaven National Laboratory; 1997.
2. Cal-Gonzalez J, et al. Positron range effects in high resolution 3D PET imaging, nuclear science symposium conference record (NSS/MIC). IEEE; 2009.

Physics of PET and Respiratory Gating

2

April-Louise Smith and Richard Manber

Contents

2.1 PET Physics

Positron emission tomography (PET) is an imaging technique that detects radiolabelled tracers, which have been injected into the body. PET uses radioisotopes which emit energy in the form of positrons (β^+). Positrons are positively charged energetic electrons emitted from nuclei. As the positron interacts with the surrounding tissue, it quickly loses energy. Once the majority of energy is lost it will combine with an electron and converts energy annihilating; subsequently forming two gamma rays (γ) of equal energy (511 keV) in opposite directions(Fig. 2.1). These gamma rays can then be detected by external detectors and used to produce a 3D image.

PET scanners have multiple detectors positioned in a ring around the patient, which allows simultaneous gamma ray detection (Fig. 2.2). Two gamma rays from

A.-L. Smith (✉) · R. Manber
University College London Hospitals NHS Foundation Trust, London, UK
e-mail: april-louise.smith@nhs.net

K. Agrawal et al. (eds.), *PET/CT Imaging*, Clinicians' Guides to Radionuclide Hybrid Imaging, https://doi.org/10.1007/978-3-030-75476-1_2

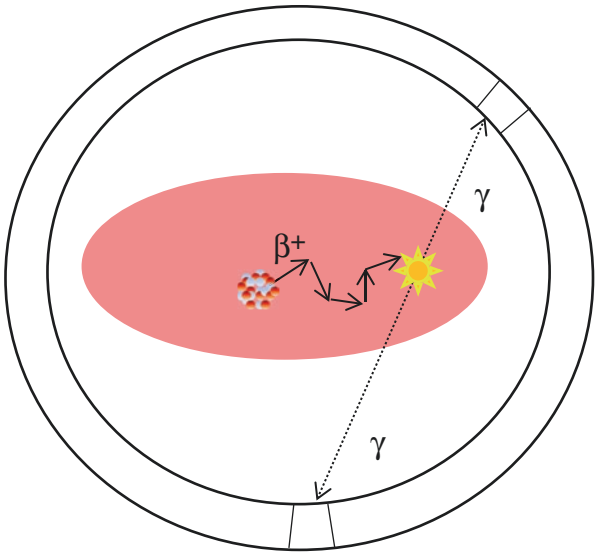

Fig. 2.1 Diagram to show radioisotope decay viaβ^+ emission, the interaction with surrounding tissue and annihilation producing two 511 keV gamma rays that are detected on the PET ring of detectors. (Diagram not to scale)

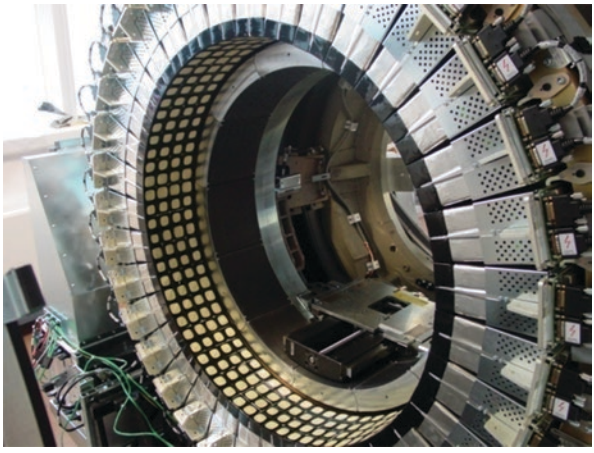

Fig. 2.2 Inside a multi-detector ring PET scanner

an annihilation create a line of response (LOR) indicating a pathway where the annihilation has occurred. If the gamma rays are detected within a set timing window(~10 ns), this is called a 'Coincidence Event'.

If the event detected is due to an annihilation (back-to-back gamma rays), it is known as a 'True Event' giving a correct LOR (Fig. 2.3a). However, if two separate interactions occur simultaneously and are detected; this is considered a 'Random Event' (Fig. 2.3b). Scatter Events occur when the positron annihilates and either one or both the gamma rays are scattered by the surrounding tissue, changing their path (Fig. 2.3c). Scattered and random events result in incorrect LOR, which can introduce noise into the image.

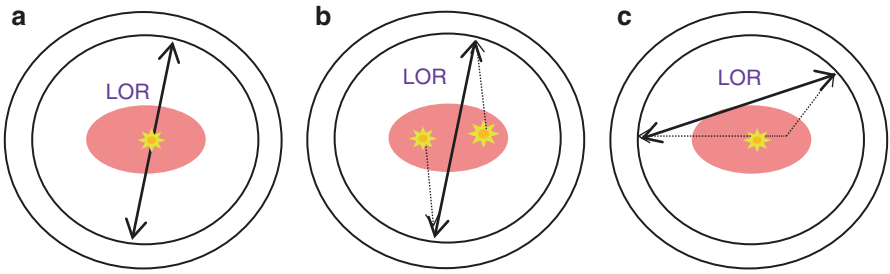

Fig. 2.3 Diagrams showing different coincidence events. (**a**) True Event showing a correct LOR, (**b**) Random Event where two separate events are detected within the coincidence window, giving an incorrect LOR. (**c**) Scatter Event, where one photon is scattered and both photons are then detected, also giving an incorrect LOR

There are a number of correction methods for scattered and random events that can be applied to improve the image quality. In addition, normalisation corrections are applied to account for different sensitivities of the detector blocks and dead-time corrections to compensate for high count rates. Another important correction is for attenuation. In PET acquisitions, some of the emitted photons are attenuated by the surrounding tissue and not detected. This gives rise to artefacts showing the outer edge with increased intensity and central areas with lower intensity. Computed tomography (CT) images can be used to create a map of this attenuation which can be used to correct the PET data. Magnetic resonance (MR) data can also be used to create an attenuation correction map in PET/MR systems, by segmenting the images and assigning corresponding attention factors for that specific tissue. In older scanners, attenuation correction is performed using a transmission scan with an external rod source.

2.2 Reconstruction

Once injected with a radiopharmaceutical, a number of interactions will occur in the patient tissue which can be accumulated over time. This gives projections at different angles, representing the distribution of radioactivity within the tissue (Fig. 2.4a, b). The images are then reconstructed using either filtered back projection (FBP) or iterative reconstruction using ordered subset expectation maximisation (OSEM) or maximum likelihood expectation maximisation (MLEM).

2.3 PET Tracers

There are a number of radiopharmaceuticals available for PET imaging. ^{18}F (Flourine-18) labelled compounds are most commonly used; ^{18}F has a slightly longer half-life compared to other PET tracers which allows it to be transported and not require an onsite cyclotron. In addition to half-life, different radionuclides vary in

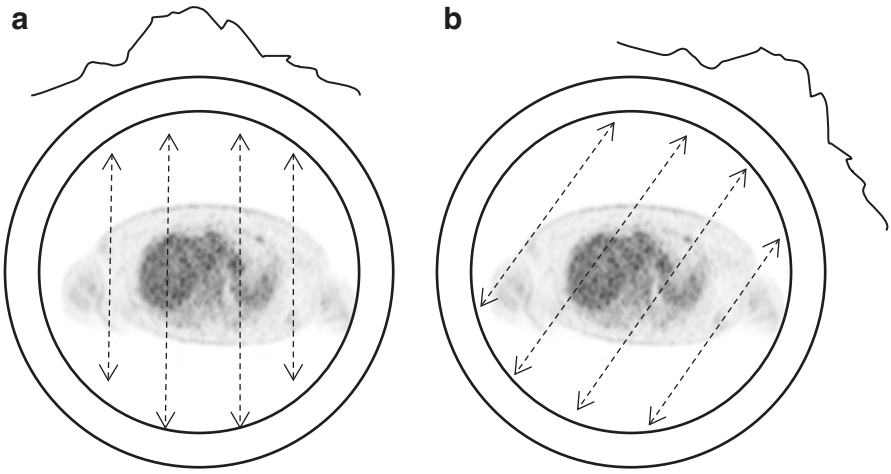

Fig. 2.4 PET reconstruction. The detected events generate lines of response (LoR), these give projections of the distribution at different angles (**a**) and (**b**). A number of projections surrounding the patient are then reconstructed to build a 3D image

Table 2.1 Some examples of radionuclides that can be used in PET

Radioisotope	Half-life	β^+ energy, max (keV)	β^+ Range (mm)	Mode of production
^{18}F	110 m	633 (97%)	0.6	Cyclotron
^{11}C	20.4 m	960 (100%)	1.1	Cyclotron
^{13}N	9.96 m	1199 (100%)	1.5	Cyclotron
^{15}O	2.03 m	1732 (100%)	2.5	Cyclotron
^{68}Ga	68 m	822 (1%) 1899 (88%)	2.9	Generator
^{82}Rb	75 s	1523 (83.3%) 1157 (10.2%)	5.9	Generator

Data references: ^{18}F [1]; ^{11}C, ^{13}N, ^{15}O, ^{68}Ga [2]; ^{82}Rb [3]

properties that can have effects on imaging parameters. Positron range affects the spatial resolution, since the annihilation can occur at a distance away from where the positron was produced. The abundance of positrons produced from each decay can also have effects on the sensitivity. As well as, effecting imaging parameters, the different radionuclides have different radiochemistry, allowing them to be labelled to desired pharmaceuticals. Some examples of PET isotopes are outlined in Table 2.1.

2.4 PET Images

The reconstructed images can be viewed in a number of ways. A stack of images is created and can be viewed in the different planes, as shown in Fig. 2.5.Hybrid imaging also allows fused data for anatomical localisation, as shown in Fig. 2.6. Because

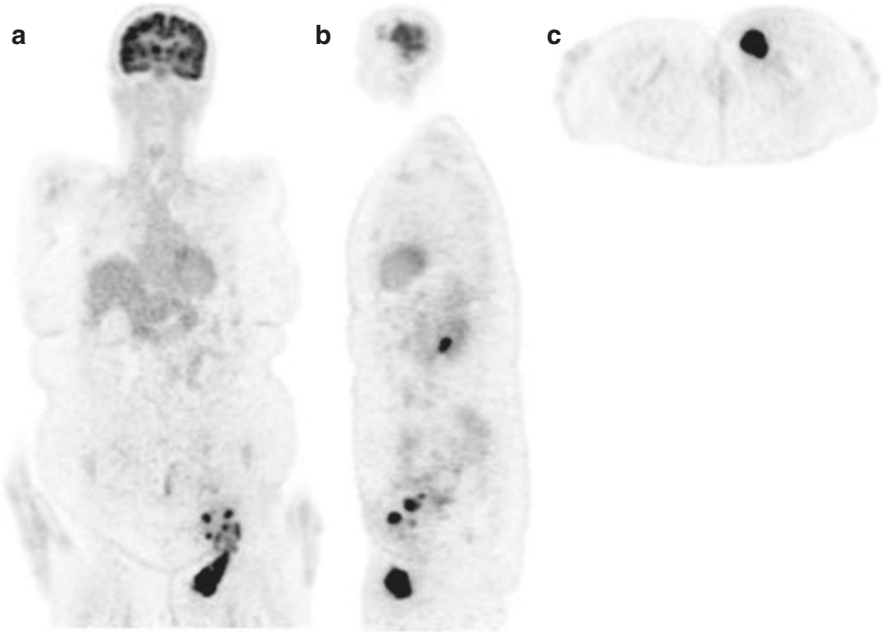

Fig. 2.5 An example ^{18}F-FDG whole body PET acquisition using ordered subset expectation maximisation (OSEM) with time of flight (TOF). (**a**) Coronal slices, (**b**) sagittal slices and (**c**) transaxial slices

PET data are corrected for physical processes, quantitative data of activity concentration per unit volume (kBq/ml) can be calculated. When normalised to available activity concentration by factoring in, e.g. patient body mass, the standardised uptake value (SUV) can be determined. This allows longitudinal comparisons—taking into account variations between injected activity and patient's weight between time points, to give a representation of the uptake in the lesion'.

2.5 Respiratory Gating

There are many artefacts that can affect image quality—one of which is motion. This can cause potential spatial mismatch between CT and PET, which can give attenuation correction artefacts as CT images are acquired in seconds compared to PET which is time averaged over a number of minutes. In addition to this, respiratory motion may introduce further errors, particularly when imaging the thorax or abdomen. Figure 2.7 shows mismatch between PET and MR data of the liver due to respiratory motion. PET data is acquired over several minutes, covering many respiratory cycles, which can introduce blurring into resultant images. One approach to overcome this problem is to acquire a respiratory signal and split the PET data into different respiratory states, either viewing separately or retrospectively combining, to form one motion-corrected image.

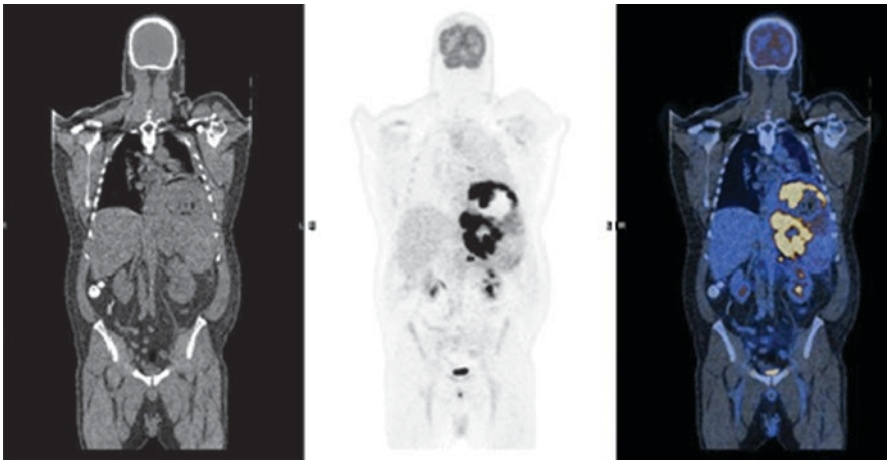

Fig. 2.6 ^{18}F-FDG whole body PET/CT acquisition showing CT, PET, fused PET/CT in the coronal plane

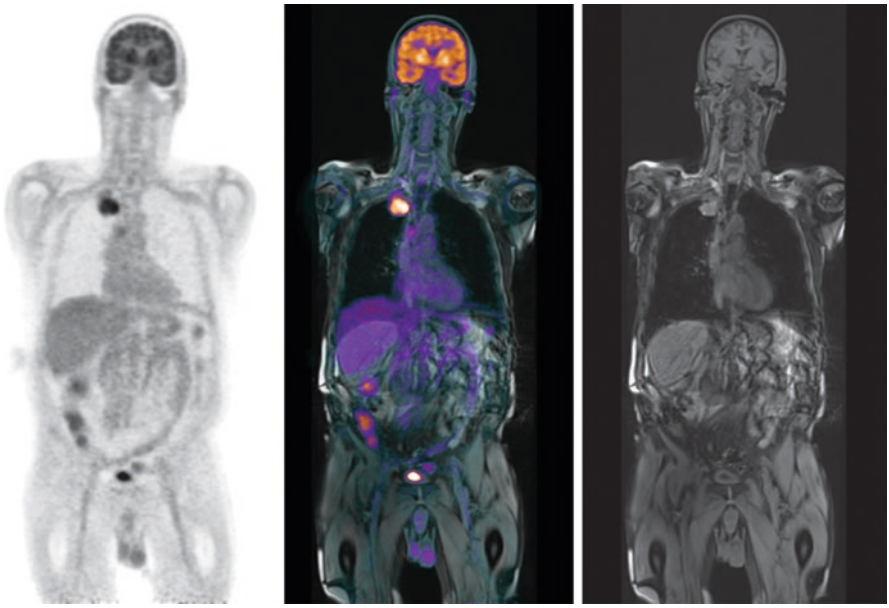

Fig. 2.7 ^{18}F-FDG whole body PET/MR showing PET, PET/MR fused and MR in the coronal plane

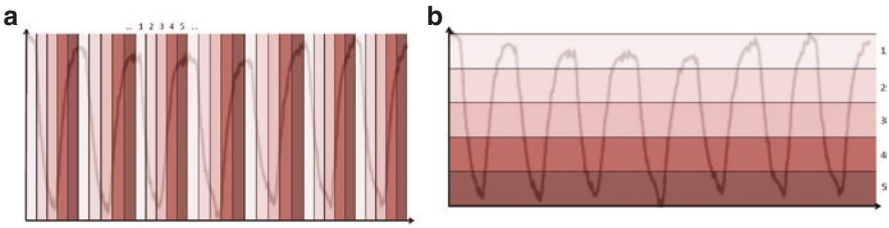

Fig. 2.8 Gating respiratory data using numbers of bins (**a**) or amplitude (**b**)

In order to track respiration, diaphragm displacement can be examined, using imaging techniques. Or external sensors can be used to detect motion. Pressure sensor belts are clinically available, identifying low pressure during expiration and high pressure during inspiration. In addition, real-time position management (RPM) uses a camera to track two infrared markers on a box positioned on the patient's chest.

Using these tracking techniques, the breathing signal can be synchronised with the imaging data, by binning or gating into groups of data at similar respiratory states. The main methods are gating by amplitude or phase. Phase gating splits the data within each respiratory cycle, into a number of bins between each inhalation peak (Fig. 2.8a) whereas amplitude gating splits the data based on the value of respiratory signal (Fig. 2.8b). Once the data is binned, one option is to create one 'exhale' image using data from one gate. This will reduce sensitivity; therefore, increased scan-time is required to achieve the same contrast. Another method is to use all the data for the different gates and register them to one gate, preserving full image contrast.

2.6 Recent Developments

There are various software advances that improve image quality which can be factored into PET reconstructions. These include time of flight (TOF) [4], which looks at the time at which two photons are received from the annihilation compared to each other, to give a better estimation of where the annihilation occurred along the LoR. There are also reconstruction algorithms that take into account the detector geometry, point spread function (PSF) [5], and an algorithm that can iteratively reconstruct going to full convergence, Bayesian penalised likelihood (BPL), algorithm [6]. In addition to this, recent advances in detectors have seen the use of solid state detectors, initially pioneered for PET/MR systems as the use photomultiplier tubes (PMT) are not compatible with the magnetic field. These detectors replace photomultiplier tubes with semiconductor readout arrays allowing more compact design and improved detecting capabilities.

Key Points

- There are many artefacts that can affect image quality—one of which is motion.
- Motion can cause potential spatial mismatch between CT and PET, which can give attenuation correction artefacts as CT images are acquired in seconds compared to PET which is time averaged over a number of minutes.
- With tracking techniques, the breathing signal can be synchronised with the imaging data, by binning or gating into groups of data at similar respiratory states.
- Phase gating splits the data within each respiratory cycle, into a number of bins between each inhalation peak.
- Amplitude gating splits the data based on the value of respiratory signal.
- Time of flight (TOF) looks at the time at which two photons are received from the annihilation compared to each other, to give a better estimation of where the annihilation occurred along the LoR.

References

1. Jolla L. Radionuclide data sheets. University of California; 2009. https://ehs.ucsd.edu/rad/radionuclide/radionuclide_datasheets.html. Accessed May 2016.
2. Delacroix D, Guerre JP, Leblanc P, Hickman C. Radionuclide and radiation protection handbook. Nuclear Technology Publishing; 2002. p. 98.
3. Jadvar H, Parker JA. Clinical PET and PET/CT—chapter 2 radiotracers. Springer; 2005. p. 45–67.
4. Vandenberghe E, Mikhaylova E, D'Hoe E, Mollet P, Karp JS. Recent developments in time-of-flight PET. EJNMMI Phy. 2016;3:3.
5. Rahmima A, Qi J, Sossi V. Resolution modelling in PET imaging: theory, practice, benefits and pitfalls. Med Phys. 2013;40(6):064301.
6. Ross S. GE healthcare Q.clear, White paper. Ross; 2014. rev 3.

The Physics of PET/CT for Radiotherapy Planning

3

Matt Aldridge

Content

The role of radiotherapy is to deliver a prescribed radiation dose to a target volume whilst minimising the dose to surrounding organs at risk (OAR). The tumour control probability (TCP) increases with absorbed dose until certain local control is achieved. However, the escalation of absorbed dose is generally limited by normal-tissue-complication probability (NTCP).

Advanced radiotherapy techniques such as intensity modulated radiation therapy (IMRT) and proton/ion therapy offer a high degree of conformity to a target volume, with much less normal tissue receiving a high dose for a given target dose. These may allow dose escalation to the target for the same NTCP as conventional radiotherapy, thus providing the potential for better disease control.

The most important component of radiation therapy treatment planning is the delineation of the gross tumour volume (GTV), Fig. 3.1. The GTV is the macroscopically demonstrable extent and location of the tumour. The clinical target volume (CTV) is extended from the GTV to include subclinical malignant disease with a certain probability of occurrence considered relevant for therapy. The planning target volume (PTV) is a larger volume that takes account of geometrical uncertainties such as organ motion and setup variations.

Traditionally, standard practice has been to delineate the target volumes on a CT dataset, sometimes after fusion with other modalities such as magnetic resonance

M. Aldridge (✉)
University College London Hospitals NHS Foundation Trust, London, UK
e-mail: matthew.aldridge@uclh.nhs.uk

K. Agrawal et al. (eds.), *PET/CT Imaging*, Clinicians' Guides to Radionuclide Hybrid Imaging, https://doi.org/10.1007/978-3-030-75476-1_3

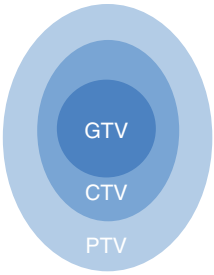

Fig. 3.1 Target volumes used in radiotherapy treatment planning. *GTV* gross tumour volume, *CTV* clinical target volume, *PTV* planning target volume

Table 3.1 Radiopharmaceuticals used to assess molecular pathways

Radiopharmaceuticals	Cellular pathway
^{18}F-fluro-2-deoxy-D-glucose (^{18}F-FDG)	Glucose metabolism
^{18}F-fluro-ethyl-tyrosine (^{18}F-FET)	Protein synthesis
^{18}F-3′-deoxy-3′-fluoro-thymidine (^{18}F-FLT)	Cell proliferation
^{18}F-fluoro-methyl-D-tyrosine (^{18}F-FMT)	Protein synthesis
^{11}C-methionine (^{11}C-MET)	Protein synthesis
^{11}C-acetate	Fatty-acid metabolism
^{18}F-fluoro-misonidazole (^{18}F-FMISO)	Hypoxia
^{68}Ga-DOTATATE	Somatostatin receptor expression

imaging, but recently PET/CT has been used as the functional imaging tool such that planning volumes are based on the metabolic uptake. Hence, PET may be used to modify the GTV and has the potential to identify hypermetabolic regions that may be smaller than the morphological appearance of the tumour. In addition, the size of the clinical target volume (CTV) may be modified by the inclusion or absence of PET avid lymph nodes.

The most commonly used radiopharmaceutical is 2-[^{18}F] fluoro-2-D-deoxyglucose (^{18}F-FDG). Other radiopharmaceuticals to assess various molecular pathways in tumour biology are summarised in Table 3.1.

A major advantage of PET imaging is the quantitative assessment of tumour uptake by standardised uptake value (SUV). This is defined as the uptake of a radiopharmaceutical, normalised to the injected dose and body weight. It is commonly used for prognosis, response monitoring and definition of treatment volumes. There are a number of biological and technical factors that influence the measure of SUV, and guidelines to minimise the error have been published [1, 2].

The widespread availability of large-bore integrated PET/CT systems, together with fixed radiation therapy positioning laser systems has enabled radiotherapy planning of metabolic target volumes to be realised. A single-scan approach can be used that enables the radiotherapy plan to be generated on the PET and/or CT dataset.

With the advent of wide bores, a flat therapy couch top with a carbon fibre overlay can be securely fitted to the PET/CT couch to achieve the same geometry as the radiotherapy couch top (Fig. 3.2). The rigidity of the couch top should ensure minimal sag in the extended PET position. Immobilisation devices can be attached to the

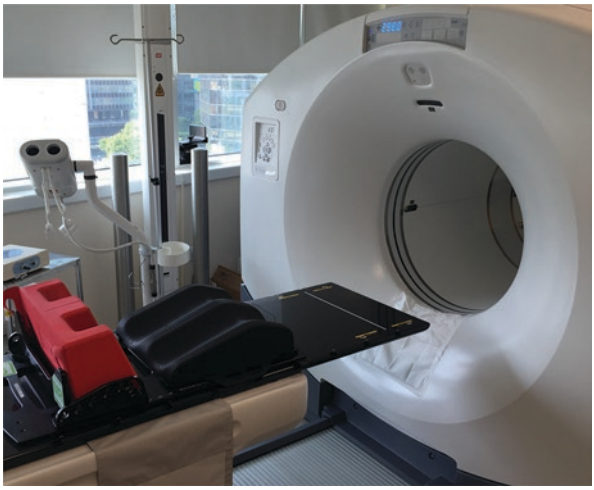

Fig. 3.2 PET/CT with radiotherapy planning setup. The laser light system is mounted in front of the gantry. A flat-top couch is attached to the bed, with immobilisation device for consistency with the treatment unit

couch top consistent with the table tops in the treatment unit. The dedicated radiotherapy laser system is generally positioned in front of the PET/CT gantry and provides a coordinate system in three axes such that appropriate marks can be placed on the patient's skin or immobilisation device to reproduce the position in the treatment room.

Appropriate QA, generally performed by the radiotherapy physics team needs to be performed to ensure consistency with the treatment room lasers.

Because of the inherent resolution limitation and partial volume effect in PET systems, accurate delineation of the gross tumour volume (GTV) is a major consideration in the application of PET/CT for radiotherapy planning [3–5]. Delineation errors may result in sub-optimal loco-regional disease control because of inadequate coverage or to increased toxicity of the treatment because of excessive coverage of normal tissues.

Manual delineation of PET images is the easiest method, but is very operator-dependent, particularly since altering the window levels can vary the perception of tumour volume, despite using the CT images as anatomic boundaries.

More accurate methods utilise automatic or semi-automatic segmentation methods that reduce the GTV significantly and reduce interobserver variability. A thresholding method is easy to implement with all voxels having an intensity higher than threshold (SUV = 2.5) considered as target [6]. Alternatively, for regions of reduced signal-to-noise, a percentage threshold may be used, with a commonly used value of 40% of the maximum value in the target region [7].

Gradient based auto-contouring methods utilise image processing techniques such as edge enhancement using partial volume correction methods. Gradient based segmentation is then performed by evaluating the image gradient of a line profile across a tumour region of the PET image.

Respiratory motion is another technical challenge for lesions located in the thorax and upper abdomen. As breath-hold techniques are not achievable in long

acquisition time PET protocols, respiratory motion may manifest in a visual appearance of smearing of the activity distribution in the tumour, with a loss of contrast and overestimation of the lesion volume.

There are several respiratory monitoring systems available for gating purposes based on different physical properties [8].

1. Pressure sensitive belt.
2. Spirometry system.
3. Strain-gauge belt.
4. Temperature sensor.
5. Opto-electronic system.

These techniques work by synchronising the PET and CT acquisitions to the patient's respiratory cycle, with the result that well-registered PET and CT images are produced corresponding to specific phases of the breathing cycle. This has the effect of potentially reducing the PTV, with increased effectiveness of radiotherapy treatment and less side-effects.

Key Points

- The role of radiotherapy is to deliver a prescribed radiation dose to a target volume whilst minimising the dose to surrounding organs at risk (OAR).
- The most important component of radiation therapy treatment planning is the delineation of the gross tumour volume (GTV).
- The GTV is the macroscopically demonstrable extent and location of the tumour.
- The clinical target volume (CTV) is extended from the GTV to include subclinical malignant disease with a certain probability of occurrence considered relevant for therapy.
- The planning target volume (PTV) is a larger volume that takes account of geometrical uncertainties such as organ motion and setup variations.
- Delineation errors may result in sub-optimal loco-regional disease control because of inadequate coverage.
- Manual delineation of PET images is the easiest method, but is very operator-dependent.
- More accurate methods utilise automatic or semi-automatic segmentation methods that reduce the GTV significantly and reduce interobserver variability.

References

1. Boellaard R, et al. EANM procedure guidelines for tumour PET imaging: version 1.0. Eur J Nucl Med Mol Imaging. 2010;37:181–200.
2. Sattler B, et al. PET/CT (and CT) instrumentation, image reconstruction and data transfer for radiotherapy planning. Radiother Oncol. 2010;96:288–97.
3. Caldwell CB, et al. Observer variation in contouring gross tumor volume in patients with poorly defined non-small-cell lung tumors on CT: the impact of 18FDG-hybrid PET fusion. Int J Radiat Oncol Biol Phys. 2001;51(4):923–31.
4. Schinagl DA, Vogel WV, Hoffmann AL, van Dalen JA, Oyen WJ, Kaanders JH. Comparison of five segmentation tools for 18F-fluorodeoxy-glucose-positron emission tomography-based target volume definition in head and neck cancer. Int J Radiat Oncol Biol Phys. 2007;69:1282–9.
5. Zaidi H, Naqa IE. PET-guided delineation of radiation therapy treatment volumes: a survey of image segmentation techniques. Eur J Nucl Med Mol Imaging. 2010;37:2165–87.
6. Nestle U, Kremp S, Schaefer-Schuler A, et al. Comparison of different methods for the delineation of 18F-FDG PET-positive tissue for target volume definition in radiotherapy of patients with non-small cell lung cancer. J Nucl Med. 2005;46:1342–8.
7. Biehl KJ, Kong F-M, Dehdashti F, et al. 18F-FDG PET definition of gross tumor volume for radiotherapy of non-small cell lung cancer: is a single standardized uptake value threshold approach appropriate? J Nucl Med. 2006;47:1808–12.
8. Nehmeh SA, Erdi YE. Respiratory motion in positron emission tomography/computed tomography: a review. Semin Nucl Med. 2008;38:167–76.

^{18}F-FDG and Non-FDG PET Radiopharmaceuticals

4

James Ballinger and Gopinath Gnanasegaran

Contents

The content of this chapter has originally been published in: Szyszko (Ed.) PET/CT in Esophageal and Gastric Cancer © Springer 2016.

J. Ballinger (✉)
Guy's and St Thomas' Hospital, London, UK

School of Biomedical Engineering and Imaging Sciences, King's College London, London, UK
e-mail: jim.ballinger@kcl.ac.uk

G. Gnanasegaran
Department of Nuclear Medicine, Royal Free NHS Foundation Trust, London, UK

K. Agrawal et al. (eds.), *PET/CT Imaging*, Clinicians' Guides to Radionuclide Hybrid Imaging, https://doi.org/10.1007/978-3-030-75476-1_4

4.1 Introduction

Positron emission tomography/computed tomography (PET/CT) is one of the key imaging techniques in oncology. Hybrid PET/CT provides both structural and metabolic information and in general improves sensitivity, specificity and nuclear medicine physician's confidence.

Fluorine-18 (^{18}F) is the most commonly used positron-emitting radionuclide label in clinical practice. It is produced using a cyclotron and has a physical half-life of 110 min. The most widely used tracer at present is the glucose analogue, 2-fluoro-2-deoxyglucose (FDG) (Table 4.1).

4.2 PET Radiopharmaceuticals

4.2.1 ^{18}F-FDG

^{18}F-FDG has a role in localising, characterising, staging and monitoring treatment response and evaluating recurrent disease in a variety of cancer types. However, increased FDG uptake is not specific to cancer cells. FDG accumulates in cells, in proportion to glucose utilisation [1–5]. In general, increased glucose uptake is a characteristic of most cancers and is in part mediated by overexpression of the

Table 4.1 Oncology PET radiopharmaceuticals [1–15]

Class	Radiopharmaceutical	Clinical application
Oncology: ^{18}F	Fludeoxyglucose (FDG)	Glucose metabolism
	Fluoride	Bone metabolism
	Fluoro-L-thymidine (FLT)	DNA synthesis
	Fluoromethylcholine (FCh)	Phospholipid synthesis
	Fluoroethylcholine (FEC)	Phospholipid synthesis
	Fluoroethyltyrosine (FET)	Protein synthesis
	Fluoromisonidazole (FMISO)	Hypoxia
	Fluoroazomycin arabinoside (FAZA)	Hypoxia
	Fluoroerythronitroimidazole (FETNIM)	Hypoxia
	Fluciclatide	Angiogenesis
	F-galacto-RGD	Angiogenesis
	Fluciclovine (Axumin®)	Amino acid transport
	F-DCFPyL (PyL™)	Prostate-specific membrane antigen
Oncology: ^{11}C	Acetate	Membrane synthesis
	Choline	Phospholipid synthesis
	Methionine	Protein synthesis
Oncology: ^{68}Ga	DOTATOC (Somakit-TOC®)	Somatostatin receptor
	DOTATATE (Netspot®)	Somatostatin receptor
	HA-DOTATATE	Somatostatin receptor
	DOTANOC	Somatostatin receptor
	PSMA-11	Prostate-specific membrane antigen
	NOTA-RGD	Angiogenesis
Oncology: ^{124}I	Iodide	Sodium iodide symporter
	MIBG	Neuronal activity

Table 4.2 Properties of positron-emitting radionuclides used in clinical practice

Radionuclide	Half-life	Positron energy (max, MeV)	Other emissions	Means of production
Carbon-11	20 min	0.96	–	Cyclotron
Nitrogen-13	10 min	1.20	–	Cyclotron
Oxygen-15	2 min	1.74	–	Cyclotron
Fluorine-18	110 min	0.63	–	Cyclotron
Copper-62	10 min	2.93	–	Generator
Copper-64	13 h	0.65	Beta, gamma	Cyclotron
Gallium-68	68 min	1.83	–	Generator
Rubidium-82	76 s	3.15	–	Generator
Zirconium-89	79 h	0.40	Gamma	Cyclotron
Iodine-124	4.2 days	1.50	Gamma	Cyclotron

Table 4.3 Common oncology PET radiopharmaceuticals and their mechanism of uptake [1–15]

Radiotracer	Mechanism of uptake
^{18}F-Fluorodeoxyglucose	Uptake by GLUT-1 transporter followed by phosphorylation by hexokinase
Sodium ^{18}F-fluoride	Incorporated within hydroxyapatite in proportion to bone metabolism
^{68}Ga-labelled peptides	Binds to peptide receptor, most commonly somatostatin receptor
^{18}F-Choline ^{11}C-Choline	Incorporation into phosphatidylcholine as part of cell wall synthesis
^{11}C-Methionine	Amino acid transport
^{18}F-Fluorothymidine ^{11}C-Thymidine	Phosphorylated by thymidine kinase in proliferating cells; FLT not incorporated into DNA
^{68}Ga-PSMA/^{18}F-PyL	Binds to active substrate recognition site of prostate-specific membrane antigen

GLUT-1 glucose transporter and increased hexokinase activity [1–5]. The net result is an increased accumulation of FDG within tumour cells at a rate greater than in normal tissue. Active inflammatory changes can also result in increased FDG uptake, due to increased glucose utilisation by activated granulocytes and mononuclear cells [1–5] (Tables 4.1, 4.2, and 4.3). The principal route of excretion of FDG from the bloodstream is via the urinary tract. The biodistribution of ^{18}F-FDG varies on several factors such as (a) fasting state, (b) medications, (c) duration of the ^{18}F-FDG and Non-FDG PET Radiopharmaceuticals uptake period post tracer injection, (d) variant metabolism and (e) incidental pathology and is discussed in detail in Chap. 8.

4.2.2 Non-FDG Radiopharmaceuticals

In addition to ^{18}F-FDG, there are several cyclotron- and generator-based radiolabelled molecules used in clinical PET/CT imaging. Sodium fluoride (^{18}F-NaF), ^{68}Ga-labelled peptides, ^{18}F-choline, ^{11}C-choline, etc., each has clinical applications and is discussed in detail in this pocket book series titled *PET Radiotracers*. While FDG is the workhorse of oncological PET imaging, it is non-specific as it monitors

the ubiquitous process of glucose metabolism. Alternative tracers tend to be more specific in their targeting and application. Some attempt to probe the hallmarks of cancer, such as uncontrolled proliferation, angiogenesis, evasion of apoptosis and tissue invasion. Tumour microenvironment, such as hypoxia, has also been probed. However, the tracers which have come into wider use tend to be those which monitor specific features such as membrane synthesis incorporating choline, prostate-specific membrane antigen (PSMA) expression and somatostatin receptor expression.

4.3 Conclusion

It is likely that the range of positron-emitting radiopharmaceuticals in routine clinical use will continue to expand in the coming years.

Key Points

- Fluorine-18 (^{18}F) is the most commonly used positron-emitting radionuclide label in clinical practice.
- Fluorine-18 (^{18}F) is produced using a cyclotron and has a physical half-life of 110 min.
- The most widely used tracer at present is the glucose analogue, 2-fluoro-2-deoxyglucose (FDG). FDG is the workhorse of oncological PET imaging. FDG is actively transported into the cell mediated by a group of structurally related glucose transport proteins (GLUT).
- Increased FDG uptake is not specific to cancer cells and often will accumulate in areas with increased metabolism and glycolysis.
- The principal route of excretion of FDG from the bloodstream is via the urinary tract.
- Non-FDG tracers include sodium fluoride (^{18}F-NaF), ^{68}Ga-labelled peptides, ^{18}F-choline, and ^{11}C-choline.

References

1. Torizuka T, Tamaki N, Inokuma T, et al. In vivo assessment of glucose metabolism in hepatocellular carcinoma with FDG-PET. J Nucl Med. 1995;36:1811–7.
2. Cook GJR, Fogelman I, Maisey MN. Normal physiological and benign pathological variants of ^{18} F-FDG PET scanning: potential for error in interpretation. Semin Nucl Med. 1996;26:308–14.
3. Warburg O. On the origin of cancer cells. Science. 1956;123:309–14.
4. Cook GJR, Maisey MN, Fogelman I. Normal variants, artefacts and interpretative pitfalls in PET imaging with ^{18}F-fluoro-2-deoxyglucose and carbon-11-methionine. Eur J Nucl Med. 1999;26:1363–78.

5. Culverwell AD, Scarsbrook AF, Chowdhury FU. False-positive uptake on 2-[18F]-fluoro-2-deoxy-D-glucose (FDG) positron-emission tomography/computed tomography (PET/CT) in oncological imaging. Clin Radiol. 2011;66:366–82.
6. Shreve PD, Anzai Y, Wahl RL. Pitfalls in oncologic diagnosis with FDG PET imaging: physiologic and benign variants. Radiographics. 1999;19:61–77.
7. Delbeke D, Coleman RE, Guiberteau MJ, et al. Procedure guideline for tumour imaging with 18 F-FDG PET/CT 1.0. J Nucl Med. 2006;47:885–95.
8. Boellaard R, Delgado-Bolton R, Oyen WJ, et al. FDG PET/CT: EANM procedure guidelines for tumour imaging: version 2.0. Eur J Nucl Med Mol Imaging. 2015;42:328–54.
9. Beheshti M, Mottaghy FM, Payche F, et al. 18F-NaF PET/CT: EANM procedure guidelines for bone imaging. Eur J Nucl Med Mol Imaging. 2015;42:1767–77.
10. Virgolini I, Ambrosini V, Bomanji JB, et al. Procedure guidelines for PET/CT tumour imaging with 68Ga-DOTA-conjugated peptides: 68Ga-DOTA-TOC, 68Ga-DOTA-NOC, 68Ga-DOTA-TATE. Eur J Nucl Med Mol Imaging. 2010;37:2004–10.
11. Juweid ME, Cheson BD. Positron-emission tomography and assessment of cancer therapy. N Engl J Med. 2006;2(354):496–507.
12. Fendler WP, Eiber M, Beheshti M, et al. 68Ga-PSMA PET/CT: joint EANM and SNMMI procedure guideline for prostate cancer imaging: version 1.0. Eur J Nucl Med Mol Imaging. 2017;44:1014–24.
13. Nanni C, Zanoni L, Bach-Gansmo T, et al. [18F]Fluciclovine PET/CT: joint EANM and SNMMI procedure guideline for prostate cancer imaging: version 1.0. Eur J Nucl Med Mol Imaging. 2020;47:579–91.
14. Unterrainer M, Eze C, Ilhan H, et al. Recent advances of PET imaging in clinical radiation oncology. Radiat Oncol. 2020;15:88.
15. Lau J, Rousseau E, Kwon D, et al. Insight into the development of PET radiopharmaceuticals for oncology. Cancers (Basel). 2020;12:1312.

PET/CT Imaging: Patient Instructions and Preparation

5

Shaunak Navalkissoor, Thomas Wagner, Gopinath Gnanasegaran, Teresa Szyszko, and Jamshed B. Bomanji

Contents

5.1 Introduction

^{18}F-FDG is a frequently used molecular imaging modality in the evaluation of cancer patients. A high-quality ^{18}F-FDG PET study should be repeatable (same result produced if imaged on the same system) and reproducible (similar result if imaged at different sites). An essential component of this is adequate patient preparation to ensure study reproducibility and technical quality. Rigorous instructions should be followed regarding patient procedure. In addition, adequate referral information is important so that the correct timing of study and imaging protocol can be followed, e.g. lung gating for a base of lung lesion. This section addresses some of these

The content of this chapter has originally been published in: Szyszko (Ed.) PET/CT in Esophageal and Gastric Cancer © Springer 2016.

S. Navalkissoor (✉) · T. Wagner · G. Gnanasegaran · T. Szyszko
Department of Nuclear Medicine, Royal Free NHS Foundation Trust, London, UK
e-mail: s.navalkissoor@nhs.net

J. B. Bomanji
Institute of Nuclear Medicine, University College London, London, UK

K. Agrawal et al. (eds.), *PET/CT Imaging*, Clinicians' Guides to Radionuclide Hybrid Imaging, https://doi.org/10.1007/978-3-030-75476-1_5

Table 5.1 Contents of PET/CT request [1–5]

1. Patient name, date of birth, address and hospital identifier number
2. Clinical indication
3. Clinical question to be answered
4. Oncological history: Site of tumour (if known), recent biopsy (site, date of biopsy and results if known) and comorbidity
5. Drug allergies and allergy to contrast agents
6. Diabetes status, if relevant (IDDM, NIDDM) and treatment
7. Renal function
8. Therapeutic interventions: Type and date of last treatment (chemotherapy, surgery, radiotherapy, bone marrow stimulants and steroids administration)
9. Result and availability of previous imaging
10. Height and body weight
11. Referring clinician's contact details: (a) to discuss about the referral, (b) to contact during emergency and (c) to send the reports
12. Date at which results of the PET or PET/CT study must be available

issues and summaries of required clinical information, patient preparation, procedure and imaging parameters are shown in Tables 5.1, 5.2, and 5.3.

FDG is a glucose analogue and is transferred intracellularly by glucose transporters. Many tumour cells overexpress glucose transporter proteins and hexokinase intracellularly, which allows FDG to be used to image these tumours.

5.2 Patient Preparation

One of the main aims in patient preparation is to reduce the hyperinsulinemic state, which occurs with recent glucose ingestion. Increased glucose levels cause competitive inhibition of ^{18}F-FDG uptake by active cells leading to decreased tumour (or other active process) to background ratio. Increased insulin secondary to elevated blood glucose also increases translocation of GLUT4, thereby shunting ^{18}F-FDG to organs with high density of insulin receptors (e.g. skeletal muscles). Patients should thus fast for at least 6 h prior to the study to ensure low insulin levels. EANM guidelines suggest that patients with blood glucose <11 mmol/L can have FDG administered, whilst patients with glucose >11 mmol/L need to be rescheduled. Patients with diabetes (particularly with insulin-based treatments) need to be carefully scheduled to avoid a hyperinsulinemic state. (An example of scheduling includes a late morning appointment with an early breakfast and insulin injection). If glucose control is not achieved, then the PET scan can be rescheduled.

Other patient preparations aim to reduce tracer uptake in normal tissues, thus increasing target to nontarget uptake. Patients should be hydrated adequately to decrease the concentration of FDG in the urine, decreasing artefacts and potentially reducing radiation dose. Drinking water is permitted; however, flavoured water contains sugar and cannot be consumed prior to the PET scan. Patients should be advised to dress warmly on the way to the PET suite and should be kept in a warm room prior to the administration of FDG. This is to avoid accumulation of FDG in

Table 5.2 General instructions for an ^{18}F-FDG PET scan [1–5]

Appointment
1. Send leaflets related to the scan and instructions
2. Confirm appointment
3. Medications list if any
4. History of diabetes, fasting state and recent infection/intervention
Before arrival
1. Fast, except for water (for at least 6 h before the injection of ^{18}F-FDG for most studies, at least 4 h before dedicated neuroimaging). Avoid chewing gum
(a) Morning appointment: Patient should not eat after midnight [preferably have a light meal (no alcohol) during the evening prior to the PET study]
(b) Afternoon appointment PET study: Patient may have a light breakfast before 8.00 a.m. (no sugars or sugar-containing fillings/products)
2. Advise adequate pre-hydration
3. Intravenous fluids containing dextrose or parenteral feedings should be withheld for 4–6 h before radiotracer injection
4. Consider if intravenous contrast material is to be used for CT
Before injecting
1. The blood glucose level should be checked and documented
FDG PET study can be performed: If plasma glucose level is <11 mmol/L (or <200 mg/dL)
FDG PET study should be rescheduled: If plasma glucose level is ≥11 mmol/L (or >200 mg/dL) depending on patients circumstances
2. Keep the patient in a warm room for 30–60 min before the injection and during the uptake period and maintain warmth with blankets during scan to reduce uptake in the brown fat (orazepam, diazepam and beta-blockers may help to reduce uptake by brown fat uptake if problematic)
3. Check patient's ability to lie still for the duration of the scan and ability to put his or her arms overhead
4. Ask for history of claustrophobia
5. If intravenous contrast material is to be used, patients should be screened for iodinated contrast material allergy, renal disease and use of metformin for diabetes mellitus treatment
6. Take a brief history and document site of malignancy, including recent investigations and treatment history: Surgery, radiation, chemotherapy
7. The recommended interval from FDG injection to scan (uptake period) is 60 min

Table 5.3 ^{18}F-FDG PET/CT imaging parameters [1–5]

Routine imaging: Skull base to upper thigh
Additional views: Lower limb views, dedicated head and neck or occasionally scan to vertex are acquired as necessary
Brain imaging is frequently omitted in many institutions routinely (poor sensitivity of FDG PET for brain metastases)
Typical adult administered activities: 185–370 MBq (5–10 mCi), up to 400 MBq
Largest effective dose administered: Urinary bladder
Whole body effective dose of PET study is approximately 0.02 mSv/MBq or 7–8 mSv for an adult administered activity of 370 MBq. CT dose depends on local protocol

activated brown fat. In some cases with no contraindications to oral beta-blockers, propranolol (1 mg/kg, maximum 40 mg) can be given at least 90 min before FDG injection to reduce FDG uptake in brown adipose tissue. This is especially important in young patients. Strenuous physical activity should be avoided for at least 6 h

Table 5.4 Example of low-carbohydrate high-fat diet provided to patients prior to FDG PET cardiac imaging

Do not eat the following:
Sugar in any form (including natural's sugars in fruits)
No starches, e.g. pasta, breads, cereals, rice and potatoes
No vegetables with high carbohydrate content, no carrots or beetroot
No chocolates, sweets, chewing gums, mints and cough syrups
No processed products, e.g. processed deli meats
No sweetener substitutes like Canderel or Splenda
No milk or milk products
No cheese or cheese products
No nuts
No fruits
No alcohol
You can eat the following:
Poultry: Fatty unsweetened chicken and Turkey (fried or boiled, NOT grilled)
Meats: Fatty unsweetened, red meat, bacon, ham (fried or boiled, NOT T grilled)
Fish: Any fish (fatty unsweetened, fried or boiled, NOT grilled)
Shellfish: Any non-processed shellfish
Eggs: Fried, scrambled preparation without milk, omelette prepared without milk or vegetables
Butter and margarine
Vegetables: Cucumber, broccoli, lettuce, celery, mushroom, green pepper, cabbage, spinach, asparagus, radish
Drinks: Mineral water (still or sparkling), coffee, tea, herbal tea (without milk or sugar)

prior to the scan to avoid excessive skeletal uptake. During the uptake period, the patient should not talk and avoid reading or chewing, to reduce uptake in these respective muscles [6].

If a lesion near the myocardium or the myocardium itself is being evaluated for suspected disease, careful patient preparation is required to limit cardiac uptake. There are several options to decrease normal glucose uptake by the myocardium. These include a high-fat diet with no or low carbohydrate content (to minimise serum glucose/insulin release and increase free fatty acids) for 24 h before the scan (Table 5.4). Other mechanisms to reduce cardiac uptake include extended fasting for up to 18 h before the scan (to switch the myocardial energy substrate from glucose to fatty acids) and intravenous bolus of heparin (50 IU/kg) given 90 min prior to ^{18}F-FDG injection (suppression of myocardial FDG uptake) [7].

Review of patients' medication should be performed, e.g. steroids in high doses may cause hyperglycaemic states and, in patients with suspected vasculitis, may reduce the sensitivity of the test; metformin may cause diffuse large bowel uptake due to increased glucose utilisation of the intestinal mucosa. If intravenous contrast is going to be administered, metformin needs to be withheld on the day of the test and for a further 48 h.

5.3 Timing of FDG PET Scan After Treatment

When the PET scan is being protocolled, adequate information about previous treatments should be available to the person authorising the request to ensure accurate timing, e.g. in chemotherapy response assessments in lymphoma, the ^{18}F-FDG PET

scan should not be performed too early to avoid false negatives due to tumour stunning or false positives due to inflammatory uptake. An interval of at least 10 days should be allowed post-chemotherapy (interim PET) or at least 3 weeks at the end of chemotherapy to allow evaluation of response to chemotherapy. If patients are undergoing radiotherapy, the recommended post-therapy interval is 2–3 months.

Key Points

- Rigorous instructions should be followed regarding patient procedure.
- Adequate referral information is important so that the correct timing of study and imaging protocol can be followed.
- Increased glucose levels cause competitive inhibition of ^{18}F-FDG uptake.
- Increased insulin secondary to elevated blood glucose increases translocation of GLUT4.
- Patients should thus fast for at least 6 h prior to the study to ensure low insulin levels.
- Patients with blood glucose <11 mmol/L can have FDG administered, whilst patients with glucose >11 mmol/L need to be rescheduled (EANM guidelines).
- Patients with diabetes (particularly with insulin-based treatments) need to be carefully scheduled to avoid a hyperinsulinemic state.
- Patients should be hydrated adequately to decrease the concentration of FDG in the urine, decreasing artefacts and potentially reducing radiation dose.
- Keep the patient in a warm room for 30–60 min before the FDG injection.
- Strenuous physical activity should be avoided for at least 6 h prior to the scan.
- An interval of at least 10 days should be allowed post-chemotherapy (interim PET) or at least 3 weeks at the end of chemotherapy to allow evaluation of response to chemotherapy.
- In patients undergoing radiotherapy, the recommended post-therapy interval is 3 months to allow evaluation of response.

References

1. Delbeke D, Coleman RE, Guiberteau MJ, et al. Procedure guideline for tumour imaging with ^{18}F-FDG PET/CT 1.0. J Nucl Med. 2006;47(5):885–95.
2. Boellaard R, O'Doherty MJ, Weber WA, et al. FDG PET and PET/CT: EANM procedure guidelines for tumour PET imaging: version 1.0. Eur J Nucl Med Mol Imaging. 2010;37(1):181–200.
3. Boellaard R, Delgado-Bolton R, Oyen WGJ, Giammarile F, Tatsch K, Eschner W, et al. FDG PET/CT: EANM procedure guidelines for tumour imaging: version 2.0. Eur J Nucl Med Mol Imaging. 2015;42:328–54.
4. Juweid ME, Cheson BD. Positron-emission tomography and assessment of cancer therapy. N Engl J Med. 2006;354(5):496–507.

5. Graham MM, Wahl RL, Hoffmans JM, Yaps JT, Sunderland JT, et al. Summary of the UPICT protocol for ^{18}F-FDG PET/CT imaging in oncology clinical trials. J Nucl Med. 2015;56:955–61.
6. IAEA Human Health Series No. 26 standard operating procedures for PET/CT: a practical approach for use in adult oncology. https://www-pub.iaea.org/MTCD/Publications/PDF/Pub1616_web.pdf.
7. Osborne MT, Hulten EA, Murthy VL, Skali H, Taqueti VR, Dorbala S, DiCarli MF, Blankstein R. Patient preparation for cardiac fluorine-18 fluorodeoxyglucose positron emission tomography imaging of inflammation. J Nucl Cardiol. 2017;24(1):86–99.

^{18}F-FDG PET/CT Imaging: Normal Variants, Pitfalls and Artefacts

6

Kanhaiyalal Agrawal, Gopinath Gnanasegaran, Evangelia Skoura, Alexis Corrigan, and Teresa Szyszko

Contents

6.1 Introduction

In recent years, positron emission tomography (PET)/computed tomography (CT) has gained widespread clinical acceptance in oncology. It is being used extensively in the diagnosis, staging, restaging, therapy response evaluation of

The content of this chapter has originally been published in: Szyszko (Ed.) PET/CT in Esophageal and Gastric Cancer © Springer 2016

K. Agrawal (✉)
Department of Nuclear Medicine, All India Institute of Medical Sciences (AIIMS), Bhubaneswar, India

G. Gnanasegaran · E. Skoura · T. Szyszko
Department of Nuclear Medicine, Royal Free NHS Foundation Trust, London, UK

A. Corrigan
Maidstone and Tunbridge Wells NHS Trust, Tunbridge Wells, UK

K. Agrawal et al. (eds.), *PET/CT Imaging*, Clinicians' Guides to Radionuclide Hybrid Imaging, https://doi.org/10.1007/978-3-030-75476-1_6

tumours (Table 6.1) along with several benign indications in cardiology and neurology. Fluorine-18 (^{18}F) 2-fluoro-2-deoxy-D-glucose (FDG) is the most commonly used positron-emitting radiotracer in PET/CT studies. In this chapter, we will mainly focus on normal variants and artefacts in ^{18}F-FDG PET/CT studies.

^{18}F-FDG is a glucose analogue labelled with a positron-emitting isotope ^{18}F. It is transported into cells through glucose transporters and phosphorylated by enzyme hexokinase to ^{18}F-FDG-6-phosphate [1]. The cell membrane is impermeable to both glucose 6-phosphate and ^{18}F-FDG-6-phosphate. However, the latter cannot be degraded further via the glycolysis pathway and remains trapped within the cell. ^{18}F-FDG is accumulated in malignant tissues more avidly than within the normal tissues due to increased glucose metabolism rate, increased expression of glucose transporters and highly active hexokinase bound to mitochondria of malignant tissue in comparison to normal tissue. However, ^{18}F-FDG uptake is also known to occur in inflammation, infection and healing tissues. This is partly due to the fact that infiltrated granulocytes and tissue macrophages use glucose as energy source. In inflammation, the granulocytes and macrophages are activated and hence, glucose metabolism increases [2].

There can be variable degree of physiological tracer uptake in the various organs in the ^{18}F-FDG PET/CT scans (Fig. 6.1) (Table 6.2) [3–16]. Recognition of physiological tracer distribution is essential in avoiding incorrect image interpretation. Sometimes special patient preparation is needed to suppress the physiological tracer uptake to identify pathology in some organs [14]. It is important that patient is relaxed on the day of the study and should maintain silence to avoid muscle uptake [5]. Brown fat uptake can be suppressed by keeping the patient warm or sometimes by administration of oral beta-blockers and benzodiazepines, especially in patients with suspected pathology in the neck and mediastinum. Similarly, cardiac ^{18}F-FDG PET imaging needs either prolonged fasting or special low-carbohydrate high-fat diet to suppress physiological uptake in the myocardium [14]. It is always better to avoid administering insulin to the patient on the day of study as this may lead to

Table 6.1 Clinical role of PET/CT imaging in oncology

Diagnosis
Localisation
Staging
Restaging
Treatment response
Recurrent disease or relapse
Radiotherapy planning
Guiding metabolic biopsy
Grading tumours

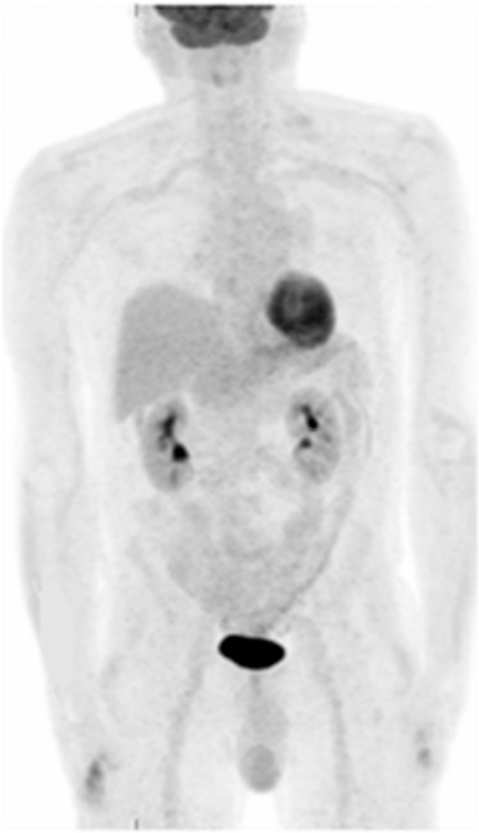

Fig. 6.1 Maximum intensity projection (MIP) [18]F-FDG PET/CT image shows normal physiologic tracer distribution in the brain, heart, liver, stomach, bowel, testes and excretion through kidneys into urinary bladder. [It is essential to recognise normal physiological uptake in order to interpret FDG PET images correctly]

increased background activity in the fat and muscles and decreases uptake in the tumour [5]. Physiological tracer activity in the urinary tract may mask pathologic conditions. Good hydration and use of intravenous diuretics should be considered to decrease the urinary stasis in the kidneys and ureters. It also dilutes the urine activity in the urinary bladder and helps in better evaluation of surrounding structures like the prostate gland.

[18]F-FDG PET study immediately after chemotherapy and radiotherapy introduces false positive findings [5–9, 12–13, 16]. Hence, at least a gap of 3 weeks following chemotherapy and 3 months following radiotherapy to perform [18]F-FDG PET study should be considered to reduce the false positives. Scanning performed immediately after surgery or biopsy may show falsely increased tracer localisation due to post-surgical inflammation. In addition, infection such as pneumonia, tuberculosis, osteomyelitis leads to false positives in oncology patients [2, 5–9, 12–13, 16].

Table 6.2 ^{18}F-FDG PET scan appearances and physiological variation [5–9, 12–13, 16]

Organ	Physiological uptake/variation	Comments
Brain	Intense uptake in cortex, basal ganglia and thalami (Fig. 6.2a)	Metastases are best assessed with MRI
Ocular muscles	Moderate or intense tracer uptake Related to eye movement during uptake period (Fig. 6.2b)	Patient should be advised to rest quietly in darkened room
Breast	Low grade diffuse uptake within breast is normal due to proliferative glandular tissue. Higher uptake may be seen in adolescent girls with dense breasts (Fig. 6.2d) The uptake in the areola is variable, but prominent uptake may be seen	Markedly increased in lactating breast. The amount of radioactivity within milk from breasts is low. The infant is more likely to receive radiation exposure from close contact with the breast, rather than from milk
Bone marrow	Low diffuse uptake in haematopoietic bone marrow is physiological	
Brown fat	Neck, paraspinal, retroperitoneal fat, etc.	Patient waiting areas should be kept warm. Drug intervention (may be helpful)
Endometrium	Central moderate uptake within uterus is normal during ovulatory and secretory phases	Menstrual history is important and tracer uptake may be pathological in postmenopausal women
Liver	Mild to moderate uptake (relatively homogeneous) (Fig. 6.2e)	
Spleen	Homogeneous uptake slightly less than to liver (Fig. 6.2e)	
GI tract	Highly variable Increased tracer uptake with a focal, diffuse or segmental distribution could be physiologic (Fig. 6.3) and more marked in patients taking the anti-diabetic drug such as metformin	Focal areas of increased uptake usually warrant further evaluation
Heart	Variable ranging from negligible to intense uptake (Fig. 6.4) depending on its metabolic state at the time of the study	Partly depends on fasting state (may be suppressed by prolonged fast or low-carbohydrate high-fat diet). However, in PET cardiac imaging, the main aim is to increase cardiac uptake of FDG and increasing uptake in cardiac cells can be achieved by increasing the serum insulin level or decreasing the free fatty acid level

Table 6.2 (continued)

Organ	Physiological uptake/variation	Comments
Muscles	Mild uptake is physiological Symmetrical diaphragmatic, intercostals and strap muscle uptake could be physiological or may relate to increased respiratory effort in patients with pulmonary disease (Fig. 6.5)	Tracer uptake is increased in patients who are not suitably fasted or following exercise/ exertion (proper clinical history is useful in these cases) (Fig. 6.6)
Ovary	During midcycle moderate increased uptake in the adnexal lesions is normal (unilateral or bilateral) (Fig. 6.7)	Menstrual history is important and may be pathological in postmenopausal women. Bilateral adnexal and uterine activity is likely to represent physiological ovarian and uterine uptake in a premenopausal woman
Salivary glands	Low grade tracer uptake is physiological and is often symmetrical	
Urinary tract	Increased activity within urinary tract is normal (Fig. 6.2f)	Good hydration and voiding are advised before imaging
Testes	Mild to moderate symmetrical uptake is physiological and declines with age (Fig. 6.2h)	
Thymus	Low to moderate uptake in children and young adults is normal (Fig. 6.8)	Often reactivated post-chemotherapy and should correlate with age of patient and medical history/treatment
Thyroid	Diffuse or focal uptake is often seen (Fig. 6.9)	Diffuse uptake is seen in patients with Graves' disease, subacute thyroiditis or Hashimoto's thyroiditis Focal uptake is often seen in thyroid nodules and should be further evaluated with fine needle aspiration
Tonsils	Common and variable. Often symmetrical and may relate to local infection/inflammation	
Vocal cords	Variable: moderate and symmetrical (Fig. 6.10)	Relates to phonation during uptake period. Unilateral uptake requires further evaluation—may relate to tumour or potentially unilateral vocal cord palsy

Imaging on hybrid PET/CT scanners may lead to misregistration due to differences in breathing patterns and patient movement between CT and PET image acquisitions [5–9]. Patient movement may be avoided by instructing the patient to lie down still during the scan or sometimes by using sedation judiciously in patient with severe pain and in children. Misregistration can be minimised by performing the CT scan during normal expiration. In hybrid PET/CT studies, low dose CT data

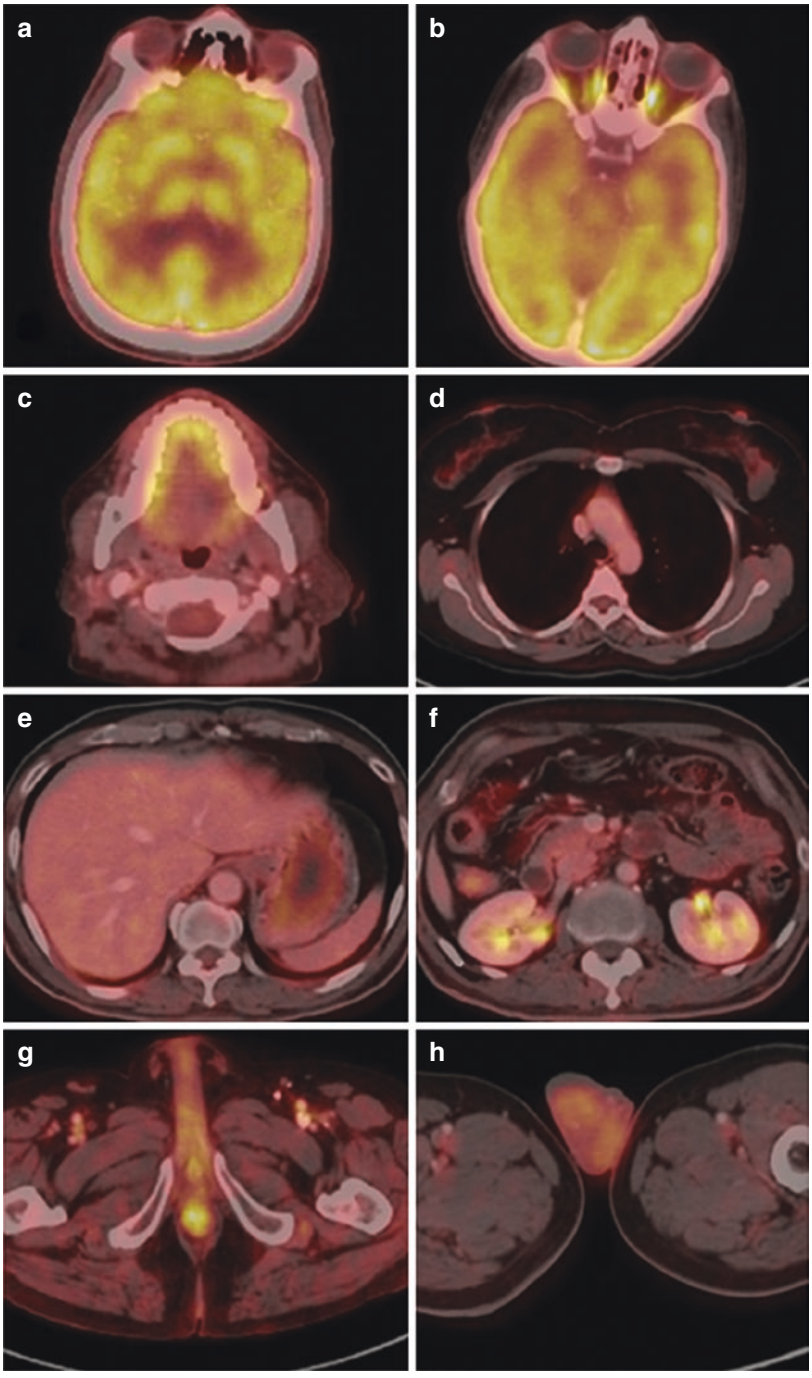

Fig. 6.2 Axial fused PET/CT images from different ^{18}F-FDG PET/CT studies show physiological tracer uptake in (**a**) brain, (**b**) medial and lateral rectus muscles of orbits, (**c**) tongue, (**d**) breasts, (**e**) liver and collapsed stomach wall, (**f**) kidneys, (**g**) rectum, (**h**) testes

is used for attenuation correction of PET data. However, high density contrast agents or metallic objects may lead to over correction if CT data is used for attenuation correction [5]. This leads to falsely increased tracer activity at these sites. Similarly, parts of brain may show falsely decreased uptake due to under attenuation correction of PET data if there is patient movement. Reviewing the non-attenuation corrected data is helpful in avoiding such misinterpretation. Another potential problem with low dose CT for attenuation correction is beam hardening artefacts, particularly in larger patients. This can lead to inaccurate attenuation correction. However, recently with many centres using diagnostic quality CT in PET/CT studies, this issue is not very frequent. Also, as this is commonly caused by the patient's arms being in the field of view, it can be avoided by placing arms above the head during imaging. However, if head and neck are the area of interest, it is advised to scan the patient in arms down position. Truncation artefacts are rare but difficult problems with hybrid scanner. These occur in cases where field of view of PET is larger in comparison to CT part [5].

False positives and false negatives can be countered in ^{18}F-FDG PET studies (Tables 6.3, 6.4, and 6.5). Tracer extravasation leads to false positive tracer

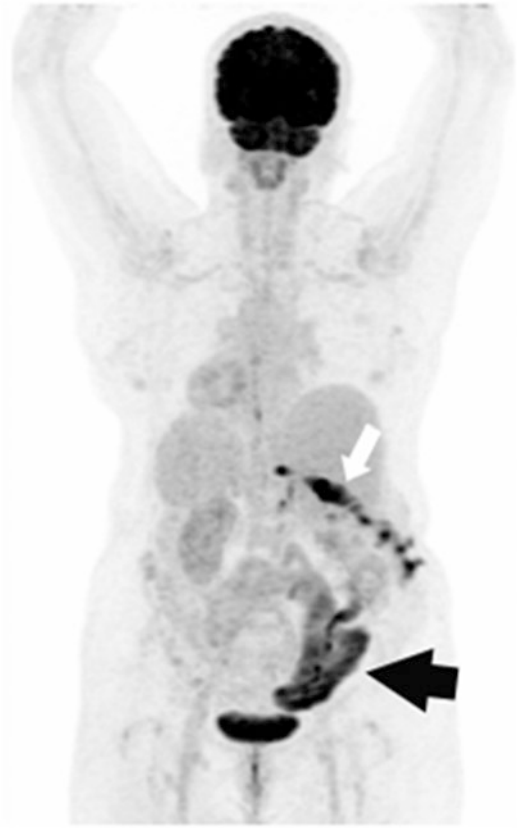

Fig. 6.3 Maximum intensity projection (MIP) ^{18}F-FDG PET image demonstrates intense tracer uptake (white arrow) in the anterior abdominal wall at the site of surgical incision in a patient with recent open cholecystectomy. [Increased uptake after surgery persists for several weeks and ideally the PET scan should be delayed for at least 6 weeks following surgery]. There is also increased uptake in the large intestine (black arrow). [GI uptake is highly variable and is increased with metformin use]

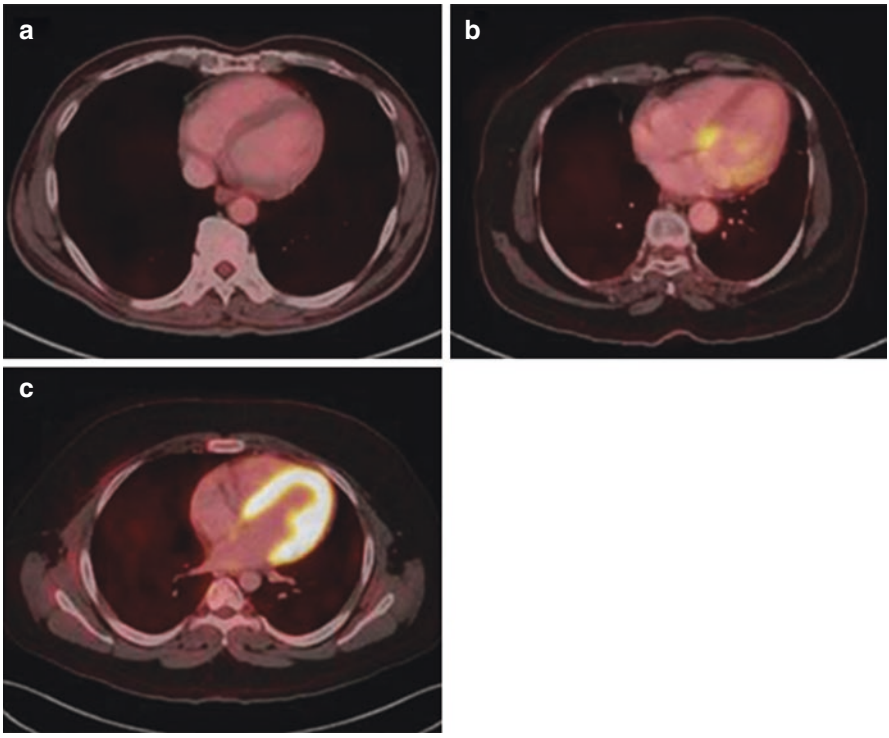

Fig. 6.4 ^{18}F-FDG PET/CT studies show different pattern of physiological tracer uptake in the myocardium varying from negligible (**a**), segmental (**b**) to diffuse intense uptake (**c**). [Variable myocardial uptake depends partly on fasting state and may be suppressed by prolonged fast or a low-carbohydrate high-fat diet. In PET cardiac imaging, the main aim is to increase cardiac uptake of FDG by increasing the serum insulin level]

accumulation at the site of injection (Fig. 6.18). Knowledge of site of injection is essential in correct interpretation of PET studies. Most of the false positives are due to infectious and inflammatory conditions [5–9]. In addition, many benign tumours may show false positive ^{18}F-FDG uptake. Similarly, some benign tumours show photopenia on PET images (Fig. 6.19). Small lesions beyond the resolution of PET scanners usually do not show ^{18}F-FDG uptake. Further, many cancers, such as lung carcinoid, are generally negative of ^{18}F-FDG PET studies. These false interpretations can be reduced by including CT findings in the PET/CT reports.

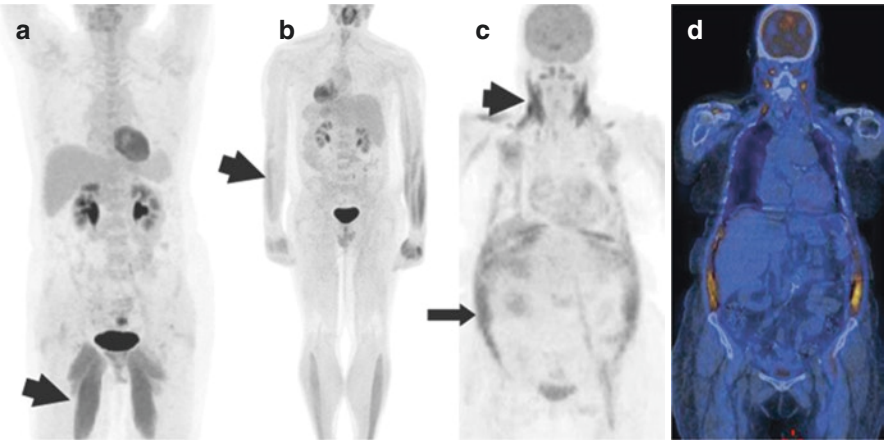

Fig. 6.5 (**a**, **b**) MIP ^{18}F-FDG PET image shows uptake in the skeletal muscles (arrows) likely due to overuse or muscular strain. This may obscure peripheral primary tumours, e.g. in melanoma. (**c**, **d**) MIP and coronal fused ^{18}F-FDG PET/CT images show increased tracer uptake in the respiratory muscles in a patient with breathing difficulty. The diffuse uptake in the abdominal muscles may mimic peritoneal uptake and caution is advised. [In general, exercising muscles, post-exercise uses glucose (energy substrate), in contrast, resting muscles predominantly use free fatty acids. Therefore, patients should avoid strenuous/severe exercise for at least a day prior to imaging]

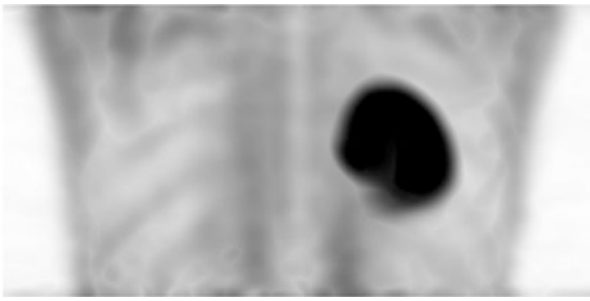

Fig. 6.6 MIP ^{18}F-FDG PET image of a patient for cardiac viability study shows diffuse increased tracer uptake in the muscles due to glucose loading and insulin administration. [Diffuse muscle uptake is often seen when the serum insulin level is elevated/increased]

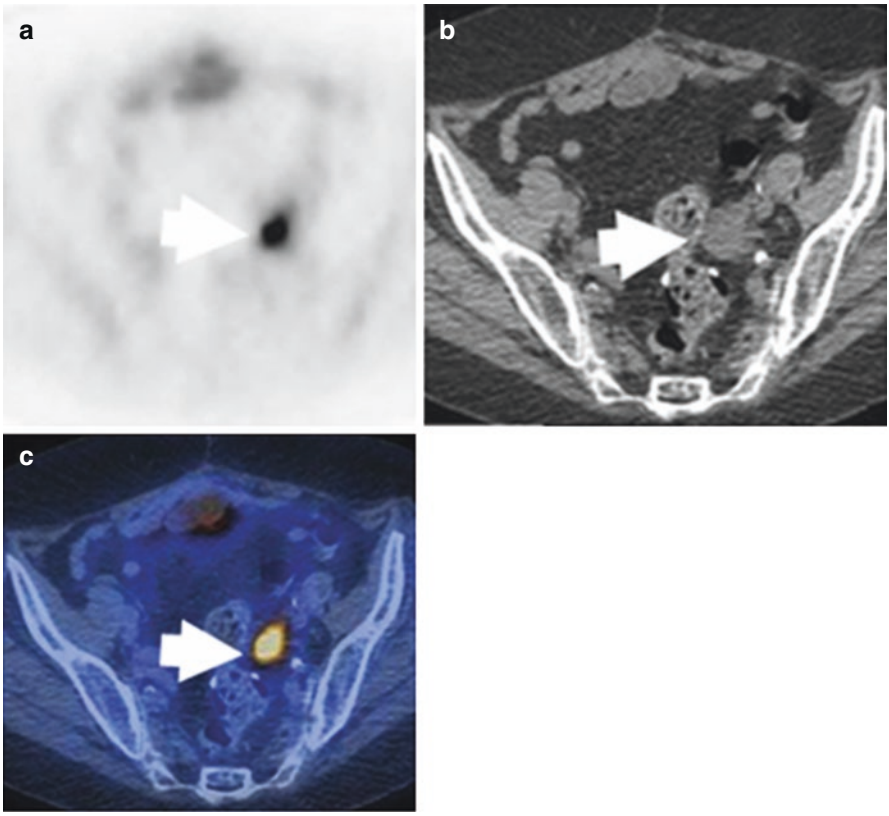

Fig. 6.7 Physiological tracer uptake in the left adnexa (arrow) [Adnexal and uterine activity is likely to represent physiological ovarian and uterine uptake in a premenopausal woman and is usually seen midcycle. A corpus luteum cyst can present as a 'ring' of peripheral uptake in the adnexa. It is important to check the patient's menstrual history. Increased adnexal or uterine uptake in a postmenopausal woman warrants further investigation]

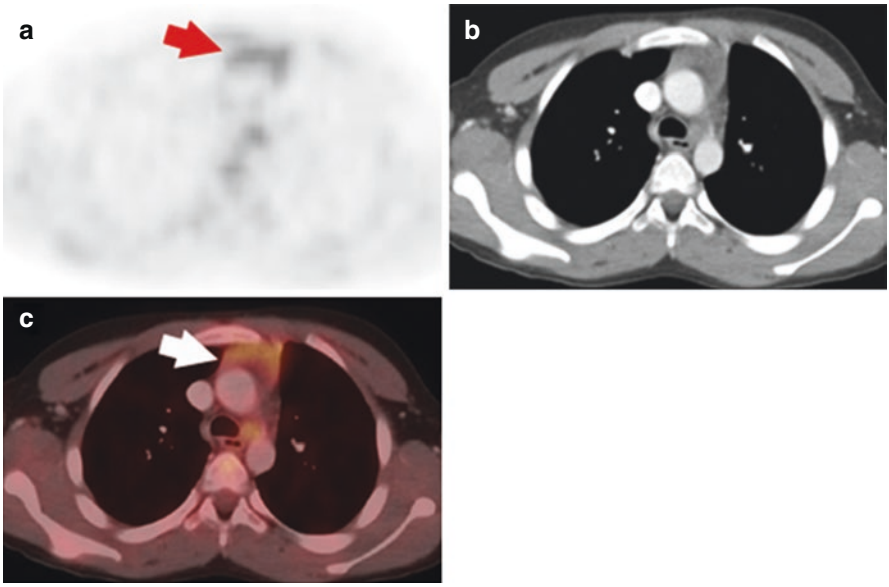

Fig. 6.8 Transaxial PET (**a**), CT (**b**) and fused (**c**) images demonstrate diffuse and homogeneous uptake (arrow in **a**) in the thymus following chemotherapy due to thymic rebound hyperplasia. [Thymic tissue is often reactivated post-chemotherapy and is normally seen in children and young adults]

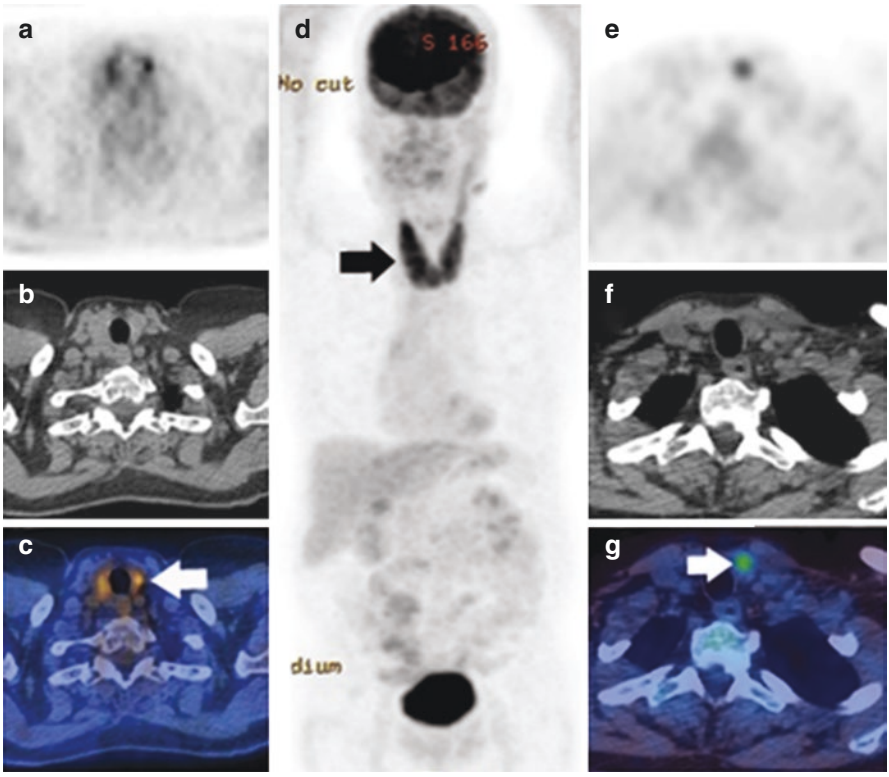

Fig. 6.9 ^{18}F-FDG PET/CT studies (**a**–**c**) transaxial PET, CT and fused images demonstrate diffuse homogenous tracer uptake in a normal size thyroid gland in a patient with known thyroiditis, (**d**) MIP image shows intense diffusely increased uptake (arrow) in enlarged thyroid gland in a patient with known Graves' disease, (**e**–**g**) transaxial PET, CT and fused images show focal uptake (arrow) in the left thyroid lobe. [Diffuse uptake is seen in patients with Graves' disease, subacute Thyroiditis or Hashimoto's thyroiditis and thyroid function tests should be recommended; focal uptake in the thyroid can be malignant in approximately 1/3rd of patients and should be further evaluated with ultrasound and FNA]

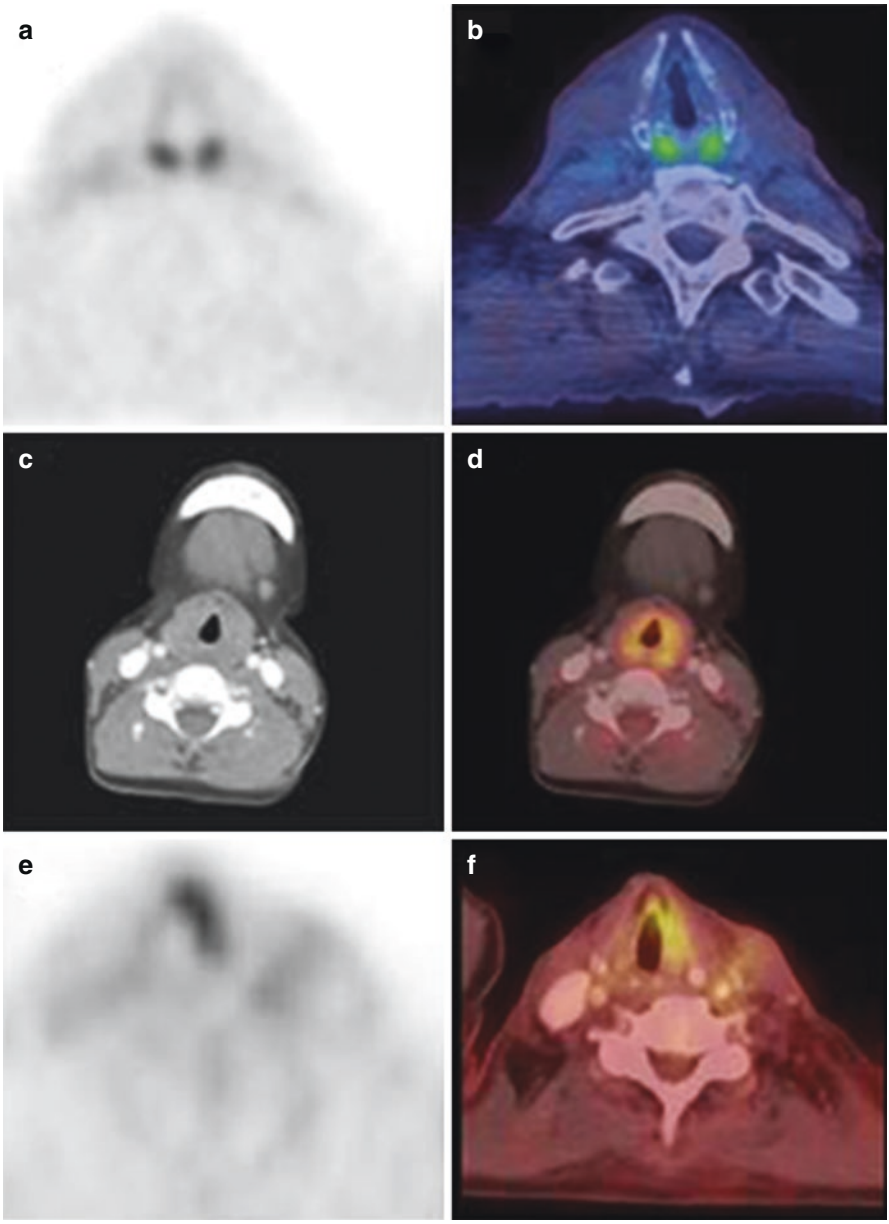

Fig. 6.10 (**a**, **b**) axial [18]F-FDG PET and fused PET/CT images show symmetrically increased tracer uptake in the arytenoid muscles. (**c**, **d**) axial CT and fused [18]F-FDG PET/CT images show symmetrically increased tracer uptake in the laryngeal muscles. [This should be minimised in patients with head and neck cancer by maintaining silence after tracer injection]. (**e**, **f**) Axial [18]F-FDG PET and fused PET/CT images show asymmetrical increased tracer uptake in the left vocal cord due to recurrent laryngeal nerve palsy on the right side. [When there is asymmetrical uptake in the vocal cords, it is the normal vocal cord that demonstrates increased uptake and the side with no increased uptake is the side with the nerve palsy]

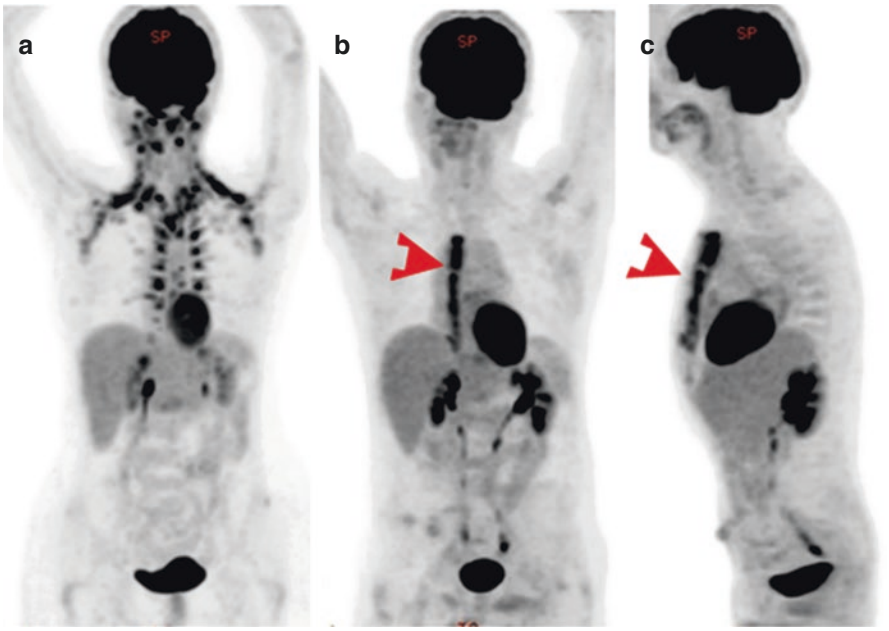

Fig. 6.11 Maximum intensity projection (MIP) ^{18}F-FDG PET images demonstrate (**a**) physiological brown fat uptake in the neck, supraclavicular fossae, mediastinum and suprarenal region, (**b**, **c**) intense tracer uptake in the sternum in patient with recent sternotomy (arrowheads)

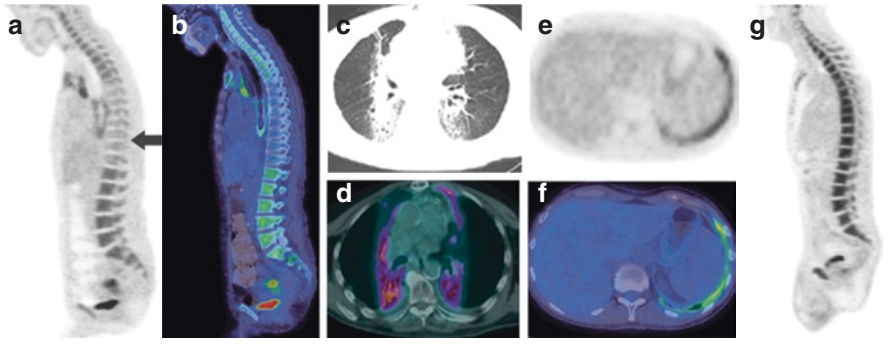

Fig. 6.12 ^{18}F-FDG PET/CT studies: (**a**, **b**) sagittal PET and fused PET/CT images show decreased tracer uptake in the thoracic vertebrae due to prior radiation therapy to this site [photopenia/decreased uptake in the bone is seen at the site of radiotherapy]; (**c**, **d**) transaxial CT and fused PET/CT images demonstrate increased uptake in para-mediastinal lung fibrosis after radiotherapy and should be read cautiously; (**e**, **f**) transaxial PET and fused PET/CT images demonstrate increased uptake in the left pleura with history of previous talc pleurodesis due to chronic granulomatous reaction [evaluation of mesothelioma is difficult following talc pleurodesis as the resulting increased pleural uptake can persist for several years]; (**g**) MIP image shows reactive diffuse tracer uptake in the bone marrow following chemotherapy in a lymphoma patient

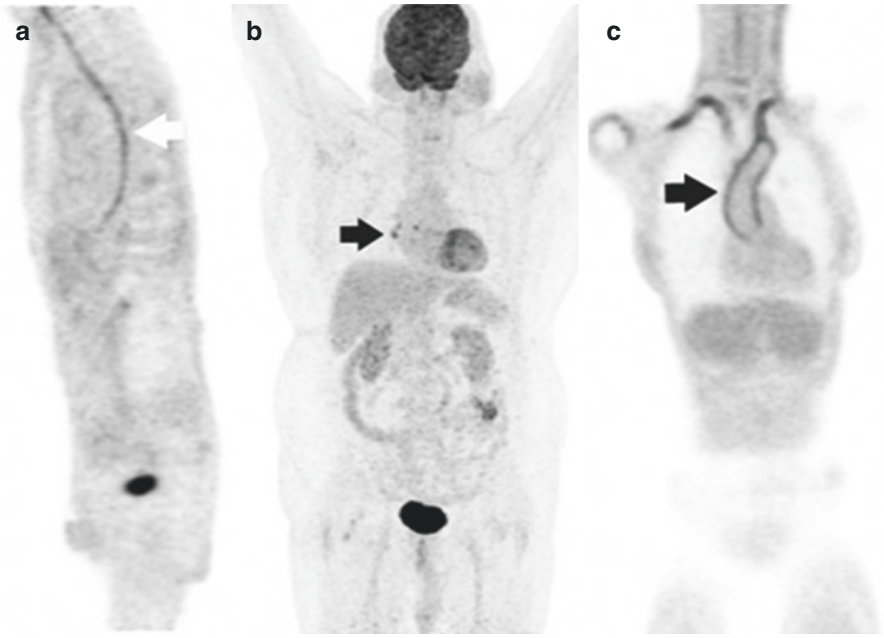

Fig. 6.13 (**a**) MIP ^{18}F-FDG PET image of a patient shows linear tracer uptake (arrow) in throughout the length of oesophagus with no gross morphological changes suggestive inflammatory activity (esophagitis), (**b**) MIP ^{18}F-FDG PET image of a follow-up patient of gall bladder carcinoma shows FDG uptake in the mediastinal lymph nodes (arrow) with no other site of significant hypermetabolism likely due to inflammation/infection, (**c**) Coronal PET image of a patient with large vessel vasculitis shows diffusely increased FDG uptake in the wall of the aorta and its main branches. [If a patient is on steroids, this can result in a false negative PET study in the evaluation of vasculitis and ideally steroid therapy needs to be stopped for at least 3 weeks before the PET scan]

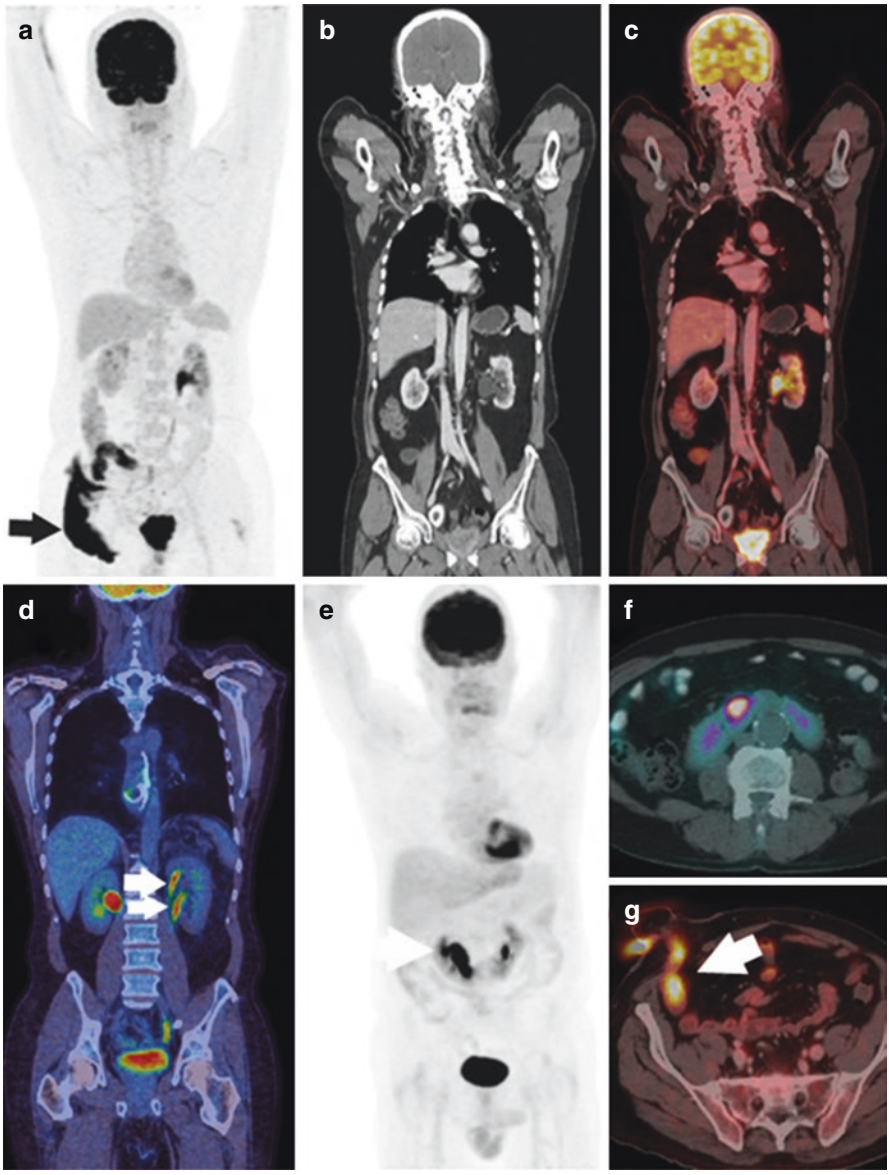

Fig. 6.14 MIP (**a**), coronal CT (**b**) and fused ^{18}F-FDG PET/CT (**c**) images of a patient with hydronephrosis of the left kidney show tracer retention in the dilated pelvi-calyceal system of the left kidney. (**a**, **g**) Intense physiological tracer uptake is also noted in the ileostomy loop (arrow). Coronal fused ^{18}F-FDG PET/CT image (**d**) of a patient duplex left kidney shows tracer uptake in two ureters (arrows), which may be mistaken as a lymph node on transaxial images. MIP (**e**) and transaxial fused ^{18}F-FDG PET/CT (**f**) images of a patient with horse shoe kidney show tracer activity within the fused kidneys in the midline of the abdomen

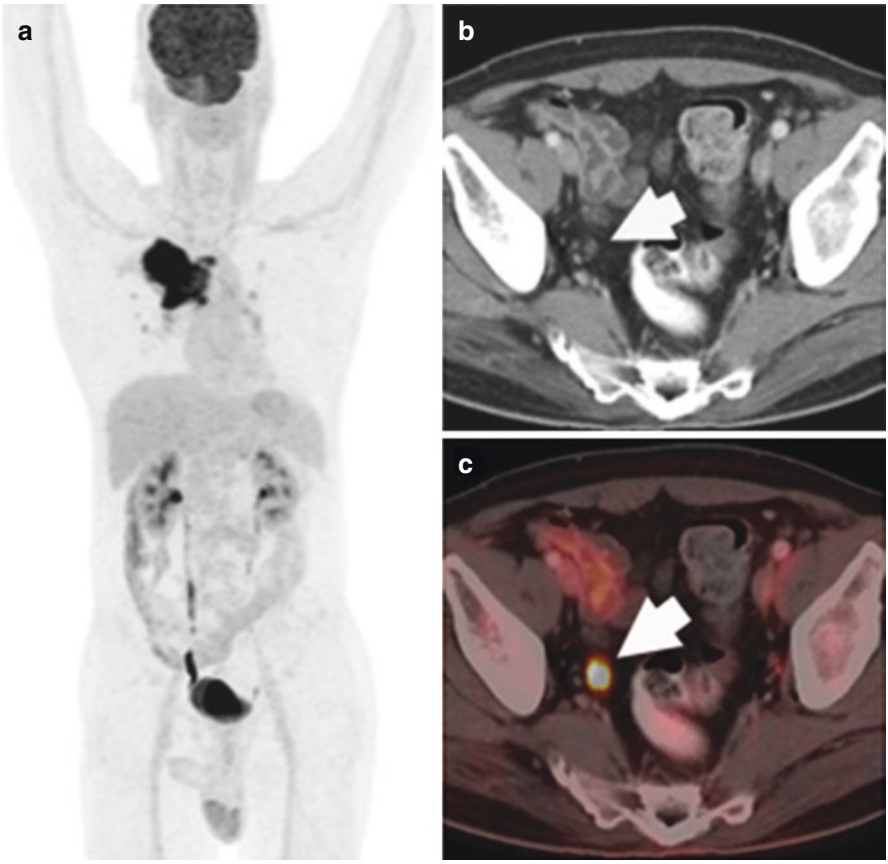

Fig. 6.15 Tracer uptake in the dilated ureter may mimic a lymph node (arrows in **b**, **c**). [Correlation of tracer activity on the MIP image (**a**) and following the ureter on transaxial images are helpful]

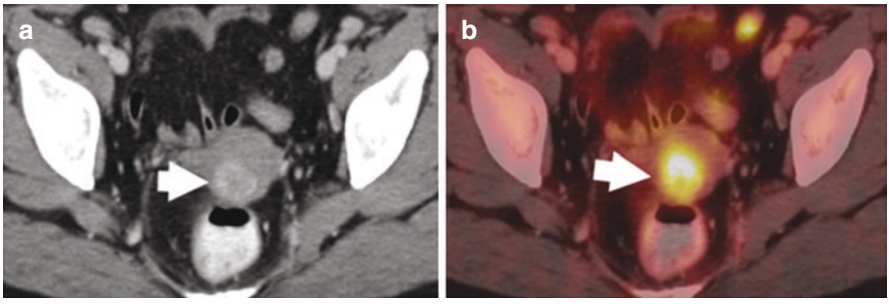

Fig. 6.16 Intense tracer uptake is seen in an enhancing soft tissue lesion in the uterine wall suggestive of fibroid. [Any increased uptake in the uterus in a postmenopausal woman should be investigated and an ultrasound advised in the first instance]

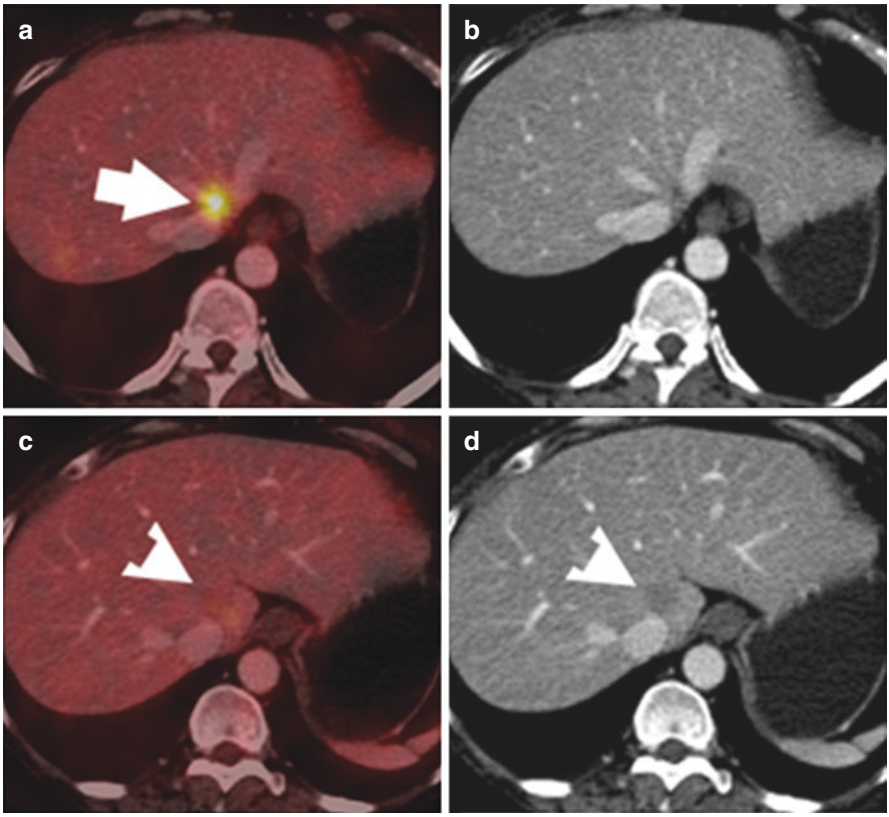

Fig. 6.17 Misregistration: Transaxial fused ^{18}F-FDG PET/CT and CT images show a hypodense hepatic lesion (arrow head in **d**) that has been misplaced to slightly higher-level during PET image acquisition (arrow in **a**) due to differences in breathing patterns between CT and PET image acquisitions. Note there is no lesion on CT image (**b**) corresponding to apparent site of tracer uptake on fused image (arrow in **a**) [In general, motion artefacts and reconstruction artefacts are usually self-evident in most cases]. Therefore, the hypodense lesion is falsely appearing as non-FDG avid (**c**)

Table 6.3 ^{18}F-FDG scans: false positive and false negative tracer uptake in head/neck region [5–9, 12, 13, 16]

False positive	False negative
Physiological uptake Brown adipose tissue (Fig. 6.11a) *Inflammatory processes* Post-surgical Post-radiotherapy Granulomatous disease Post-chemotherapy Thyroiditis (Fig. 6.9) Benign neoplasms Pleomorphic adenomas Thyroid adenomas (Fig. 6.9) Salivary gland tumours Artefacts Misalignment between PET and CT data (attenuation correction artefacts)	• Small size • Recent high-dose steroid therapy • Hyperglycaemia and hyperinsulinaemia • Low grade and well differentiated tumours • Misalignment between PET and CT data (attenuation correction artefacts)

Table 6.4 ^{18}F-FDG scans: false positive and false negative tracer uptake in thorax [5–9, 12, 13, 16]

False positive	False negative
Physiological uptake Brown adipose tissue (Fig. 6.11a) Thymus (children and young adults) Lactating breast and areolae (Fig. 6.2) Skeletal and smooth muscles (Fig. 6.5) Oesophagus *Inflammatory processes* Post-surgical (Fig. 6.11b, c) Post-radiotherapy (Fig. 6.12a–d) Granulomatous disease (Fig. 6.12e, f) Post-chemotherapy (Fig. 6.12g) Infection/inflammation (Fig. 6.13) Drainage tubes Oesophagitis (Fig. 6.13a) Vasculitis (Fig. 6.13c) Fungal infection Post-chemotherapy Thymic rebound hyperplasia (Fig. 6.8) Artefacts Misalignment between PET and CT data (attenuation correction artefacts)	• Small size • Recent high-dose steroid therapy • Hyperglycaemia and hyperinsulinaemia • Low grade and well differentiated tumours • Bronchioalveolar carcinomas • Lobular carcinomas of the breast

Table 6.5 ^{18}F-FDG scan: false positive and false negative tracer uptake in abdomen and pelvis [5–9, 12, 13, 16]

False positive	False negative
Physiological uptake	Small size
Brown adipose tissue	Recent high-dose steroid therapy
Skeletal and smooth muscles (Fig. 6.5)	Hyperglycaemia and hyperinsulinaemia
Stomach (Fig. 6.2e)	Low grade tumours
Bowel (diffuse)	Well differentiated carcinomas
Kidney and urinary bladder (Fig. 6.14)	Hepatocellular carcinoma
Ureters and urethra (Figs. 6.14 and 6.15)	Neuroendocrine tumours
Uterus during menses or corpus luteum cyst	Mucous secreting tumours
Ileostomy loop (Fig. 6.14)	Prostate carcinoma
Inflammatory processes	
Drainage tubes	
Post-surgical (Fig. 6.3)	
Post-radiotherapy	
Post-chemotherapy	
Inflammatory bowel disease	
Cholecystitis	
Pancreatitis	
Psoas abscess	
Benign neoplasms	
Adrenal adenoma	
Ovarian cystadenoma	
Uterine fibroid (Fig. 6.16)	
Artefacts	
Misalignment between PET and CT data (attenuation correction artefacts) (Fig. 6.17)	

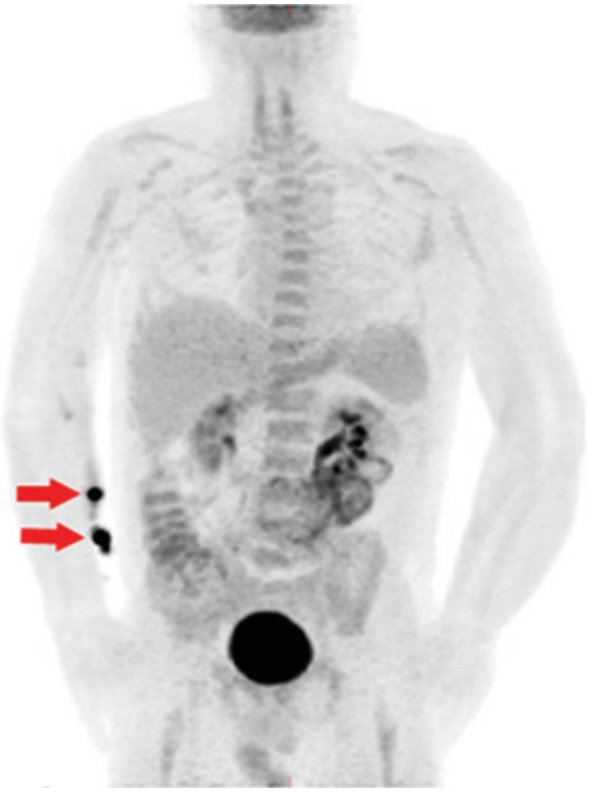

Fig. 6.18 MIP ^{18}F-FDG PET image shows tracer extravasation at the site of injection (arrows). [A local view of the extravasation site is often undertaken to establish what proportion of the administered activity remains at the extravasation site. The SUV measurements will also be affected]

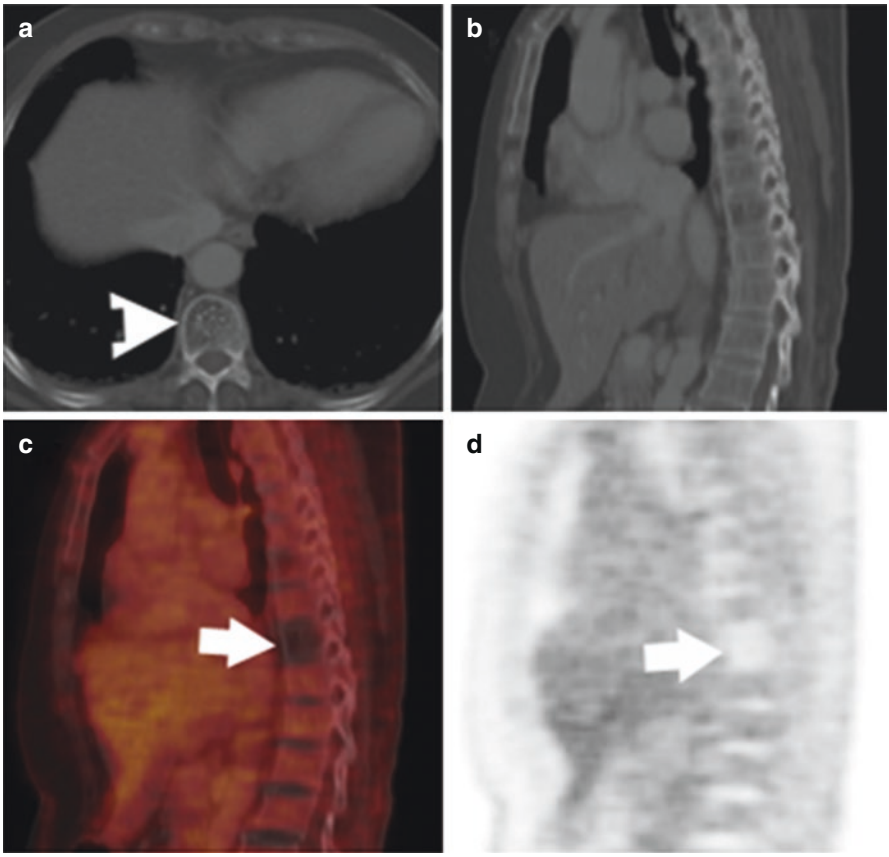

Fig. 6.19 Focal photopenia (arrows in **c**, **d**) is observed in a vertebral hemangioma showing 'polka-dot appearance' on CT image (**b**, arrow head in **a**). [Vertebral hemangiomata can be 'hot' or 'cold' on FDG PET imaging]

6.2 Conclusions

It is vital to know the normal variants and artefacts for accurate interpretation of ^{18}F-FDG PET/CT studies. Furthermore, recognising false positive and false negatives is equally important for correct reporting.

Key Points

- ^{18}F-FDG is transported into cells through glucose transporters and phosphorylated by enzyme hexokinase to ^{18}F-FDG-6-phosphate.
- ^{18}F-FDG is accumulated in malignant tissues more avidly than within the normal tissues.
- ^{18}F-FDG uptake is also known to occur in inflammation, infection and healing tissues.
- ^{18}F-FDG PET/CT scans often show variable degree of physiological tracer uptake which is noted in various organs.
- Recognition of physiological tracer distribution is essential in avoiding wrong image interpretation.
- ^{18}F-FDG PET study immediately after chemotherapy and radiotherapy may introduce false positive findings.
- Misregistration is noted due to differences in breathing patterns and patient movement between CT and PET image acquisition.
- False positives and false negatives can be countered in ^{18}F-FDG PET studies.
- Artefacts in PET/CT imaging may be due to (a) metallic objects, (b) respiration/patient movement and (c) oral or intravenous contrast agents.
- It is vital to recognise normal variants and artefacts to avoid misinterpretation.
- Recognising false positives and false negatives is important for accurate reporting.

Acknowledgements Dr. Nerriman, Dr. Riyamma and Dr. Halsey for contributing images for the chapter on PET/CT imaging: normal variants, pitfalls and artefacts.

References

1. Agrawal K, Mittal BR, Bansal D, et al. Role of F-18 FDG PET/CT in assessing bone marrow involvement in pediatric Hodgkin's lymphoma. Ann Nucl Med. 2013;27(2):146–51.
2. Mittal BR, Agrawal K. FDG-PET in tuberculosis. Curr Mol Imaging. 2014;3(3):211–5.
3. Cook GJR, Fogelman I, Maisey MN. Normal physiological and benign pathological variants of ^{18}F-FDG PET scanning: potential for error in interpretation. Semin Nucl Med. 1996;26:308–14.

4. Cook GJR, Maisey MN, Fogelman I. Normal variants, artefacts and interpretative pitfalls in PET imaging with ^{18}F-fluoro-2-deoxyglucose and carbon-11 methionine. Eur J Nucl Med. 1999;26:1363–78.
5. Cook GJ, Wegner EA, Fogelman I. Pitfalls and artifacts in 18FDG PET and PET/CT oncologic imaging. Semin Nucl Med. 2004;34:122–33.
6. Culverwell AD, Scarsbrook AF, Chowdhury FU. False-positive uptake on 2-[^{18}F]-fluoro-2-deoxy-D-glucose (FDG) positron-emission tomography/computed tomography (PET/CT) in oncological imaging. Clin Radiol. 2011;66:366–82.
7. Shreve PD, Anzai Y, Wahl RL. Pitfalls in oncologic diagnosis with FDG PET imaging: physiologic and benign variants. Radiographics. 1999;19:61–77.
8. Delbeke D, Coleman RE, Guiberteau MJ, et al. Procedure guideline for tumour imaging with ^{18}F-FDG PET/CT 1.0. J Nucl Med. 2006;47:885–95.
9. Boellaard R, O'Doherty MJ, Weber WA, et al. FDG PET and PET/CT: EANM procedure guidelines for tumour PET imaging: version 1.0. Eur J Nucl Med Mol Imaging. 2010;37:181–200.
10. Segall G, Delbeke D, Stabin MG, et al. SNM practice guideline for sodium 18F-fluoride PET/CT bone scans 1.0. J Nucl Med. 2010;51:1813–20.
11. Juweid ME, Cheson BD. Positron-emission tomography and assessment of cancer therapy. N Engl J Med. 2006;354:496–507.
12. Gorospe L, Raman S, Echeveste J, et al. Whole-body PET/CT: spectrum of physiological variants, artifacts and interpretative pitfalls in cancer patients. Nucl Med Commun. 2005;26:671–87.
13. Shammas A, Lim R, Charron M. Pediatric FDG PET/CT: physiologic uptake, normal variants, and benign conditions. Radiographics. 2009;29:1467–86.
14. Harisankar CN, Mittal BR, Agrawal KL, et al. Utility of high fat and low carbohydrate diet in suppressing myocardial FDG uptake. J Nucl Cardiol. 2011;18:926–36.
15. Agrawal K, Weaver J, Ngu R, et al. Clinical significance of patterns of incidental thyroid uptake at (^{18})F-FDG PET/CT. Clin Radiol. 2015;70(5):536–43.
16. Corrigan AJ, Schleyer PJ, Cook GJ. Pitfalls and artifacts in the use of PET/CT in oncology imaging. Semin Nucl Med. 2015;45(6):481–99.

7 ^{68}Ga-DOTA-Peptides PET/CT: Physiological Biodistribution, Variants and Pitfalls

Ashik Amlani, Keerthini Muthuswamy, Kanhaiyalal Agrawal, Shaunak Navalkissoor, and Gopinath Gnanasegaran

Contents

7.1 Introduction

Gallium-68 (^{68}Ga)-DOTA-peptides PET/CT is increasingly used in the diagnosis of tumours expressing high levels of somatostatin receptors (SSTRs) (Figs. 7.1, 7.2, and 7.3). In general, pathological SSTRs are found in high concentrations in, amongst others, neuroendocrine tumours (NETs), pheochromocytoma and paraganglioma [1] (Table 7.1). ^{68}Ga is the positron emitter and is labelled to a somatostatin

A. Amlani · K. Muthuswamy
Department of Radiology, Guy's and St Thomas' NHS Foundation Trust, London, UK

K. Agrawal
Department of Nuclear Medicine, All India Institute of Medical Sciences (AIIMS), Bhubaneswar, India

S. Navalkissoor (✉) · G. Gnanasegaran
Department of Nuclear Medicine, Royal Free NHS Foundation Trust, London, UK
e-mail: s.navalkissoor@nhs.net

K. Agrawal et al. (eds.), *PET/CT Imaging*, Clinicians' Guides to Radionuclide Hybrid Imaging, https://doi.org/10.1007/978-3-030-75476-1_7

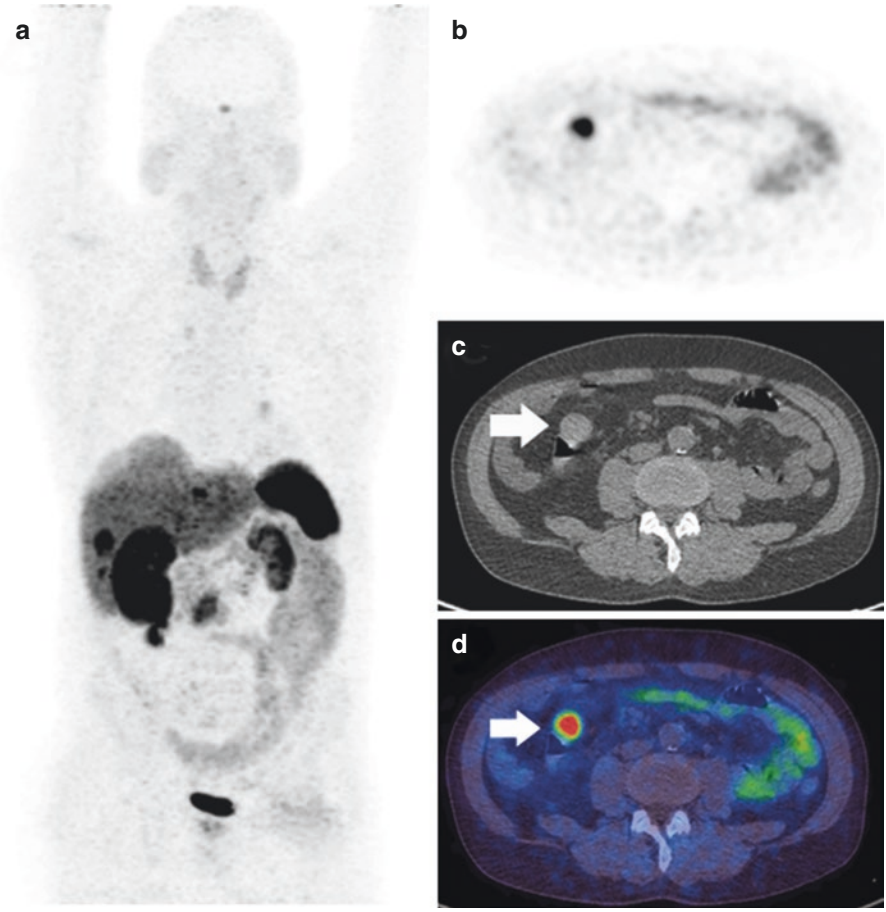

Fig. 7.1 ^{68}Ga-DOTA-TATE PET/CT study with maximum intensity projection (**a**), axial PET (**b**), axial CT (**c**) and axial fused PET/CT (**d**) images shows focal intense uptake of tracer (arrow) within small bowel in keeping with primary midgut neuroendocrine tumour. There is increased tracer uptake of tracer within several liver metastases and within a mesenteric mass on the maximum intensity projection image (**a**)

analogue via the compound 1,4,7,10-tetraazacyclododecane-1,4,7,10-tetraacetic acid (DOTA) [2]. Currently, three common analogues are available—[^{68}Ga-DOTA^{0}-Tyr^{3}] octreotide (*^{68}Ga-DOTA-TOC*), [^{68}Ga-DOTA^{0}-1NaI^{3}] octreotide (*^{68}Ga-DOTA-NOC*) and [^{68}Ga-DOTA^{0}-Tyr^{3}] octreotate (*^{68}Ga-DOTA-TATE*) [3]. Generally, they all bind to SSTR subtype 2 but have differing affinities for other subtypes [4]. In this chapter, we focus on the normal physiological biodistribution, variants and pitfalls of ^{68}Ga-DOTA-conjugated peptides PET/CT for NETs.

The most common clinical application of ^{68}Ga-DOTA-conjugated peptide PET/CT is in the imaging of NETs [5]. A meta-analysis by Geijer et al. suggested the pooled sensitivity and specificity of SSTR PET/CT in the diagnosis of NET were

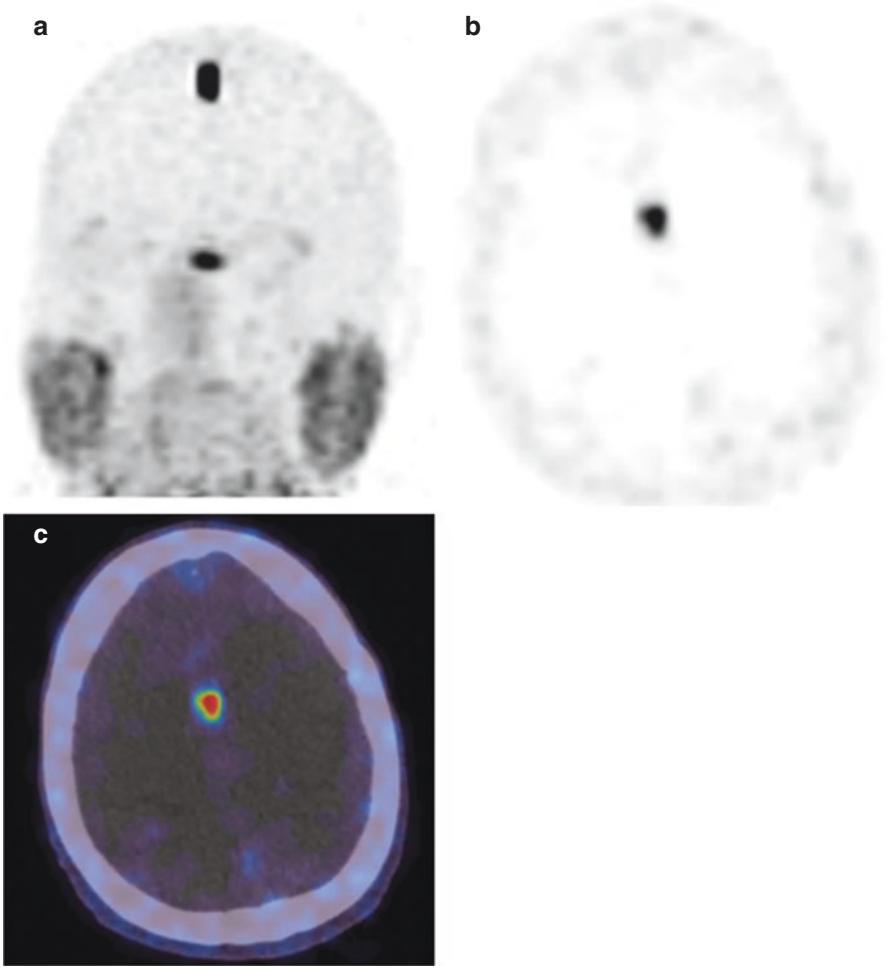

Fig. 7.2 ^{68}Ga-DOTA-TATE PET/CT study with maximum intensity projection (**a**), axial PET (**b**) and axial fused PET/CT (**c**) images shows intense focal ^{68}Ga-DOTA-TATE uptake is seen in a small midline dural based lesion suggestive of meningioma

93% and 96%, respectively [6]. ^{68}Ga-DOTA-conjugated peptide PET/CT is used as the gold standard for the detection of suspected NET primary in patients with biochemical signs and/or clinical symptoms of the disease (Table 7.2). It provides valuable additional information compared to other imaging modalities and early diagnosis may potentially direct these patients to either curative surgery or systemic therapy (if metastases are present) [7]. Similarly, in patients who have a histologically confirmed NET at sites of distant metastases, ^{68}Ga-DOTA-conjugated peptide PET/CT can be valuable in diagnosing an unknown primary when other imaging modalities are negative or equivocal [8].

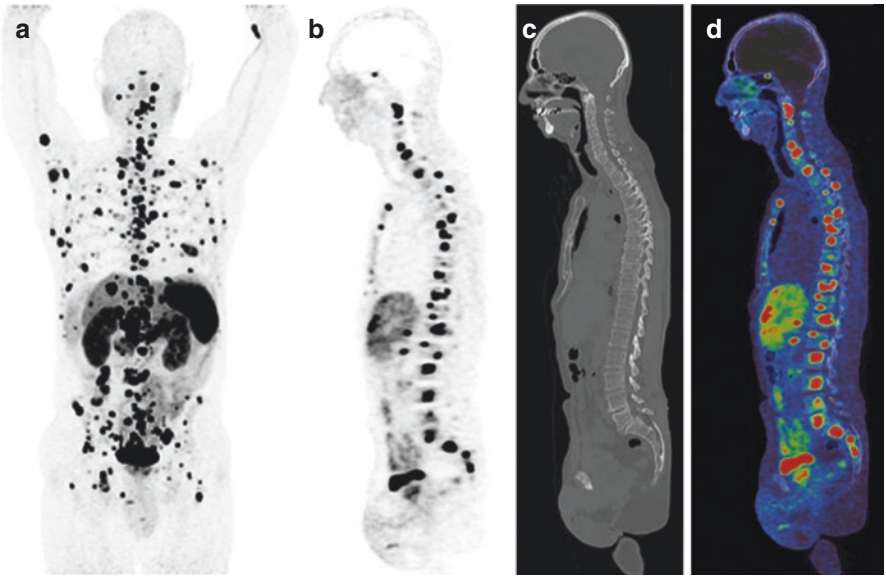

Fig. 7.3 ^{68}Ga-DOTATATE PET/CT maximum intensity projection image (**a**) shows widespread multiple skeletal, liver and nodal metastases. Sagittal PET (**b**), CT (**c**) and fused PET/CT (**d**) images show multiple skeletal metastases not seen on the CT scan (**c**)

Table 7.1 Tumours potentially visualised with ^{68}Ga-DOTA-peptide PET/CT [3, 14]

Tumours with high SST receptor expression	Tumours with low SST receptor expression
1. Sympathoadrenal system tumours – Pheochromocytoma – Paraganglioma – Neuroblastoma – Ganglioneuroma 2. Small-cell lung cancer 3. Gastroenteropancreatic tumours (Fig. 7.1) 4. Pituitary adenoma 5. Merkel cell carcinoma 6. Medullary thyroid carcinoma 7. Meningioma (Fig. 7.2)	1. Breast carcinoma 2. Melanoma 3. Renal cell carcinoma 4. Lymphomas 5. Prostate carcinoma 6. Differentiated thyroid carcinoma 7. Non-small-cell lung cancer 8. Sarcomas 9. Astrocytoma

It is important to note the complementary nature of ^{68}Ga-DOTA-peptide and ^{18}F-FDG PET/CT. In well differentiated NETs, SSTR expression is likely to be high and consequently offers good visualisation with ^{68}Ga-DOTA-conjugated peptide PET/CT. However, SSTR expression is much lower in poorly differentiated NETs and hence ^{68}Ga-DOTA-conjugated peptide uptake is likely to be low [9]. Conversely, these poorly differentiated tumours are likely to be highly metabolic and are often well visualised with ^{18}F-FDG PET/CT. This is clinically relevant because high grade NETs which are well visualised with ^{18}F-FDG PET/CT are strongly correlated with higher risk of progression [9]. Additionally, high SSTR expression (as

Table 7.2 Current and potential clinical applications of ^{68}Ga-DOTA-peptide PET/CT in neuroendocrine tumours (NETs) [1, 3]

Current clinical applications of ^{68}Ga-DOTA-peptide PET/CT in NETs	Potential clinical applications of ^{68}Ga-DOTA-peptide PET/CT in NETs
• Detection of unknown primary (Fig. 7.1)	Monitoring response to therapy
• Detection of potential metastatic disease prior to surgical intervention (Fig. 7.3)	
• Restaging of patients with known disease	
• Determine tumour SSTR status to identify suitability for somatostatin analogue therapy	
• Determine tumour suitability for peptide receptor radionuclide therapy (PRRT) (Fig. 7.4)	

demonstrated by ^{68}Ga-DOTA-conjugated peptide uptake) indicates potential suitability for somatostatin analogue as well as peptide receptor radionuclide therapy. Clinical utility outside of NETs is also well documented (Table 7.3).

7.2 Pathological Uptake

Pathological uptake can be graded using the Krenning scoring system. The scale uses the liver as a reference and is from 0 to 4 [10] (Table 7.4). Table 7.1 shows a list of tumours which show ^{68}Ga-DOTA-peptide uptake and can potentially be detected by^{68}Ga-DOTA-peptide PET/CT.

7.3 Physiological Distribution

The physiological distribution of ^{68}Ga-DOTA-peptide is mentioned in Table 7.5. Generally, the highest uptake is seen in the spleen followed by adrenal glands and kidney [2, 10]. In the spleen, salivary glands and endocrine organs, uptake is mediated by the presence of SSTRs. The high uptake in the kidneys is because ^{68}GA-DOTA-peptide is filtered at the glomerulus and only partially reabsorbed at the proximal convoluted tubule [1]. It is therefore seen throughout the urinary tract including kidneys and bladder. In general, no specific uptake is seen in brain tissue, bones, red marrow, lung and muscles [2].

7.4 Pitfalls and Artefacts

Apart from the sources of physiological uptake listed above, false positive and false negative uptake is common (Table 7.6).

Performing the scan whilst the patient is being treated with simultaneous somatostatin analogue therapy might interfere with visualisation (either reducing or enhancing detectability) as the analogue is reported to compete with the tracer for bioavailability [1, 3]. It is therefore recommended that somatostatin analogue

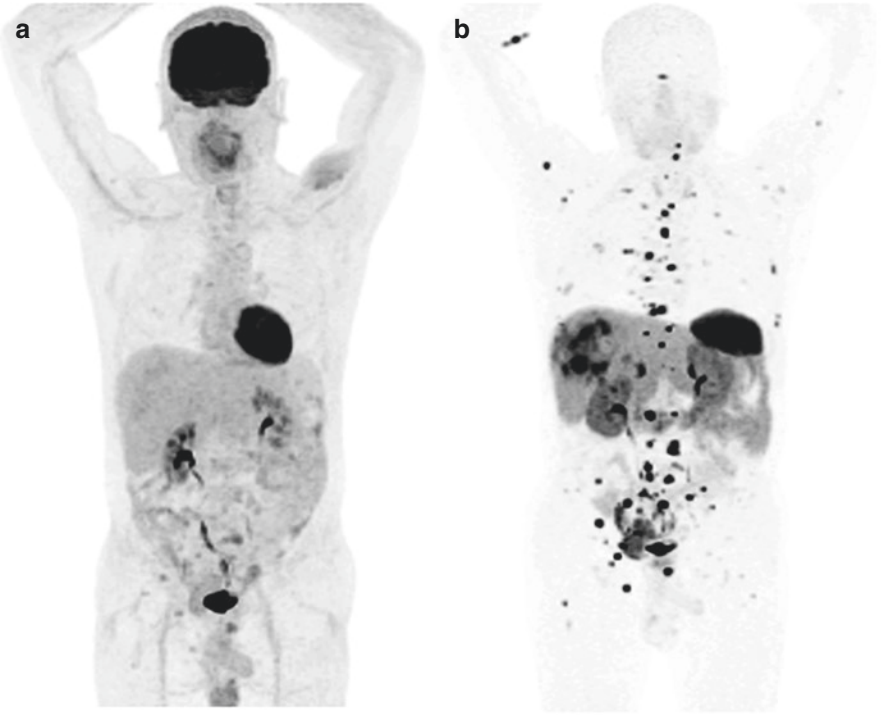

Fig. 7.4 Maximum intensity projection ^{18}F-FDG PET image (**a**) shows only low grade tracer uptake in the known skeletal metastases in the pelvic bones. Maximum intensity projection ^{68}Ga-DOTATATE PET image (**b**) shows widespread multiple skeletal, liver and nodal metastases. There is no significant FDG avid discordant disease

Table 7.3 Current and potential clinical applications of ^{68}Ga-DOTA-peptide PET/CT beyond neuroendocrine tumours (NETs) [1, 3]

Current clinical applications	Potential clinical applications
• Diagnosis of pheochromocytoma	• Medullary thyroid cancer
• Diagnosis of paraganglioma	• Merkel cell carcinoma
• Diagnosis of neuroblastoma	• Small cell carcinoma
	• Esthesio-neuroblastoma
	• Iodine negative thyroid cancer

therapy is temporarily withheld prior to PET/CT [1]. The time interval suggested is one day for short-acting analogues and 3–4 weeks for long-acting analogues [3]. However, this is still controversial for diagnostic imaging.

The well differentiated NETs usually express high SSTRs and show good tracer uptake on SSTR PET/CT and low or no uptake on FDG PET/CT (Figs. 7.4, 7.5, 7.6, 7.7, 7.8, 7.9, 7.10, 7.11, 7.12, 7.13, 7.14, 7.15, 7.16, 7.17, 7.18, 7.19, and 7.20). Conversely, the poorly differentiated NETs might express few SSTRs and might not be visualised on SSTR PET/CT despite their presence. This is a

Table 7.4 Krenning scoring system for grading of pathological uptake [10]

Krenning score	Intensity of uptake
0	No uptake
1	Uptake greater than background and less than liver
2	Uptake equal to that of liver
3	Uptake greater than that of liver and less than kidneys or spleen
4	Uptake in tumour equal to or greater than that of spleen or kidneys

Table 7.5 Tissues demonstrating physiological ^{68}Ga-DOTA-peptide uptake [1, 2, 11, 15]

High intensity uptake	Moderate intensity uptake	Variable intensity uptake
• Spleen (Figs. 7.5 and 7.6)	• Liver (Figs. 7.5 and 7.6)	• Large bowel (Fig. 7.5)
• Adrenal glands (Fig. 7.6)	• Parotid glands (Figs. 7.5 and 7.8)	• Small bowel (Fig. 7.5)
		• Choroid plexus (Fig. 7.6)
• Urinary tract (including kidneys) (Figs. 7.5 and 7.6)	• Other salivary glands (Fig. 7.1)	• Stomach (Fig. 7.6)
• Pituitary gland (Figs. 7.5 and 7.6)	• Thyroid gland (Figs. 7.5 and 7.9)	• Pancreas (heterogeneous)

Fig. 7.5 ^{68}Ga-DOTA-TATE PET maximum Intensity projection (MIP) image showing physiological tracer distribution

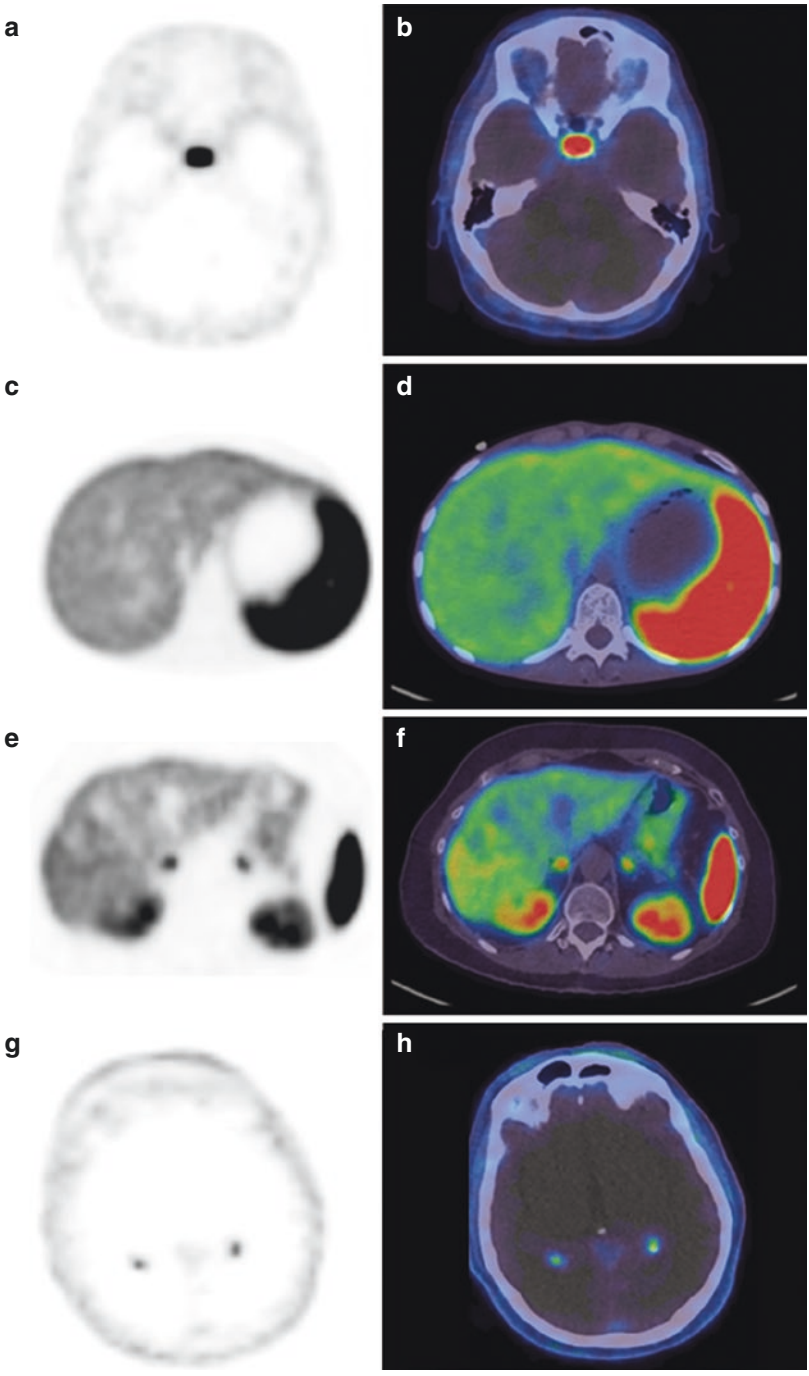

Fig. 7.6 ^{68}Ga-DOTA-TATE PET/CT images showing normal tracer distribution in the pituitary gland (**a**, **b**), liver and spleen (**c**, **d**), stomach, adrenal glands and kidneys (**e**, **f**), calcified choroid plexus (**g**, **h**)

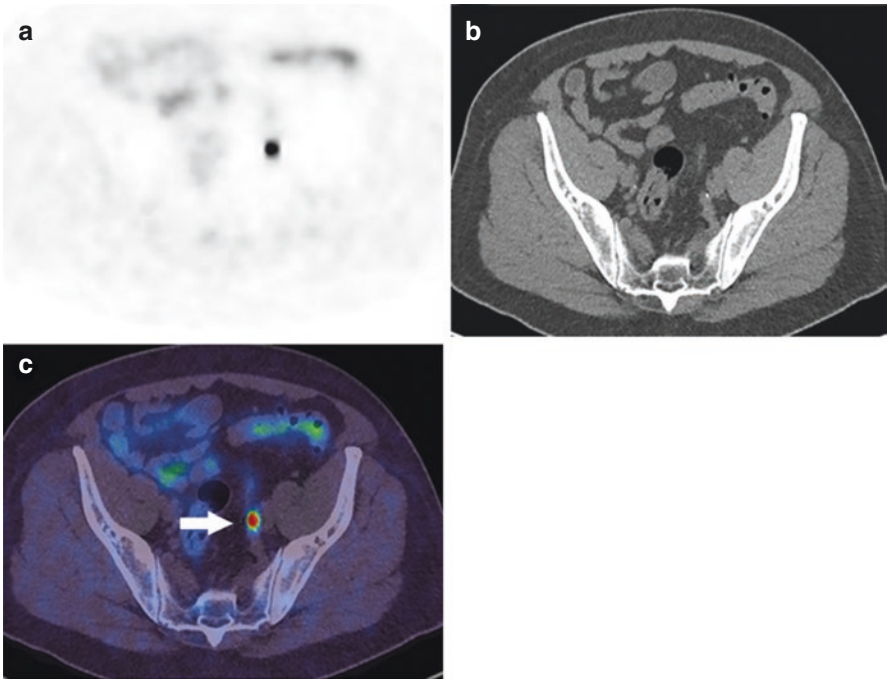

Fig. 7.7 ^{68}Ga-DOTA-TATE PET (**a**), CT (**b**) and fused PET/CT (**c**) images showing focal tracer uptake in the left ureter due to urinary tracer activity, which might be confusing to be considered as pathological. However, looking at MIP image, tracking the ureter and delayed imaging helps in avoiding the false interpretation

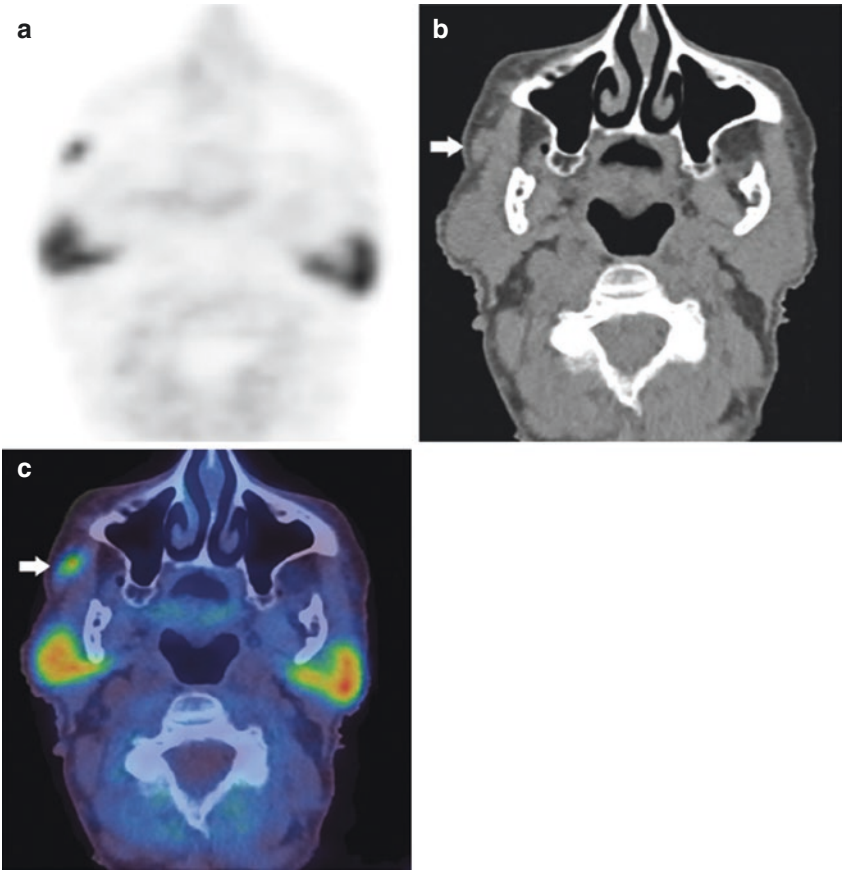

Fig. 7.8 Physiological tracer uptake in the parotid glands. Abnormal tracer uptake anterior to the right parotid is likely due to accessory parotid showing physiological tracer uptake (arrow). (**a**) PET, (**b**) CT, (**c**) fused PET/CT

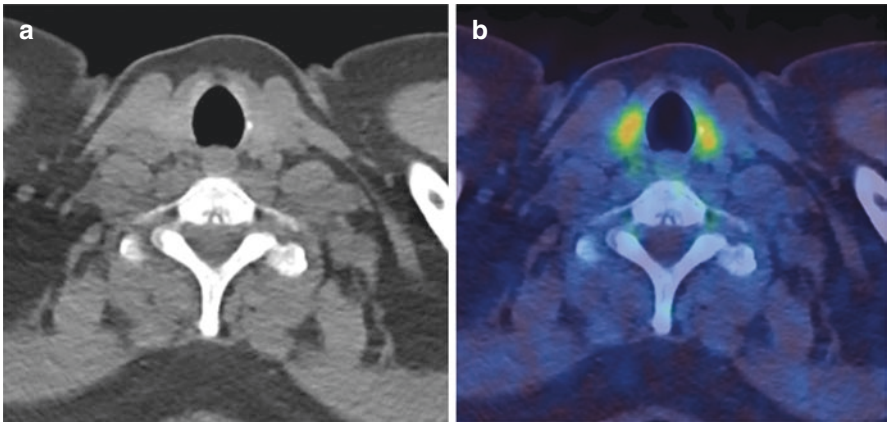

Fig. 7.9 Diffuse homogeneous physiological uptake in the thyroid gland. (**a**) CT (**b**) fused PET/CT

Table 7.6 Pitfalls in interpretation [1, 14, 16]

False positive uptake	Comments
• Physiological uptake in the pancreatic uncinate process (curvilinear morphology or ill-defined edges-best appreciated on coronal grey-scale images) (Fig. 7.10)	• Corresponding contrast enhanced CT findings and MRI imaging correlation helpful if the lesion is well-defined and focal
• Physiological uptake in the splenunculi and Intrapancreatic splenunculus (Fig. 7.11)	• Usually well-defined on CT and show high grade uptake. However, may be confused with a peritoneal deposit if placed other than splenic hilum • Imaging with 99mTc-Sulphur colloid or radiolabelled denatured cell is often useful in differentiating splenunculi from metastasis
• Stellate ganglia (Fig. 7.12)	• Potential pitfall and might be misinterpreted as lymph node uptake. Uptake is usually low grade but could be intense. More common on left side but again could be bilaterally present
• Infective/inflammatory process, e.g. reactive nodes (Fig. 7.13), sarcoidosis (Fig. 7.14), other granulomatous disease, prostatitis (Fig. 7.15), bacterial infection (Fig. 7.16), post-surgical inflammation, inflammatory changes in lung (Fig. 7.17)	• Show variable but usually low grade uptake as white blood cells and macrophages express SSTR 2
• Bone fracture site	• Low grade uptake due to inflammation. Particular attention should be paid while interpreting scan for tumour induced osteomalacia
• Inflamed joints in active rheumatoid arthritis	• Due to SSTR expression preferentially in the proliferating synovial vessels
• Degenerative bone disease (Fig. 7.18)	• As osteoblasts express SSTR, there may be uptake in osteophytes and CT findings are useful to avoid false interpretation
• Fibrous dysplasia, bone haemangioma (Fig. 7.19)	• The uptake is usually low grade and can be distinguished from metastatic disease by CT characteristics

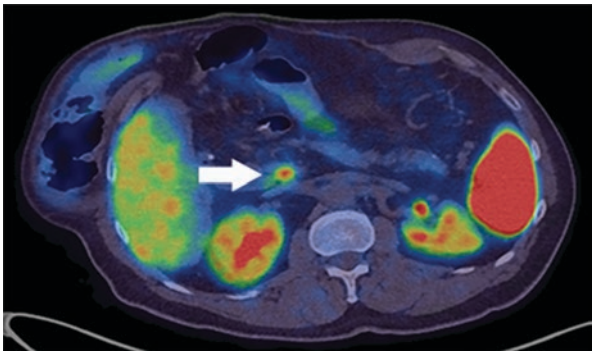

Fig. 7.10 Physiological focal uptake of tracer within the uncinate process of pancreas (arrow)

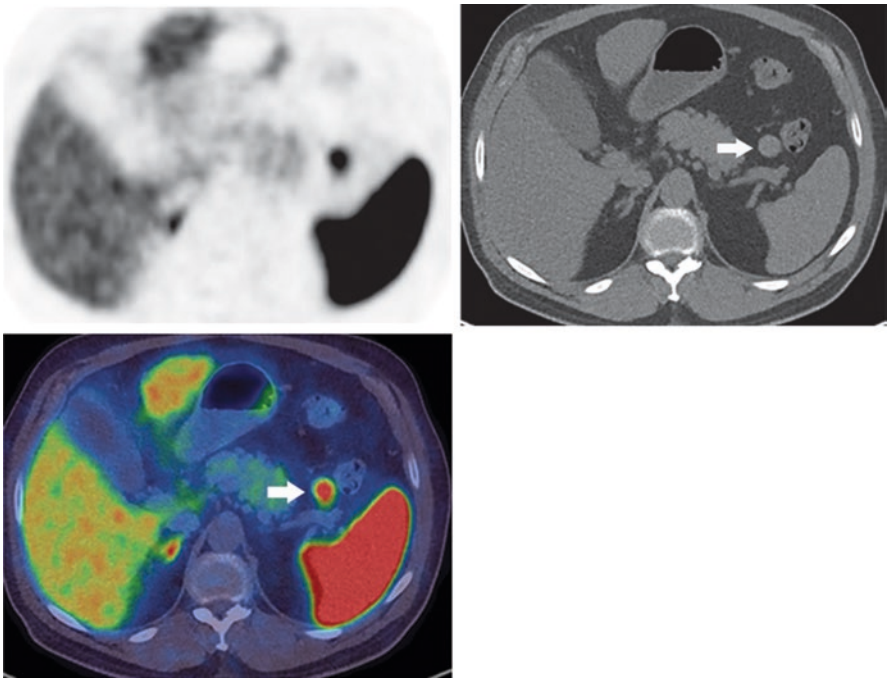

Fig. 7.11 Physiological focal uptake of tracer in a splenunculus (arrow)

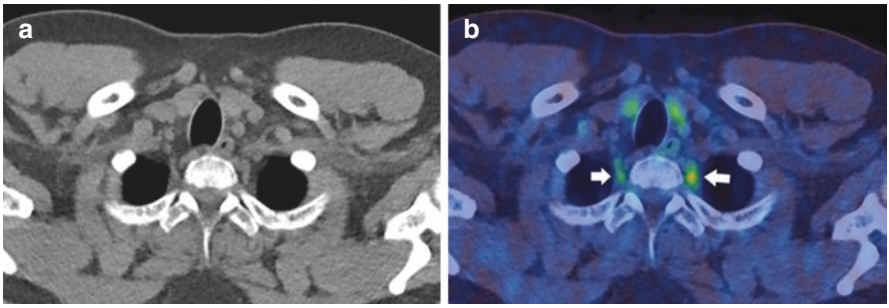

Fig. 7.12 Low grade tracer uptake in the stellate ganglia bilaterally (arrows). (**a**) CT (**b**) fused PET/CT

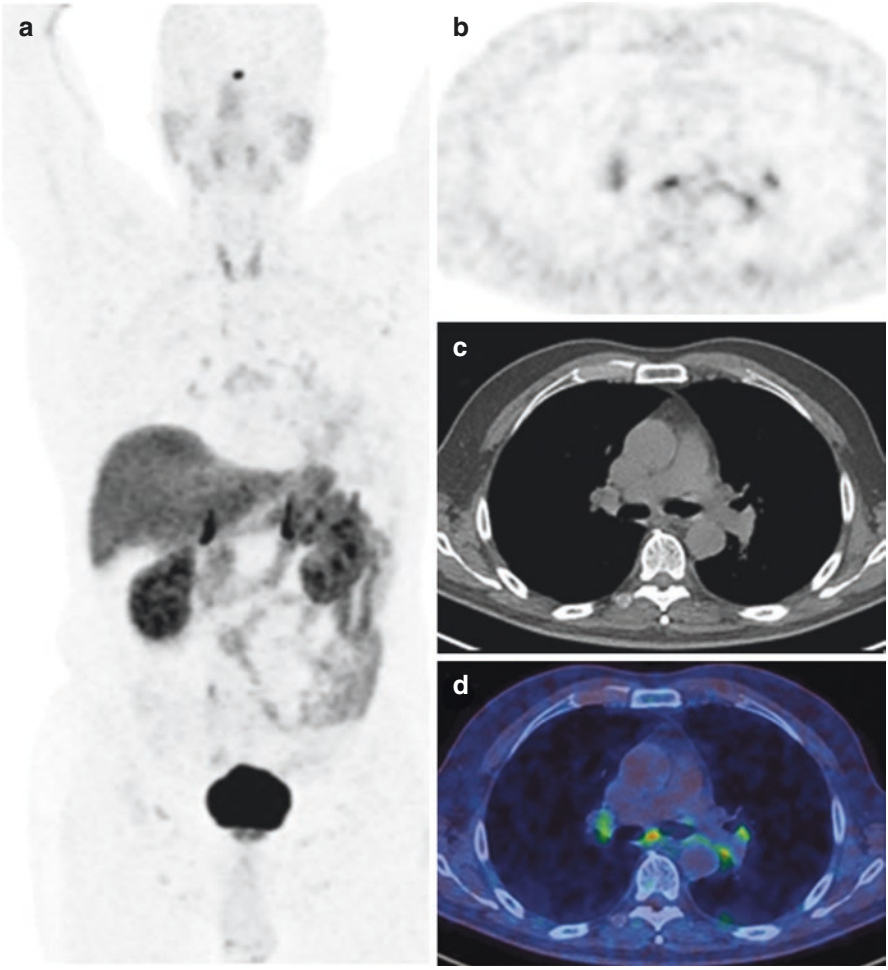

Fig. 7.13 ^{68}Ga-DOTA-TATE PET/CT study with maximum intensity projection (**a**), axial PET (**b**), axial CT (**c**) and axial fused PET/CT (**d**) images show tracer uptake in the subcarinal and hilar lymph nodes compatible with reactive changes

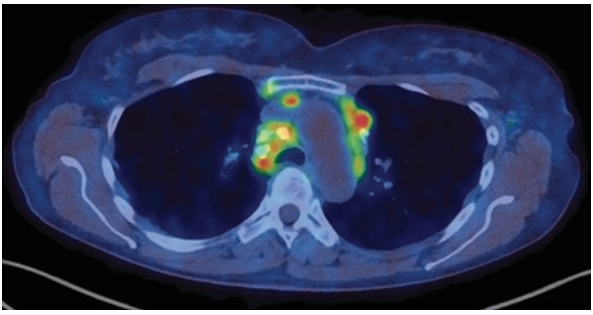

Fig. 7.14 ^{68}Ga-DOTA-TATE PET shows increased tracer uptake in the mediastinal nodes with calcification. The histopathology from lymph node was suggestive of non-caseating granulomas

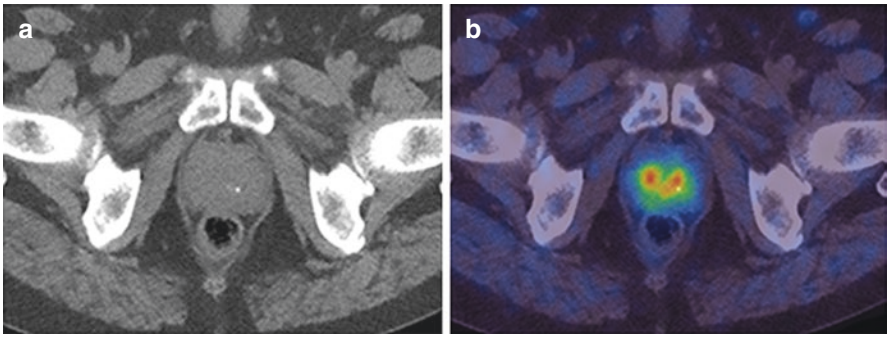

Fig. 7.15 Abnormal ^{68}Ga-DOTA-TATE uptake in the prostate gland with foci of calcification in a patient with prostatitis

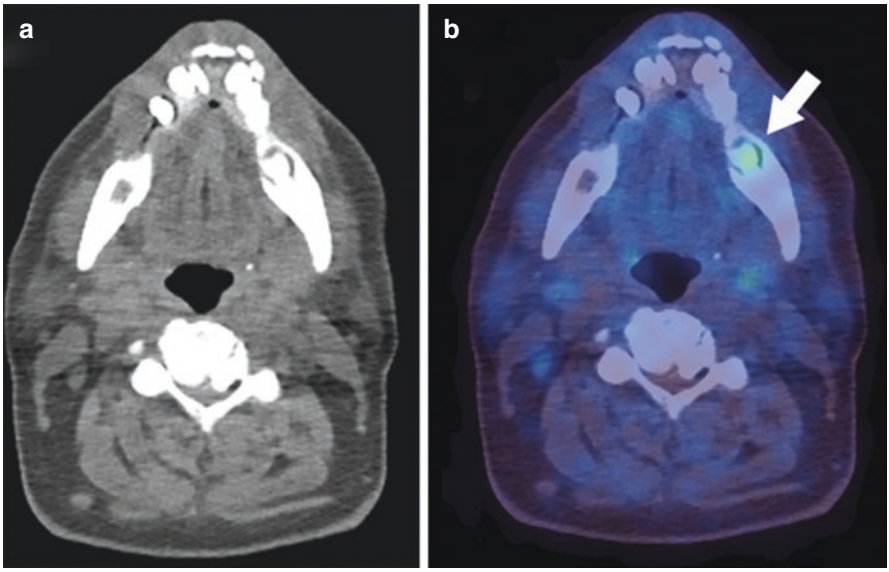

Fig. 7.16 Low grade uptake in an infected tooth (arrow)

potential false negative but concurrent ^{18}F-FDG PET/CT imaging may help to reveal these poorly differentiated types. Similarly, it is essential to recognise that different NETs may express different SSTR subtypes (although subtype 2 is the most common) [11]. All three common^{68}Ga-DOTA-peptide analogues bind to subtype 2; however, other subtype binding is variable [4]. This may influence uptake of ^{68}Ga-DOTA-peptide and hence impair visualisation of a tumour with atypical SSRT subtype expression [3].

The pancreas is a common site for pitfall [2]. It has been reported that prominent focal uptake in the uncinate process is seen in around 30% of patients [12]. However, this focal uptake can often be physiological and should be correlated with other

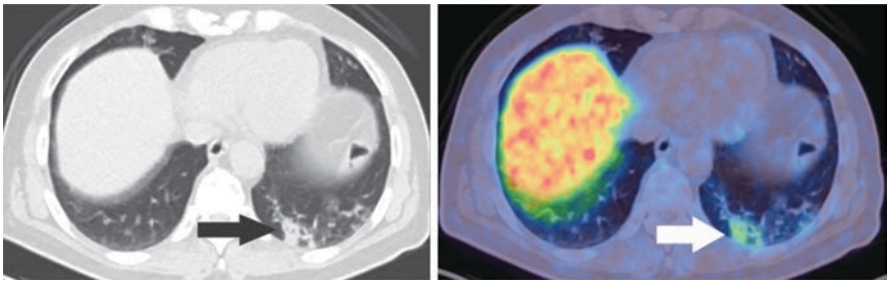

Fig. 7.17 Low grade patchy ^{68}Ga-DOTA-TATE uptake is seen in the inflammatory changes in the left lung (arrow)

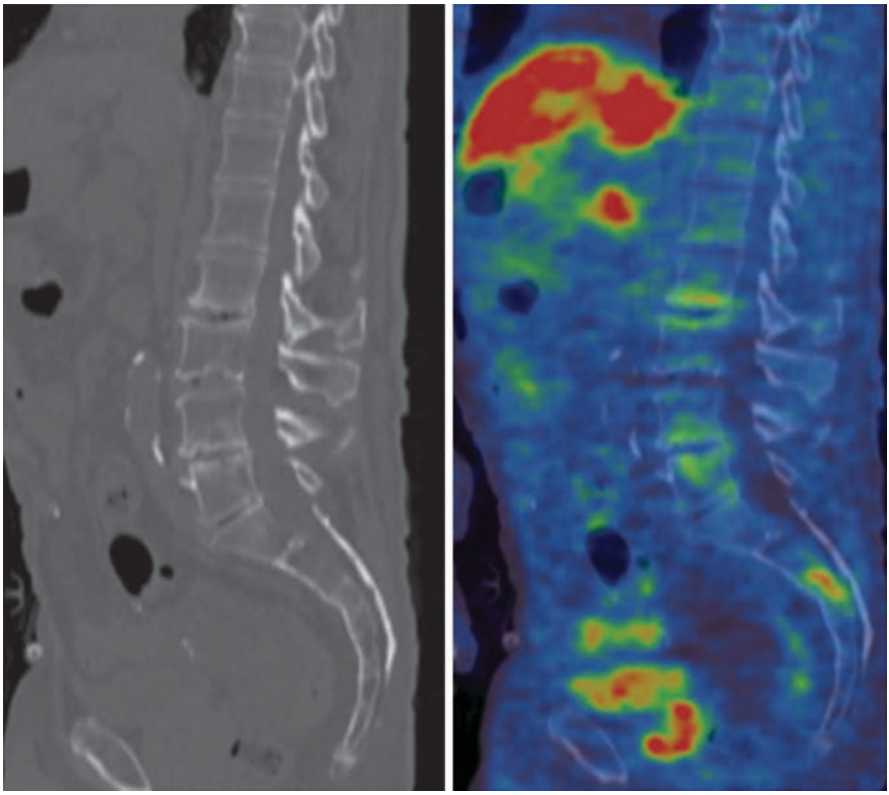

Fig. 7.18 ^{68}Ga-DOTA-TATE PET/CT study: low grade linear tracer uptake is seen in end plate degenerative changes in the lumbar spine

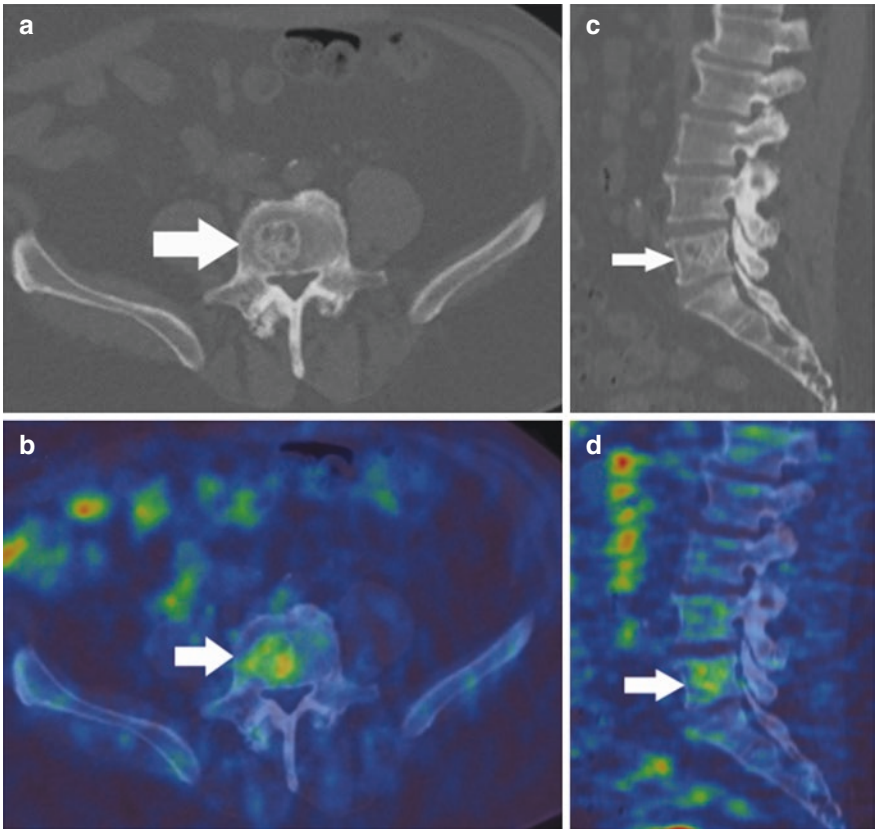

Fig. 7.19 ^{68}Ga-DOTA-TATE PET/CT study: Low grade patchy tracer uptake is seen in a haemangioma in L5 vertebral body (arrows). (**a**) CT axial (**b**) fused PET/CT axial (**c**) CT sagittal (**d**) fused PET/CT sagittal

imaging where appropriate in order to avoid erroneous reporting of pancreatic tumours [13].

As mentioned, ^{68}Ga-DOTA-peptide is filtered at the glomerulus, hence will be excreted in the urine. Urine contamination can cause false positive uptake [3].

Finally, it is important to remember that uptake could be due to a high density of SSTRs for another reason. These include osteoblastic activity, inflammation/activated lymphocytes or other tumours [1].

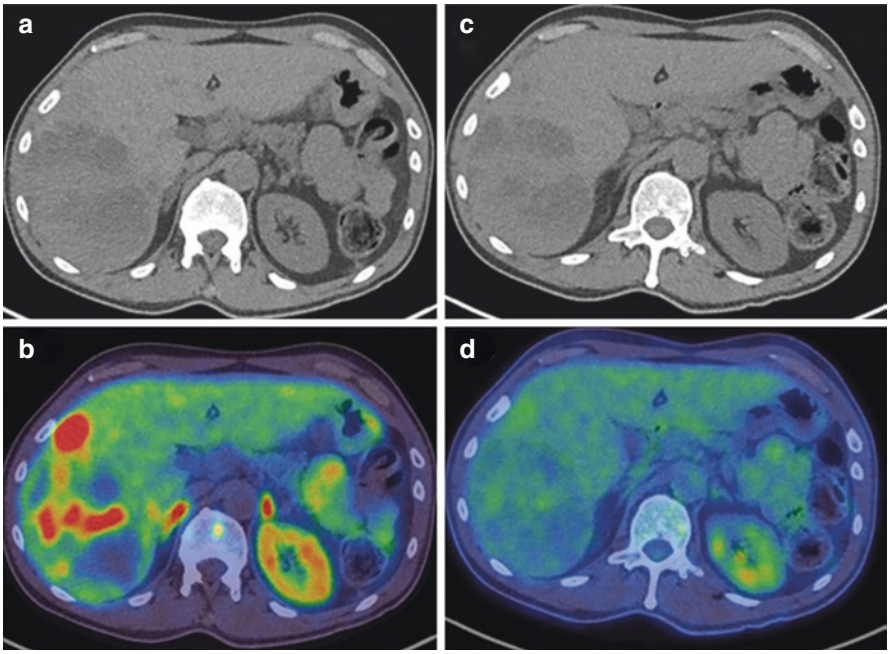

Fig. 7.20 Patient with midgut neuroendocrine tumour: Axial CT (**a**) and fused PET/CT (**b**) ^{68}Ga DOTATATE PET/CT images show increased heterogenous tracer uptake within the liver metastases. Axial CT (**c**) and fused PET/CT (**d**) ^{18}F-FDG PET/CT images show very minimal tracer uptake in the liver metastases. There is no FDG avid discordant disease

7.5 Conclusion

^{68}Ga-DOTA-peptide is a valuable PET tracer and, amongst others, offers particular utility in neuroendocrine tumours. Physiological uptake in numerous tissues as well as frequent pitfalls and sources of error must be considered when interpreting images.

Key Points

- Gallium-68 (^{68}Ga)-DOTA-peptides PET/CT is increasingly used in the diagnosis of tumours expressing high levels of somatostatin receptors (SSTRs).
- ^{68}Ga-DOTA-conjugated peptide PET/CT is used as the gold standard for the detection of suspected NET primary in patients with biochemical signs and/or clinical symptoms of the disease.
- In well differentiated NETs, SSTR expression is likely to be high and consequently offers good visualisation with ^{68}Ga-DOTA-conjugated peptide PET/CT.
- SSTR expression is much lower in poorly differentiated NETs and hence ^{68}Ga-DOTA-conjugated peptide uptake is likely to be low.

References

1. Hofman MS, Lau WF, Hicks RJ. Somatostatin receptor imaging with 68Ga DOTATATE PET/CT: clinical utility, normal patterns, pearls, and pitfalls in interpretation. Radiographics. 2015;35(2):500–16.
2. Kuyumcu S, Ozkan ZG, Sanli Y, Yilmaz E, Mudun A, Adalet I, et al. Physiological and tumoral uptake of (68)Ga-DOTATATE: standardized uptake values and challenges in interpretation. Ann Nucl Med. 2013;27(6):538–45.
3. Virgolini I, Ambrosini V, Bomanji JB, Baum RP, Fanti S, Gabriel M, et al. Procedure guidelines for PET/CT tumour imaging with 68Ga-DOTA-conjugated peptides: 68Ga-DOTA-TOC, 68Ga-DOTA-NOC, 68Ga-DOTA-TATE. Eur J Nucl Med Mol Imaging. 2010;37(10):2004–10.
4. Antunes P, Ginj M, Zhang H, Waser B, Baum RP, Reubi JC, et al. Are radiogallium-labelled DOTA-conjugated somatostatin analogues superior to those labelled with other radiometals? Eur J Nucl Med Mol Imaging. 2007;34(7):982–93.
5. Klimstra DS, Modlin IR, Coppola D, Lloyd RV, Suster S. The pathologic classification of neuroendocrine tumors: a review of nomenclature, grading, and staging systems. Pancreas. 2010;39(6):707–12.
6. Geijer H, Breimer LH. Somatostatin receptor PET/CT in neuroendocrine tumours: update on systematic review and meta-analysis. Eur J Nucl Med Mol Imaging. 2013;40(11):1770–80.
7. Hofman MS, Kong G, Neels OC, Eu P, Hong E, Hicks RJ. High management impact of Ga-68 DOTATATE (GaTate) PET/CT for imaging neuroendocrine and other somatostatin expressing tumours. J Med Imaging Radiat Oncol. 2012;56(1):40–7.
8. Prasad V, Ambrosini V, Hommann M, Hoersch D, Fanti S, Baum RP. Detection of unknown primary neuroendocrine tumours (CUP-NET) using (68)Ga-DOTA-NOC receptor PET/CT. Eur J Nucl Med Mol Imaging. 2010;37(1):67–77.
9. Nilica B, Waitz D, Stevanovic V, Uprimny C, Kendler D, Buxbaum S, et al. Direct comparison of (68)Ga-DOTA-TOC and (18)F-FDG PET/CT in the follow-up of patients with neuroendocrine tumour treated with the first full peptide receptor radionuclide therapy cycle. Eur J Nucl Med Mol Imaging. 2016;43:1585–92.
10. Kunikowska J, Krolicki L, Pawlak D, Zerizer I, Mikolajczak R. Semiquantitative analysis and characterization of physiological biodistribution of (68)Ga-DOTA-TATE PET/CT. Clin Nucl Med. 2012;37(11):1052–7.
11. Mizutani G, Nakanishi Y, Watanabe N, Honma T, Obana Y, Seki T, et al. Expression of somatostatin receptor (SSTR) subtypes (SSTR-1, 2A, 3, 4 and 5) in neuroendocrine tumors using real-time RT-PCR method and immunohistochemistry. Acta Histochem Cytochem. 2012;45(3):167–76.
12. Castellucci P, PouUcha J, Fuccio C, Rubello D, Ambrosini V, Montini GC, et al. Incidence of increased 68Ga-DOTANOC uptake in the pancreatic head in a large series of extrapancreatic NET patients studied with sequential PET/CT. J Nucl Med. 2011;52(6):886–90.
13. Krausz Y, Rubinstein R, Appelbaum L, Mishani E, Orevi M, Fraenkel M, et al. Ga-68 DOTA-NOC uptake in the pancreas: pathological and physiological patterns. Clin Nucl Med. 2012;37(1):57–62.
14. Agrawal K, Esmail AA, Gnanasegaran G, Navalkissoor S, Mittal BR, Fogelman I. Pitfalls and limitations of radionuclide imaging in endocrinology. Semin Nucl Med. 2015;45(5):440–57.
15. Kabasakal L, Demirci E, Ocak M, Decristoforo C, Araman A, Ozsoy Y, et al. Comparison of 68Ga-DOTATATE and 68Ga-DOTANOC PET/CT imaging in the same patient group with neuroendocrine tumours. Eur J Nucl Med Mol Imaging. 2012;39(8):1271–7.
16. Agrawal K, Bhadada S, Mittal BR, Shukla J, Sood A, Bhattacharya A, Bhansali A. Comparison of ^{18}F-FDG and 68Ga DOTATATE PET/CT in localization of tumor causing oncogenic osteomalacia. Clin Nucl Med. 2015;40(1):6–10.

8 ^{18}F-methylcholine (FCH) PET/CT Imaging: Physiological Distribution, Pitfalls and Imaging Pearls

Arun Kumar Reddy Gorla, Kanhaiyalal Agrawal, Ashwin Singh Parihar, and Bhagwant Rai Mittal

Contents

Over several years, functional tumour imaging has often relied on abnormal patterns of specific metabolic pathways or the overexpression of tumour specific receptors. Initial observations that demonstrated the alterations in Kennedy pathway in cancerous tissues fueled the development of radiolabelled choline and exploration of its uptake patterns in tumour cells. Subsequently, several trials and research studies established the invaluable role of choline-based radiotracers in accurate detection of biochemical relapse in patients of prostate cancer, following initial definitive treatment.

Although preliminary studies linked the increased phosphocholine (PCho) levels in tumour cells to increased cell membrane turnover and thus to

A. K. R. Gorla
Department of Nuclear Medicine, American Oncology Institute, Hyderabad, Telangana, India

K. Agrawal
Department of Nuclear Medicine, All India Institute of Medical Sciences (AIIMS), Bhubaneswar, India

A. S. Parihar · B. R. Mittal (✉)
Department of Nuclear Medicine, Postgraduate Institute of Medical Education and Research (PGIMER), Chandigarh, India

K. Agrawal et al. (eds.), *PET/CT Imaging*, Clinicians' Guides to Radionuclide Hybrid Imaging, https://doi.org/10.1007/978-3-030-75476-1_8

proliferative activity, it was only subsequently realised to be due to overexpression of the choline transporters (e.g. CLT-1) and the key enzyme, choline 1-α-kinase. Several molecules were developed to target these mechanisms; however, only ^{11}C-choline, ^{18}F-methylcholine (FCH) and ^{18}F-ethylcholine garnered widespread utilisation [1]. Since ^{11}C-choline is biochemically indistinguishable from natural choline and shows similar kinetics, it is believed to follow the pathways of naturally occurring choline. Although its favourable imaging characteristic of limited urinary clearance had the advantage in urological malignancies, the short half-life of ^{11}C (20 minutes) restricted its utilisation only to centres equipped with an on-site cyclotron. Flourine-18 methylcholine (FCH) was subsequently developed by DeGrado et al., which demonstrated slightly slower rates of incorporation than choline and higher rates of urinary clearance than ^{11}C-Choline. However, better image quality and longer half-lives provided logistic advantage over ^{11}C-choline [2]. Currently, both these tracers are in use depending on their availability and validation in various regions.

Several authors have previously reported and reviewed the several pitfalls of PET imaging with radiolabelled choline derivatives [3, 4]. In this chapter, we review the physiological distribution and pitfalls of FCH PET/CT imaging that a clinician should be aware of during the interpretation.

8.1 Physiological Tracer Distribution

After intravenous administration, significant fraction of radiolabelled choline is rapidly cleared from the circulation within 10 min, after which the plasma concentration reaches a plateau. Physiological uptake of tissues is noted most prominently in the liver, pancreas, followed by salivary glands, spleen and lacrimal glands. Mild diffuse tracer uptake is noted in the bone marrow and muscles. A recent multicentre evaluation demonstrated no significant difference in the extra-prostatic distributions of ^{11}C-choline, ^{18}F-methylcholine (FCH) and ^{18}F-ethylcholine [1]. Table 8.1 lists the organs with physiological uptake graded as per the degree of uptake.

Table 8.1 Physiological distribution [1]

Tissue uptake
High grade uptake: liver, pancreas
Moderate to high uptake: spleen, salivary glands, lacrimal glands
Low grade diffuse uptake: bone marrow, muscles
Variable uptake: small and large intestine
Tracer excretion: (less prominent with ^{11}C-choline)
Kidneys, ureters and bladder

8.2 Applications

Although choline labelled radiotracers were utilised in evaluating patients with several malignancies (including brain tumours, oesophageal cancer, hepatocellular carcinoma [5] and several others), the most important clinical application is prostate cancer imaging [6] (Fig. 8.1). Incidental detection of parathyroid adenoma in patients imaged for prostate cancer evaluation led to recent studies in evaluating its utility in evaluation of patients with primary hyperparathyroidism (Fig. 8.2). Table 8.2 lists the various malignancies evaluated using radiolabelled choline PET/CT imaging and various indications in prostate cancer.

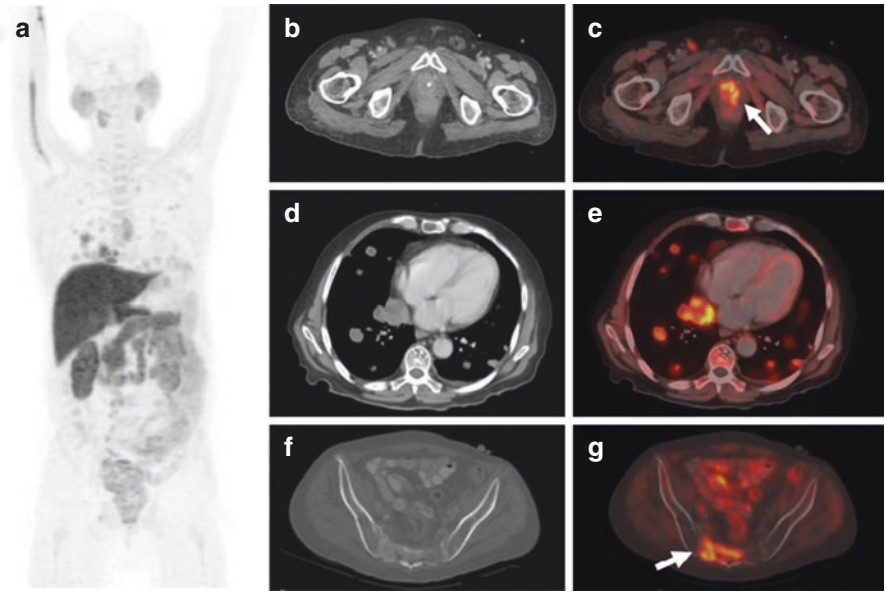

Fig. 8.1 58 year-old-man with incidentally detected elevated S. PSA—2000 ng/mL. Trans-rectal ultrasound guided biopsy from the prostate was done, which showed adenocarcinoma (Gleason's score 4 + 4 = 8). ^{18}F-Choline PET/CT done for staging showed multiple foci of increased tracer avidity in the thoracic region, abdomen and pelvis in the maximum intensity projection image (**a**). Transaxial CT and fused PET/CT images showed increased tracer avidity in a heterogeneously enhancing lesion in the entire prostate (**b**, **c**—arrow; SUVmax 5.4), multiple tracer avid bilateral lung nodules (**d**, **e**) with SUVmax 14.5 and tracer avid sclerotic lesion in the sacrum (**f**, **g**) with SUVmax 11. The patient was put on androgen deprivation therapy with anti-androgen therapy and concurrent docetaxel based chemotherapy

Table 8.2 Possible role of choline PET/CT in various malignancies

Malignancy	Role
Prostate carcinoma [6–8]	• Initial staging • Restaging • Recurrence evaluation
Malignant brain tumours [9] • Malignant gliomas • Brain metastases	• Staging • Post-treatment fibrosis vs residual disease • Recurrence evaluation
Parathyroid carcinoma [10]	• Recurrence evaluation
Lung adenocarcinoma [11]	• Evaluation of solitary pulmonary nodule
Hepatocellular carcinoma [5, 12]	• Initial staging
Urothelial carcinoma [13]	• Regional staging • Restaging
Breast carcinoma [14]	• Initial staging
Gynaecologic malignancies [15]	• Initial staging • Recurrence evaluation

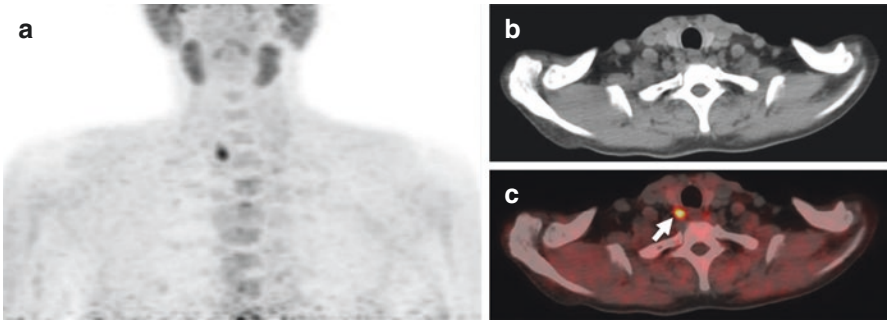

Fig. 8.2 45 year-old-man with history of renal stone disease. Biochemical examination showed elevated serum levels of calcium (12.2 mg/dL) and intact parathyroid hormone (270 pg/mL). Ultrasound of neck did not reveal any abnormality. Sestamibi scan done for detection of parathyroid adenoma did not reveal any abnormality. ^{18}F-Choline PET/CT showed a well-defined tracer avid (SUVmax 11.4) lesion postero-inferior to the right lobe of thyroid gland (~1.7 × 1.2 cm) (maximum intensity projection image—(**a**), transaxial CT—(**b**), fused PET/CT—(**c**), arrow). The patient underwent surgical resection of the lesion with the histopathology confirming the parathyroid adenoma

8.3 False Positive FCH Uptake

It is not uncommon to notice incidental sites of FCH uptake that are less likely to be related to the primary aetiology of concern (usually prostate cancer) (Figs. 8.3, 8.4, and 8.5). In such cases, all suspicious findings warrant further evaluation with imaging and/or histological correlation to rule out any atypical pattern of metastatic involvement or any synchronous malignancy (Table 8.3). Also, several benign inflammatory and non-inflammatory conditions can demonstrate variable FCH uptake due to its inherent non-specific mechanism of uptake. Knowledge of these conditions will avoid potential misinterpretation of these conditions as malignant/metastatic involvement (Table 8.4).

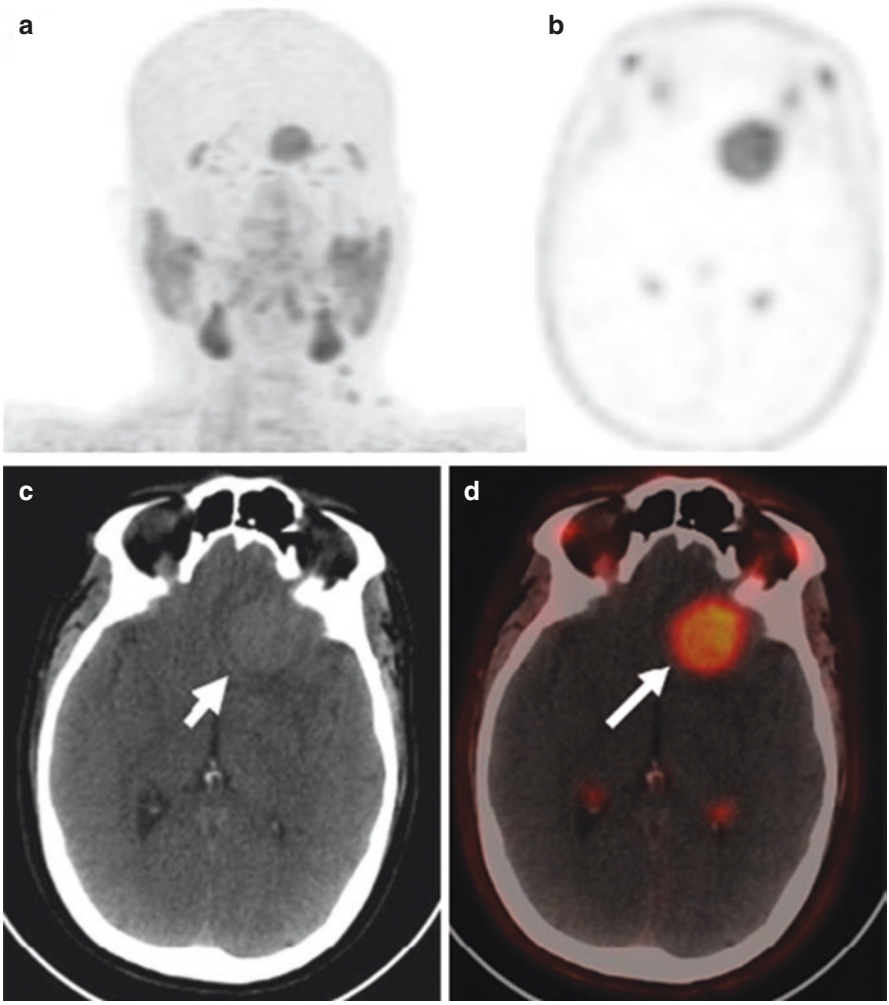

Fig. 8.3 45 year-old-man with an incidentally detected intracranial space occupying lesion on CT. MRI showed an extra-axial mass in the left frontal—basi-frontal region—likely meningioma. [18]F-Choline PET/CT showed increased tracer uptake (SUVmax 6.1) in a hyperdense lesion (~3.2 × 3.0 cm) in the left basi-frontal region (maximum intensity projection image—(**a**), transaxial PET—(**b**), CT—(**c**), fused PET/CT—(**d**)). Mass effect was also seen in the form of effacement of frontal horn of left lateral ventricle and midline shift (maximum ~7 mm) towards the right side with significant perilesional oedema. He subsequently underwent tumour resection and the histopathology was suggestive of meningioma

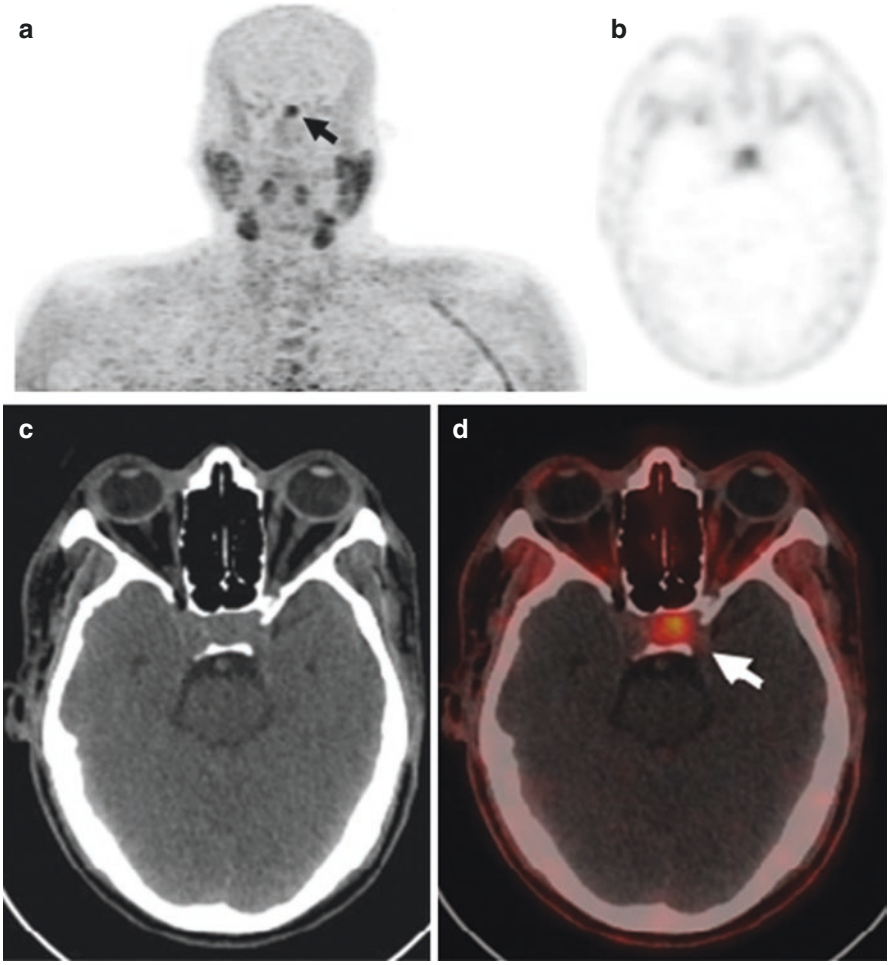

Fig. 8.4 51 year-old-man with acromegaly. MRI examination suggestive of pituitary microadenoma. ^{18}F-Choline PET/CT showed a tracer avid (SUVmax 5) hyperdense soft tissue lesion (~1.3 × 1.9 cm) in the pituitary fossa—likely pituitary macroadenoma (maximum intensity projection image—(**a**), transaxial PET—(**b**), CT—(**c**), fused PET/CT—(**d**), arrow). The patient underwent trans-sphenoidal resection of the tumour and had an uneventful post-operative recovery. The diagnosis on histopathologic examination of the resection specimen was pituitary macroadenoma

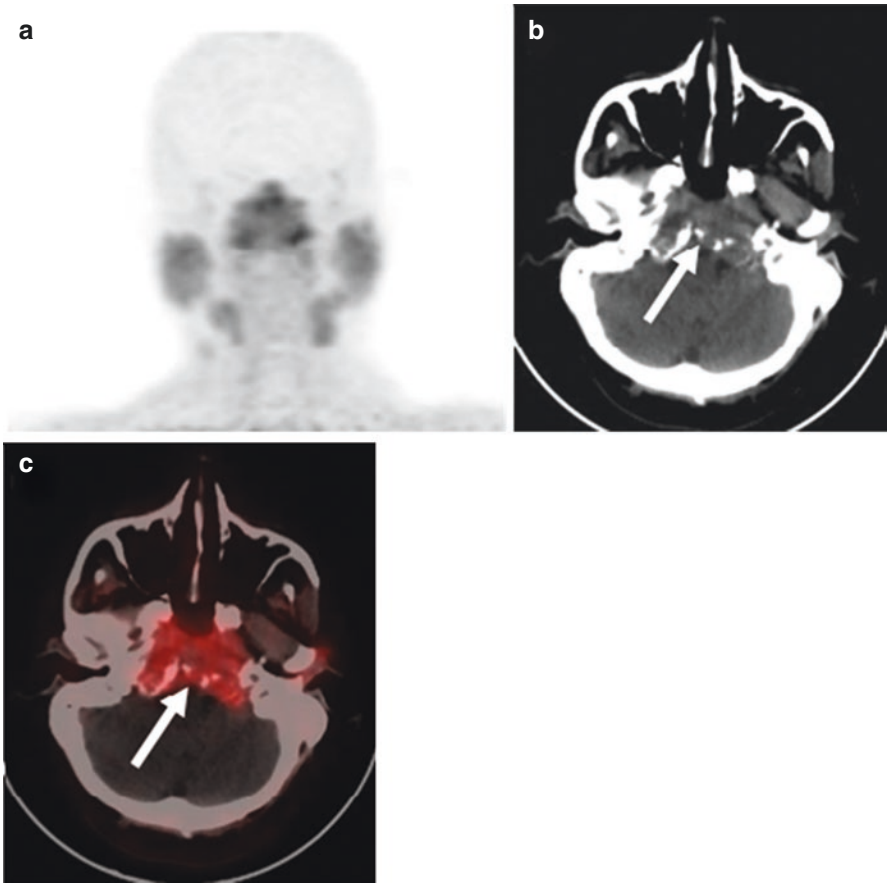

Fig. 8.5 68-year-old-man presented with complaint of headache for 1 year, gradual in onset and with increasing severity. MRI of the head was suggestive of clival chondrosarcoma. ^{18}F-Choline PET/CT showed a tracer avid (SUVmax 4.8) lytic expansile mass (~3.6 × 6.1 × 5.2 cm) at the base of the skull (maximum intensity projection image—(**a**), transaxial CT—(**b**), fused PET/CT—(**c**)). The mass was seen to cause lytic destructive changes of the base of the skull, clivus and the sella with anteriorly extension to the sphenoid sinus (arrow in (**b**, **c**)). The patient underwent tumour resection with the histopathology diagnosing the tumour as clival chordoma

8.4 False Negative Interpretation of FCH PET/CT (Table 8.5)

Some authors have reported lower detection rates of FCH PET/CT imaging in patients treated with androgen deprivation therapy [43]. However, subsequently results contrary to initial have been reported. Hence, due to lack of conclusive evidence for or against the hypothesis, currently withholding of therapy is suggested in hormone naïve patients planned for restaging. There is also report of impaired uptake of tracer in patients taking colchicine.

Administration of furosemide enhances the rapidity of tracer clearance and improves interpretation of perivesical space and avoids focal abnormal

Table 8.3 Various incidentally detected (synchronous) malignancies reported with positive radiolabelled choline uptake [16]

Head
Intracranial: Meningioma [17] (Fig. 8.3), pituitary adenoma [18] (Fig. 8.4), glioma, medulloblastoma [9], clival chordoma (Fig. 8.5)
Extracranial: Warthin's tumour, nasopharyngeal carcinoma [19]
Neck
Thyroid tumours (papillary [20], Hurthle cell, follicular carcinoma, lymphoma [21])
Parathyroid adenoma
Chest
Mediastinum: Thymic carcinoma, oesophageal carcinoma [22]
Lung carcinoma (squamous cell carcinoma) [11]
Abdomen
Adrenocortical carcinoma [23]
GI malignancies (gastric, pancreatic and colon malignancy)
Pelvis
Bladder carcinoma [13]
Testicular tumours (Leydig cell tumour)
Skeletal
Solitary: plasmacytoma [24], bone malignancy
Multifocal: multiple myeloma [25, 26], metastatic involvement due to synchronous malignancy
General
Lymphoma (DLBCL, Hodgkin's lymphoma) [27, 28]
Neurofibroma [29]
Paraganglioma [30]

Table 8.4 Reported literature on various benign conditions with positive choline uptake that can lead to potential false positive interpretation

Head and neck
Tumefactive cerebral lesions (e.g. multiple sclerosis)
Sinusitis, Oto-mastoiditis
Thyroiditis, thyroid adenoma
Parathyroid hyperplasia [31]
Brown adipose tissue [32]
Thoracic region
Mediastinitis
Esophagitis
Mediastinal lymphadenopathy (sarcoidosis, reactive)
Thymoma
Tuberculosis [33]
Diffuse lung uptake: pulmonary oedema, pulmonary inflammation
Pneumoconiosis (e.g. anthracosis) [34]
Pulmonary nodules
Pleuritis
Sclerosing hemangioma
Abdominal region

Table 8.4 (continued)

Adrenal adenoma
Meckel's diverticulum [35]
Reactive lymphadenopathy (low grade uptake)
Ureteral activity (stone, obstruction)
Seminal vesiculitis
Prostatitis, Benign prostatic nodule, prostatic abscess
Skeletal and marrow uptake
Recent trauma [36], healed fractures, osteomyelitis
Brown tumours [37], Paget's disease, fibrous dysplasia [38]
Hemangioma [39]
Diffuse marrow uptake [40]: Chronic haemoglobinopathies, proliferative marrow pathologies
Uncategorised
Non-specific systemic inflammatory lymphadenopathy
Interference due to urinary activity
Tumour thrombus
Misregistration and other technical artefacts (inherent to any PET/CT imaging)

Table 8.5 False negative interpretation

Drug interference
– Androgen deprivation therapy – Colchicine – Erythropoietin [41] – Furosemide during scan [42]
Small sized lesions (below the resolution of scanner)
Hepatic lesions (primary or metastatic; due to high physiological activity)
Interference due to urinary activity
Misregistration and other technical artefacts (inherent to any PET/CT imaging)

accumulations in the ureter. However, recently Rischke et al. reported that administration of furosemide reduced the degree of choline uptake in pelvic lymph nodes [42]. Hence, an early initial imaging followed by a delayed post-diuretic regional imaging seems to be a safer alternative. Some authors also reported that similar potential false negative interpretations are possible in patients treated with erythropoietin and chemotherapeutic drugs like docetaxel and paclitaxel [7, 41].

Key Points

- Choline labelled radiotracers were utilised in evaluating patients with several malignancies and the most important clinical application is prostate cancer imaging.
- Flourine-18 methylcholine (FCH) demonstrates slightly slower rates of incorporation and higher rates of urinary clearance than ^{11}C-choline.
- Physiological uptake of tissues is noted most prominently in the liver, pancreas, followed by salivary glands, spleen and lacrimal glands.
- There is no significant difference in the extra-prostatic distributions of ^{11}C-choline, ^{18}F-methylcholine (FCH) and ^{18}F-ethylcholine.

References

1. Calabria F, Gallo G, Schillaci O, et al. Bio-distribution, imaging protocols and diagnostic accuracy of PET with tracers of lipogenesis in imaging prostate cancer: a comparison between ^{11}C-Choline, ^{18}F-Fluoroethylcholine and ^{18}F-methylcholine. Curr Pharm Des. 2015;21:4738–47.
2. DeGrado TR, Reiman RE, Price DT, et al. Pharmacokinetics and radiation dosimetry of 18F-fluorocholine. J Nucl Med. 2002;43:92–6.
3. Calabria F, Chiaravalloti A, Schillaci O. 18F-choline PET/CT pitfalls in image interpretation. Clin Nucl Med. 2013;39:1.
4. Beheshti M, Haroon A, Bomanji JB, et al. Fluorocholine PET/computed tomography. PET Clin. 2014;9:299–306.
5. Chalaye J, Baranes L, Costentin C, et al. Dual-tracer 18F-fluorocholine and 18F-fluorodeoxyglucose PET/CT for the diagnosis of tumoral portal vein thrombosis in patients with hepatocellular carcinoma. HPB. 2016;18:e531.
6. Hara T, Kosaka N, Kishi H. PET imaging of prostate cancer using carbon-11-choline. J Nucl Med. 1998;39:990–5.
7. Wallitt KL, Khan SR, Dubash S, et al. Clinical pet imaging in prostate cancer. Radiographics. 2017;37:1512–36.
8. Hara T, Kosaka N, Kishi H. Development of (18)F-fluoroethylcholine for cancer imaging with PET: synthesis, biochemistry, and prostate cancer imaging. J Nucl Med. 2002;43:187–99.
9. Hara T, Kosaka N, Shinoura N, et al. PET imaging of brain tumor with [methyl- 11C]choline. J Nucl Med. 1997;38:842–7.
10. Thanseer NTK, Parihar A, Sood A, et al. Evaluation of recurrent parathyroid carcinoma: a new imaging tool in uncommon entity. World J Nucl Med. 2019;18:198.
11. Li M, Peng Z, Liu Q, et al. Value of 11C-choline PET/CT for lung cancer diagnosis and the relation between choline metabolism and proliferation of cancer cells. Oncol Rep. 2013;29:205–11.
12. Talbot JN, Michaud L, Grange JD, et al. Use of choline PET for studying hepatocellular carcinoma. Clin Transl Imaging. 2014;2:103–13.
13. Sassa N, Kato K, Abe S, et al. Evaluation of ^{11}C-choline PET/CT for primary diagnosis and staging of urothelial carcinoma of the upper urinary tract: a pilot study. Eur J Nucl Med Mol Imaging. 2014;41:2232–41.
14. Hara T. 18F-fluorocholine: a new oncologic PET tracer. J Nucl Med. 2001;42:1815–7.
15. Torizuka T, Kanno T, Futatsubashi M, et al. Imaging of gynecologic tumors: comparison of 11C-choline PET with 18F-FDG PET. J Nucl Med. 2003;44:1051–6.
16. Haroon A, Zanoni L, Celli M, et al. Multicenter study evaluating extraprostatic uptake of 11C-choline, 18F-methylcholine, and 18F-ethylcholine in male patients: physiological distribution, statistical differences, imaging pearls, and normal variants. Nucl Med Commun. 2015;36:1065–75.
17. Fallanca F, Giovacchini G, Picchio M, et al. Incidental detection by [11C]choline PET/CT of meningiomas in prostate cancer patients. Q J Nucl Med Mol Imaging. 2009;53:417–21.
18. Maffione AM, Mandoliti G, Pasini F, et al. Pituitary non-functioning adenoma disclosed at 18F-choline PET/CT to investigate a prostate cancer relapse. Clin Nucl Med. 2016;41:e460.
19. Wu H, Wang Q, Wang M, et al. Preliminary study of 11C-choline PET/CT for T staging of locally advanced nasopharyngeal carcinoma: comparison with 18F-FDG PET/CT. J Nucl Med. 2011;52:341–6.
20. Lalire P, Zalzali M, Garbar C, et al. Incidental detection of oxyphilic papillary thyroid carcinoma by 18F-fluorocholine PET/CT. Clin Nucl Med. 2016;41:512–3.
21. Eccles A, Challapalli A, Khan S, et al. Thyroid lymphoma incidentally detected by 18F-fluorocholine (FCH) PET/CT. Clin Nucl Med. 2013;38:755–7.
22. Kobori O, Kirihara Y, Kosaka N, et al. Positron emission tomography of esophageal carcinoma using (11)C-choline and (18)F-fluorodeoxyglucose: a novel method of preoperative lymph node staging. Cancer. 1999;86:1638–48.

23. Imperiale A, Cabral JF, Rust E, et al. 18F-fluorocholine uptake in a case of adrenal incidentaloma: possible diagnostic pitfall or potential tool for adrenocortical tumors characterization? Clin Nucl Med. 2013;38:83–4.
24. Ambrosini V, Farsad M, Nanni C, et al. Incidental finding of an 11C-choline PET-positive solitary plasmacytoma lesion. Eur J Nucl Med Mol Imaging. 2006;33:1522.
25. Florimonte L, Orunesu E, Castellani M, et al. 18F-choline PET/CT-positive lytic bone lesions in prostate cancer and accidental myeloma detection. Clin Nucl Med. 2016;41:394–6.
26. Dias AH, Bouchelouche K. Skeletal "superscan" on 18F-choline PET/CT: cases of myeloproliferative disease. Clin Nucl Med. 2016;41:173–4.
27. Garzon JG, Bassa P, Moragas M, et al. Incidental diagnosis of diffuse large B-cell lymphoma by 11C-choline PET/CT in a patient with biochemical recurrence of prostate cancer. Clin Nucl Med. 2014;39:742–3.
28. Goineau A, Colombié M, Rousseau C, et al. Incidental detection of a Hodgkin lymphoma on 18F-choline PET/CT and comparison with 18F-FDG in a patient with prostate cancer. Clin Nucl Med. 2015;40:670–1.
29. Agrawal K, Sajjan RS, Gavra M, et al. Incidental neurofibroma on 18F-fluorocholine PET/MR. Clin Nucl Med. 2015;40:e455–6.
30. Rahbar K, Fuchs M, Kemper S, et al. Imaging of a paraganglioma on C-11 choline PET/CT. Clin Nucl Med. 2009;34:119–21.
31. Cazaentre T, Clivaz F, Triponez F. False-positive result in 18F-Fluorocholine PET/CT due to incidental and ectopic parathyroid hyperplasia. Clin Nucl Med. 2014;36:328–30.
32. Balogova S, Michaud L, Vereb M, et al. 18F-fluorocholine may be taken-up by brown adipose tissue. Nuklearmedizin. 2013;52:3.
33. Vorster M, Stoltz A, Jacobs AG, et al. Imaging of pulmonary tuberculosis with 18F-fluorodeoxy-glucose and 18F-ethylcholine. Open Nucl Med J. 2014;6:17–21.
34. Pinaquy J-B, Fernandez P, Pasticier G, et al. Anthracosis mimicking mediastinal lymph node metastases with 18F-FCholine in high-risk prostate cancer. Clin Nucl Med. 2015;40:e253–4.
35. Khor LK, Loi HY, Sinha AK, et al. Incidental possible diagnosis by 18F-fluorocholine PET/CT of Meckel's diverticulum and potential pitfalls. Hell J Nucl Med. 18:157–9.
36. Leyendecker P, Imperiale A, Matern J-F, et al. Intense 18F-choline uptake after minor head injury: misleading PET/CT result in a patient with biochemical relapse of prostate adenocarcinoma. Clin Nucl Med. 2014;39:1012–3.
37. García JR, Alvarez Moro FJ, Bassa P, et al. Brown tumours due to secondary hyperparathyroidism detected by 11C-choline PET/CT. Rev Esp Med Nucl Imagen Mol. 35:209–10.
38. Gu CN, Hunt CH, Lehman VT, et al. Benign fibrous dysplasia on [(11)C]choline PET: a potential mimicker of disease in patients with biochemical recurrence of prostate cancer. Ann Nucl Med. 2012;26:599–602.
39. Savelli G, Perotti V, Rosso E, et al. 18F-fluorocholine PET/CT finding of a vertebral hemangioma. Clin Nucl Med. 2016;41(8):390.
40. Wartski M, Jehanno N, Gontier E, et al. Hyperfixation ostéomédullaire diffuse de la [18]F-fluorocholine et hémopathies chroniques. Med Nucl. 2015;39:414–7.
41. Balogova S, Huchet V, Egrot C, et al. Effect of erythropoietin on bone marrow uptake of 18F-fluorocholine in prostate cancer. Clin Nucl Med. 2013;38:200–2.
42. Rischke HC, Beck T, Vach W, et al. Furosemide diminishes [18]F-fluoroethylcholine uptake in prostate cancer in vivo. Eur J Nucl Med Mol Imaging. 2014;41:2074–82.
43. Chondrogiannis S, Marzola MC, Ferretti A, et al. Is the detection rate of 18F-choline PET/CT influenced by androgen-deprivation therapy? Eur J Nucl Med Mol Imaging. 2014;41:1293–300.

^{68}Ga-PSMA PET/CT: Normal Variants, Pitfalls and Artefacts

9

Kanhaiyalal Agrawal, Sharjeel Usmani, Abdulredha Esmail, Fahad Marafi, and Gopinath Gnanasegaran

Contents

9.1 Introduction

Prostate-specific membrane antigen (PSMA), a type II transmembrane protein expressed in all types of prostatic tissue, including benign secretory acinar epithelium, high grade prostatic intraepithelial neoplasia and prostate carcinoma(PCa) [1]. High expression of PSMA in prostate carcinoma has been investigated as molecular target for diagnostic and therapeutic applications in nuclear medicine. Recently,

K. Agrawal (✉)
Department of Nuclear Medicine, All India Institute of Medical Sciences (AIIMS), Bhubaneswar, India

S. Usmani
Department of Nuclear Medicine, Kuwait Cancer Control Center (KCCC), Shuwaikh, Kuwait

A. Esmail · F. Marafi
Department of Nuclear Medicine, Jaber Al-Ahmad Molecular Imaging Center, Kuwait City, Kuwait

G. Gnanasegaran
Department of Nuclear Medicine, Royal Free NHS Foundation Trust, London, UK

K. Agrawal et al. (eds.), *PET/CT Imaging*, Clinicians' Guides to Radionuclide Hybrid Imaging, https://doi.org/10.1007/978-3-030-75476-1_9

Glu-NH-CO-NH-Lys(Ahx)-Gallium-68-*N,N′*-bis[2-hydroxy-5-(carboxyethyl)benzyl]ethylenediamine-*N,N′*-diacetic acid (HBED-CC) [^{68}Ga-PSMA-11], a urea-based PSMA inhibitor, has been proven to have high clinical value for imaging of PCa [2].

9.2 Clinical Utility of ^{68}Ga-PSMA-11 PET/CT

Initial studies on role of ^{68}Ga-PSMA-11 PET/CT in PCa have shown promising results in diagnosis, staging and recurrence of PCa (Table 9.1) [3]. Conventionally CT or magnetic resonance imaging (MRI) is used for identification of metastatic lymph nodes in PCa during initial staging, but this relies on pathologic changes in lymph node morphology and size criteria. Studies have shown that up to 80% of metastatic lymph nodes are smaller than 8 mm threshold limit used in clinical practice [4]. Meta-analytical data demonstrated conventional CT and MRI imaging has sensitivity of 39–42% and specificity of 82% [4]. In patients with PCa, ^{68}Ga-PSMA-11 PET/CT has shown both sensitivity and specificity of 86% [3]. Afshar-Oromieh et al. retrospectively analysed the diagnostic utility of ^{68}Ga-PSMA-11 PET/CT in a large cohort of 319 PCa patients with biochemical relapse and showed on a patient based analysis sensitivity of 88.1% in detecting tumour recurrence [5]. Kratochwil et al. demonstrated that integrating ^{68}Ga-PSMA-11 PET/CT into the planning phase of radiotherapy, management is changed in 30–50% of the patients [6].

9.3 PSMA Expression in Prostate Carcinomas

PSMA is expressed several times in PCa cells compared to normal prostate cells [7]. Dysplastic changes in the prostate lead to overexpression of PSMA on the luminal surface of prostatic ducts. Increasing PCa stage and grade result in higher PSMA expression. Finally, progression to advanced and castrate resistance PCa leads to further increase in PSMA expression in prostate [8]. It should be emphasised that not all PCa demonstrate positive PSMA staining. Ninety-three percent of acinar adenocarcinomas of prostate show positive PSMA staining [9]. A rare variant of prostate carcinomas, ductal adenocarcinomas, shows positive PSMA staining in

Table 9.1 Clinical utility of ^{68}Ga-PSMA-11 PET/CT in prostate carcinoma

Potential clinical applications
• Primary staging in high-risk disease based on D'Amico classification
• Biochemical recurrence with PSA-values 0.2–10 ng/ml
• Biopsy targeting in high suspicion of prostate carcinoma
• ^{68}Ga-PSMA-11 PET/CT guided radiotherapy planning
Possible clinical applications
• Primary staging in low-risk and intermediate-risk disease based on D'Amico classification
• Treatment response evaluation in metastatic prostate carcinoma
• Active surveillance

only 86.2% cases [9]. Furthermore, PSMA staining has been shown to be of weaker intensity in high grade prostate cancers [10]. Although completely PSMA negative prostate carcinomas are rare, there may be heterogeneous PSMA expression within PCa [11]. PCa with high PSMA expression of any Gleason score frequently contains larger areas with PSMA negative cells [11].

9.4 PSMA Expression in Non-prostatic Tissues

Along with overexpression of PSMA in PCa, studies have also demonstrated its expression in non-prostatic tumour neo-vasculature [1]. Table 9.2 elaborates list of normal tissues and neoplasms expressing PSMA [10, 12]. It was also detected in hyperplastic prostate and Barrett's oesophagus. It is important to note that some variants of renal cell carcinomas, e.g. chromophobe carcinomas, oncocytomas and Wilms' tumours, did not express PSMA [10].

9.5 Pitfalls and Limitations ^{68}Ga-PSMA-11 PET/CT

With increasing clinical interest in ^{68}Ga-PSMA-11 PET/CT imaging, it is important to have knowledge of physiological distribution (Tables 9.3 and 9.4) (Figs. 9.1 and 9.2) [2, 13], normal variants and pitfalls in ^{68}Ga-PSMA-11 PET/CT imaging. These pitfalls may lead to misinterpretations of the images and potentially avoidable (Figs. 9.3, 9.4, 9.5, 9.6, 9.7, 9.8, 9.9, and 9.10). As PSMA is expressed in other tumours apart from PCa, ^{68}Ga-PSMA-11 tracer uptake has been noted in the benign and malignant tumours and other benign pathologies mentioned in Tables 9.5 and 9.6. Causes of false negative findings are enumerated in Table 9.7.

Table 9.2 Tissues expressing PSMA

Normal tissue	Neoplasms involving
• Prostate • Urinary bladder • Proximal tubules of kidney • Liver • Cortex and medulla of the adrenal gland • Oesophagus • Stomach • Small intestine • Colon • Breast • Fallopian tubes • Ovary stroma • Testicular seminiferous tubules • Hippocampal neurons and astrocytes • Ependyma	• Prostate • Kidney • Urinary bladder • Stomach • Small intestine • Colon • Lung • Adrenal gland • Testis • Glioma

Table 9.3 Physiological distribution of ^{68}Ga-PSMA-11 [2, 13]

• Renal cortex • Urinary bladder • Salivary glands (Fig. 9.2a, b) • Lacrimal glands • Liver (Fig. 9.2e) • Spleen • Duodenum (Fig. 9.2d)	Variable uptake • Nasopharyngeal mucosa • Vocal cords (Fig. 9.2c) • Thyroid • Pancreas

Fig. 9.1 ^{68}Ga-PSMA-11 PET/CT study showing physiological tracer distribution in the lacrimal glands, salivary glands, vocal cords, liver, kidneys, spleen, bowel, ureters and urinary bladder

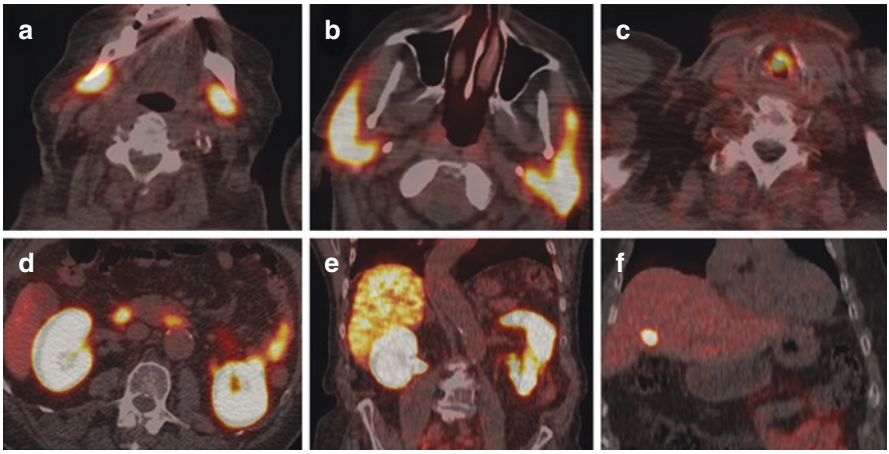

Fig. 9.2 Fused axial ^{68}Ga-PSMA-11 PET/CT images showing physiological tracer distribution in the (**a**) submandibular glands, (**b**) parotids, (**c**) vocal cords, (**d**) kidneys and duodenum, (**e**) liver and kidneys, (**f**) gall bladder

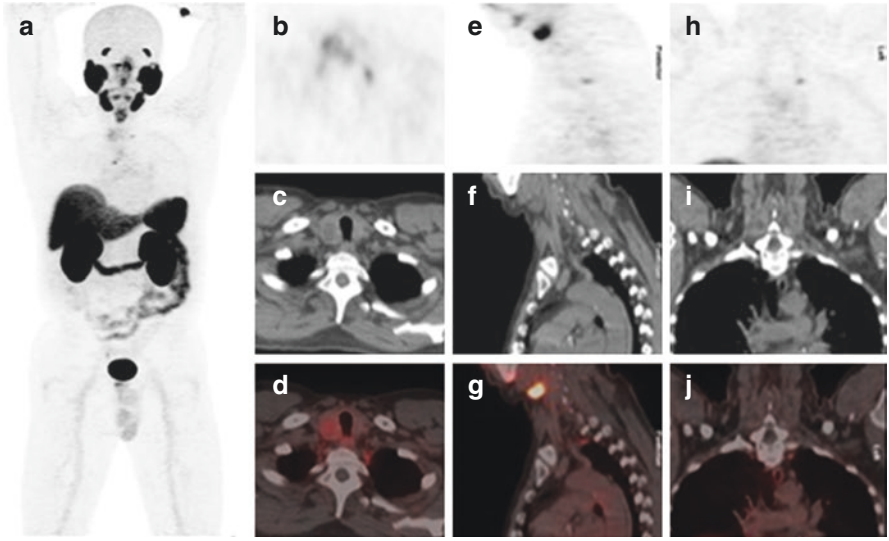

Fig. 9.3 65-years old male with prostate cancer, Gleason score of (4+3), Serum PSA 7.4 ng/ml. ^{68}Ga-PSMA-11 PET/CT MIP image (**a**) shows mild tracer uptake in the neck and upper chest region. The low grade uptake in the neck localises to a cystic lesion in the right thyroid gland likely benign lesion (**b**–**d**). The tiny focal uptake of SUVmax 3.0 is seen at bilateral thoracic inlet region at D1 level (**b**–**j**), likely uptake at cervicothoracic stellate ganglia. The uptake at D4 vertebral level with SUV max 5.7 is seen. Uptake at D1 and D4 vertebral region is likely due to normal variant uptake at sympathetic ganglia

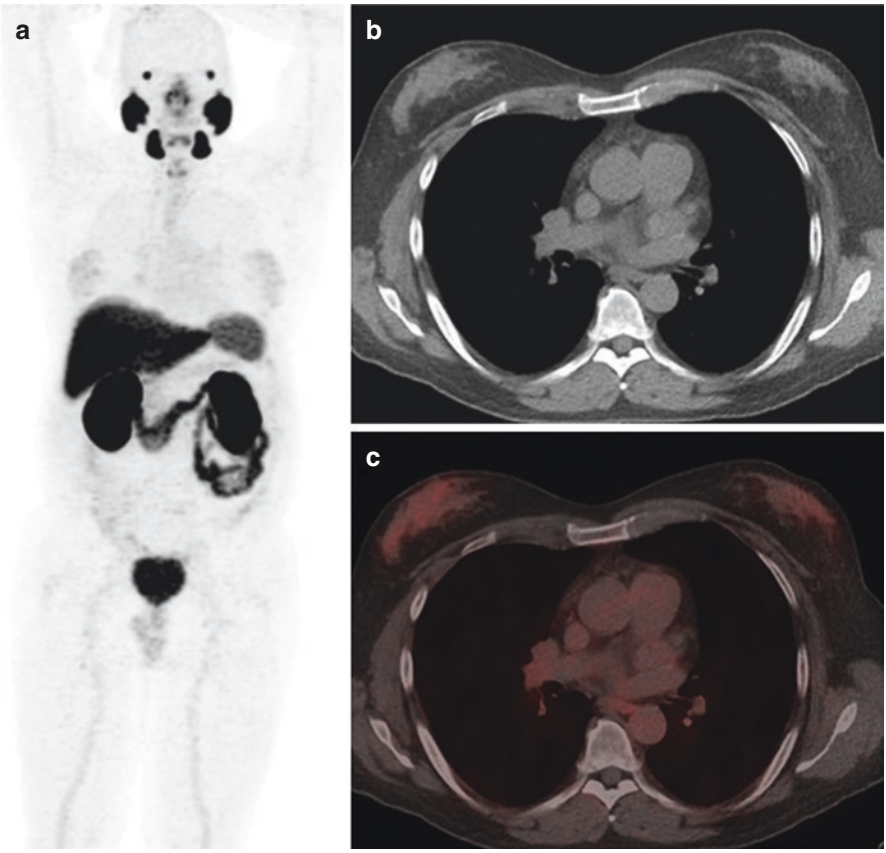

Fig. 9.4 64-years old male with prostate cancer treated with radical prostatectomy. Most recent PSA was 0.25 ng/ml. ^{68}Ga-PSMA-11 PET/CT MIP image (**a**) shows mild diffuse increase tracer uptake in the bilateral chest region localising to bilateral breast (**b**, **c**) suggestive of uptake in Gynaecomastia. This is likely related to hormonal imbalance caused by castration

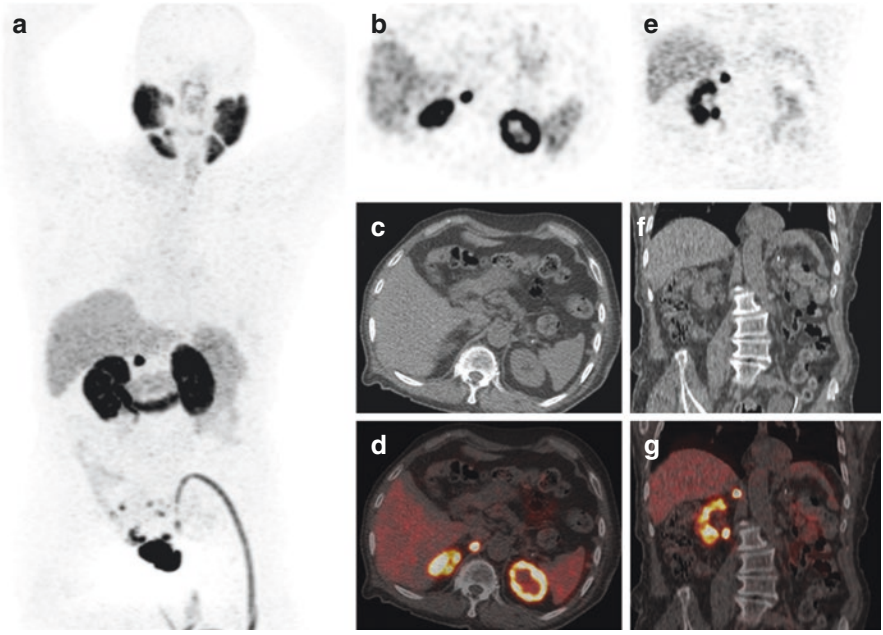

Fig. 9.5 87-year-old male with prostate cancer and PSA 23 ng/ml. ^{68}Ga-PSMA-11 PET/CT MIP image (**a**) show intense tracer activity in the right suprarenal region and multiple focal uptake in the pelvic region. The tracer uptake with SUVmax 43.6 in the right suprarenal region localises to the right adrenal gland with CT showing right adrenal nodule with low attenuation representing fat rich tissue (**b**–**g**). Findings are consistent with adrenal adenoma confirmed by follow-up MRI. The multifocal uptake in the pelvic region localises to the sacrum (SUV max 17.6) and coccyx bone (SUV max 25.2) consistent with bone metastasis (**a**)

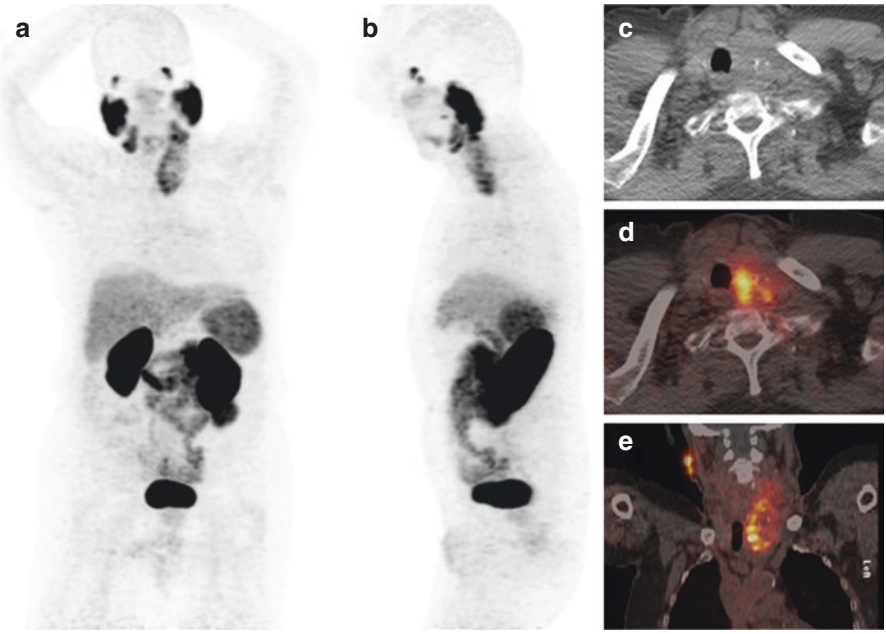

Fig. 9.6 72-year-old male with prostate cancer. Recent PSA is 0.23 ng/ml. ^{68}Ga-PSMA-11 PET/CT MIP anterior (**a**) and lateral (**b**) images show heterogenous tracer uptake in the enlarged left lobe of thyroid gland. Axial CT (**c**), PET (**d**) and fused PET/CT (**e**) images show increased tracer uptake, SUVmax 9.2, in the left thyroid mass with focal calcification. Histopathology showed papillary carcinoma of thyroid

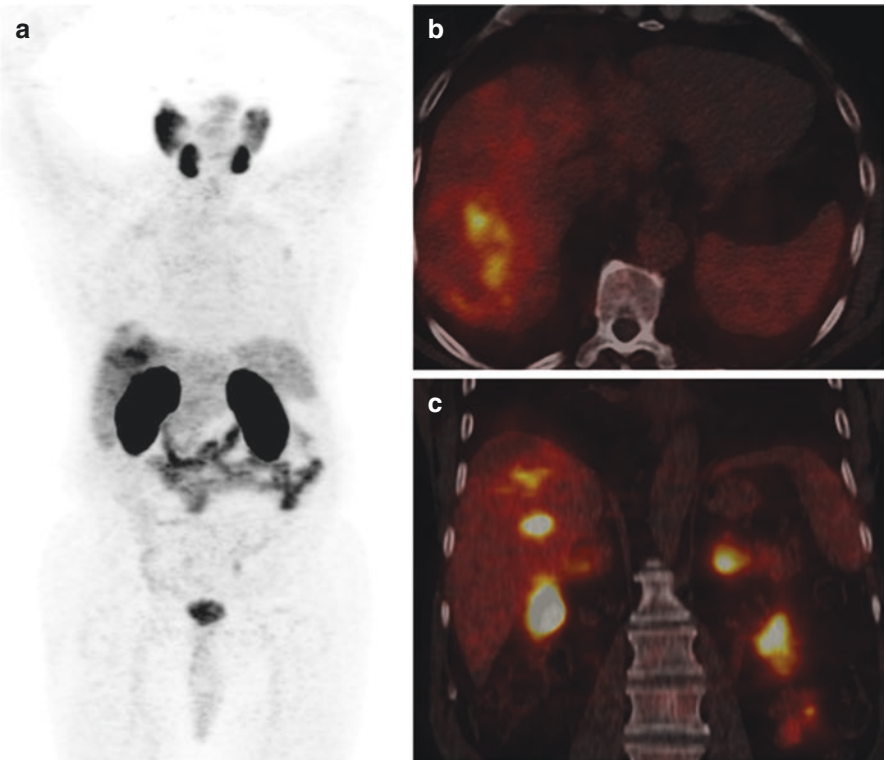

Fig. 9.7 ^{68}Ga-PSMA-11 PET/CT MIP (**a**) and fused PET/CT images (**b**, **c**) show increased heterogeneous tracer uptake in a case of hepatocellular carcinoma

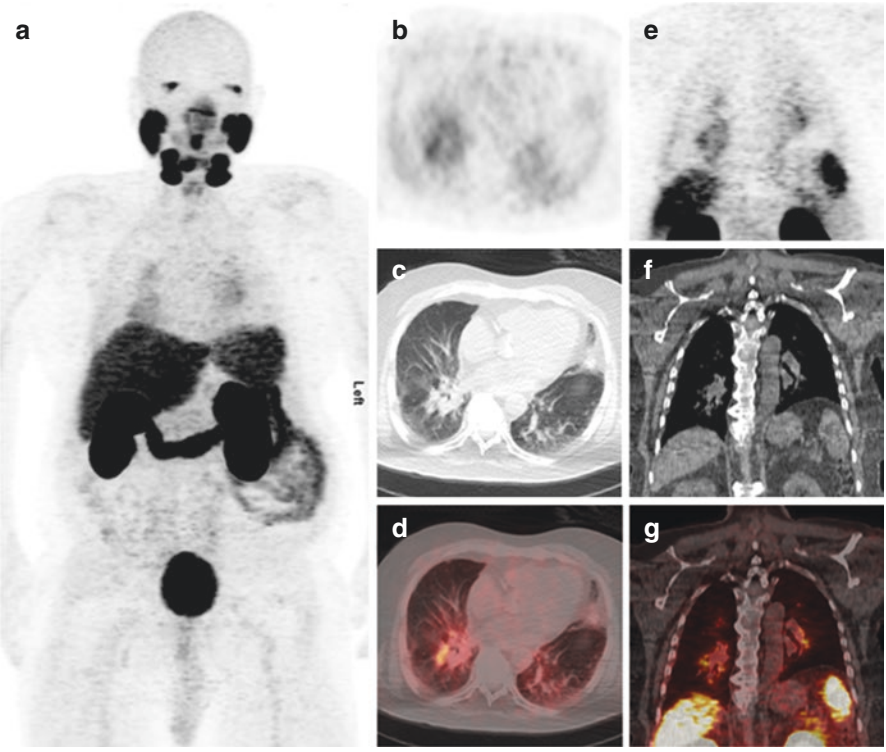

Fig. 9.8 72-year-old male with prostate cancer, with slow rising PSA. ^{68}Ga-PSMA-11 PET/CT PET image (**a**, **b**, **e**) shows diffuse increase tracer uptake in the bilateral hilar and chest region, which on CT shows diffuse infiltration and atelectatic bands (**c**, **d**, **f**, **g**). Findings are likely due to infective/inflammatory process

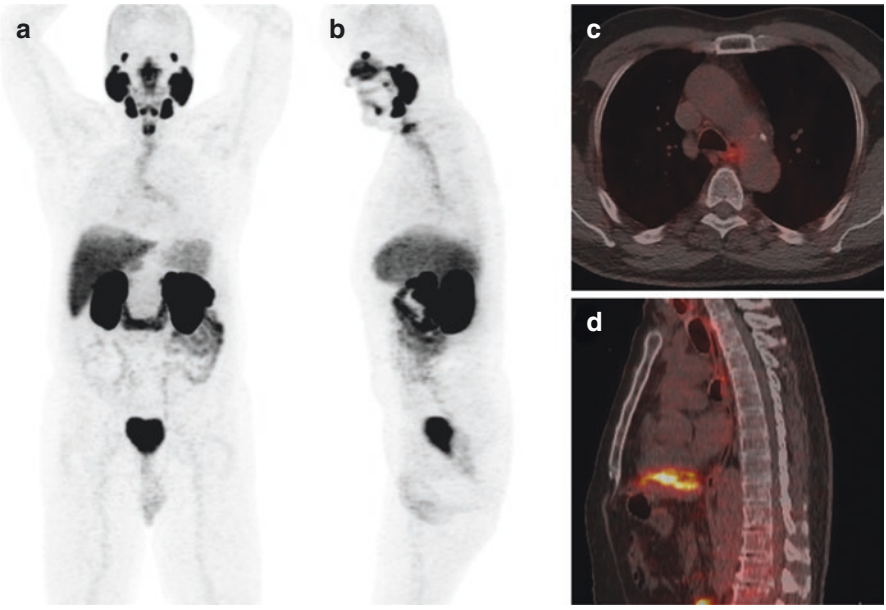

Fig. 9.9 68-year-old male with prostate cancer treated surgically. ^{68}Ga-PSMA-11 PET/CT was performed due to rising PSA. ^{68}Ga-PSMA-11 PET/CT MIP anterior (**a**) and lateral (**b**) images show linear tracer uptake in the mid chest region. This diffuse tracer uptake, SUVmax 4.7, localises to the oesophagus with no definite thickening on the CT (**c**, **d**), likely esophagitis

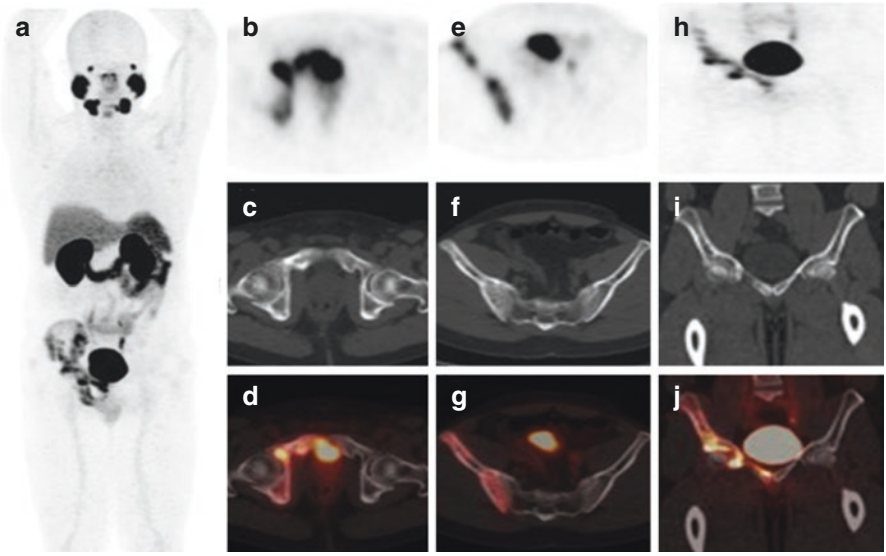

Fig. 9.10 55-year-old male with prostate cancer, with slow rising PSA. Recent PSA is 3 ng/ml. ^{68}Ga-PSMA-11 PET/CT MIP image (**a**) diffuse heterogeneous increase tracer uptake in the right hemipelvis. Transaxial (**b**–**d**, **e**–**g**) and coronal (**h**–**j**) ^{68}Ga-PSMA-11 PET/CT images show increased tracer uptake in the right-side pelvic bones showing mixed sclerotic/lytic lesion and accentuated trabecular pattern, typical for Paget's disease. These findings were confirmed by biopsy

Table 9.4 Normal variants in ^{68}Ga-PSMA-11 PET/CT

• Uptake in calcified choroid plexus [2]
• Celiac ganglia/sympathetic ganglia uptake [14] (Fig. 9.3)
• Gall bladder uptake (Fig. 9.2f) [2]
• Gynaecomastia (Fig. 9.4) [13]

Table 9.5 ^{68}Ga-PSMA-11 uptake in non-prostatic tumours

Benign	Malignant
• Follicular thyroid adenoma [15] • Adrenal adenoma (Fig. 9.5) [16] • Schwannoma [17–19]	• Adenoid cystic carcinoma of salivary gland [20] • Thyroid carcinoma [21–23] (Fig. 9.6) • Lung carcinoma [24, 25] • Breast carcinoma [26] • Neuroendocrine tumour [27] • Primary hepatocellular carcinoma [28] (Fig. 9.7) • Renal cell carcinoma [29, 30] • Rectal carcinoma [31] • Urothelial carcinoma [32] • Desmoid tumour [33] • Follicular lymphoma [34]

Table 9.6 False positive ^{68}Ga-PSMA-11 uptake in benign pathologies

• Low grade uptake in prostatitis [35]
• Benign lymph nodes [2]
• Tuberculosis [25]
• Sarcoidosis [36]
• Wegener's granulomatosis [13]
• Lung infective aetiology (Fig. 9.8)
• Oesophageal inflammation/infection (Fig. 9.9)
• Fascitis [37]
• Subacute stroke [38]
• Osteophytes [2]
• Bone fractures [39]
• Paget's disease [40] (Fig. 9.10)
• Focal urinary activity in the ureter may be mistaken for lymph nodes [41]—forced diuresis and delayed imaging are helpful

Table 9.7 False negative ^{68}Ga-PSMA-11 PET/CT in prostate carcinoma

Prostate
• Few prostate carcinomas do not express PSMA and may be false negative on ^{68}Ga-PSMA-11 PET/CT studies [9]
• Poorly differentiated prostatic carcinoma [42]
• Higher urine activity within urinary bladder may mask local recurrence—forced diuresis and use of indwelling catheter to empty the bladder prior to imaging is helpful [35, 41]
Lymph nodes
• Small size lymph nodes may be missed possibly due to partial volume effects [13]
• May be due to low PSMA expression
Metastases
• Metastases in poorly differentiated prostate carcinoma [25, 42]
• Low grade uptake in the liver metastases may be obscured due to high background uptake [3]

Key Points

- Prostate-specific membrane antigen (PSMA) is a transmembrane protein expressed in all types of prostatic tissue, including carcinoma.
- PSMA is expressed several times in PCa cells compared to normal prostate cells.
- Dysplastic changes in the prostate lead to overexpression of PSMA on the luminal surface of prostatic ducts.
- Increasing PCa stage and grade result in higher PSMA expression.
- PSMA expression is also seen in non-prostatic tumour neo-vasculature.
- Few prostate carcinomas do not express PSMA and may be false negative on radiolabelled PSMA studies.
- Low grade uptake in the liver metastases may be obscured due to high background uptake.

References

1. Chang SS, O'Keefe DS, Bacich DJ, et al. Prostate-specific membrane antigen is produced in tumor-associated neovasculature. Clin Cancer Res. 1999;5:2674–81.
2. Demirci E, Sahin OE, Ocak M, et al. Normal distribution pattern and physiological variants of 68Ga-PSMA-11 PET/CT imaging. Nucl Med Commun. 2016;37(11):1169–79.
3. Rauscher I, Maurer T, Fendler WP, et al. 68Ga-PSMA ligand PET/CT in patients with prostate cancer: how we review and report. Cancer Imaging. 2016;16:14.
4. Hovels AM, Heesakkers RA, Adang EM, et al. The diagnostic accuracy of CT and MRI in the staging of pelvic lymph nodes in patients with prostate cancer: a meta-analysis. Clin Radiol. 2008;63:387–95.
5. Afshar-Oromieh A, Avtzi E, Giesel FL, et al. The diagnostic value of PET/CT imaging with the 68Ga-labelled PSMA ligand HBED-CC in the diagnosis of recurrent prostate cancer. Eur J Nucl Med Mol Imaging. 2015;42:197–209.
6. Kratochwil C, Afshar-Oromieh A, Kopka K, et al. Current status of prostate-specific membrane antigen targeting in nuclear medicine: clinical translation of chelator containing prostate-specific membrane antigen ligands into diagnostics and therapy for prostate cancer. Semin Nucl Med. 2016;46:405–18.
7. Silver DA, Pellicer I, Fair WR, et al. Prostate-specific membrane antigen expression in normal and malignant human tissues. Clin Cancer Res. 1997;3:81–5.
8. Perera M, Papa N, Christidis D, et al. Sensitivity, specificity, and predictors of positive ^{68}Ga-prostate-specific membrane antigen positron emission tomography in advanced prostate cancer: a systematic review and meta-analysis. Eur Urol. 2016;70:926.
9. Seipel AH, Samaratunga H, Delahunt B, et al. Immunohistochemical profile of ductal adenocarcinoma of the prostate. Virchows Arch. 2014;465:559–65.
10. Kinoshita Y, Kuratsukuri K, Landas S, et al. Expression of prostate-specific membrane antigen in normal and malignant human tissues. World J Surg. 2006;30:628–36.
11. Mannweiler S, Amersdorfer P, Trajanoski S, et al. Heterogeneity of prostate-specific membrane antigen (PSMA) expression in prostate carcinoma with distant metastasis. Pathol Oncol Res. 2009;15:167–72.
12. Wernicke AG, Edgar MA, Lavi E, et al. Prostate-specific membrane antigen as a potential novel vascular target for treatment of glioblastoma multiforme. Arch Pathol Lab Med. 2011;135:1486–9.
13. Prasad V, Steffen IG, Diederichs G, et al. Biodistribution of [(68)Ga]PSMA-HBED-CC in patients with prostate cancer: characterization of uptake in normal organs and tumour lesions. Mol Imaging Biol. 2016;18:428–36.
14. Krohn T, Verburg FA, Pufe T, et al. [(68)Ga]PSMA-HBED uptake mimicking lymph node metastasis in coeliac ganglia: an important pitfall in clinical practice. Eur J Nucl Med Mol Imaging. 2015;42:210–4.
15. Kanthan GL, Drummond J, Schembri GP, et al. Follicular thyroid adenoma showing avid uptake on 68Ga PSMA-HBED-CC PET/CT. Clin Nucl Med. 2016;41:331–2.
16. Law WP, Fiumara F, Fong W, et al. Gallium-68 PSMA uptake in adrenal adenoma. J Med Imaging Radiat Oncol. 2016;60:514–7.
17. Kanthan GL, Izard MA, Emmett L, et al. Schwannoma showing avid uptake on 68Ga-PSMA-HBED-CC PET/CT. Clin Nucl Med. 2016;41:703–4.
18. Wang W, Tavora F, Sharma R, et al. PSMA expression in Schwannoma: a potential clinical mimicker of metastatic prostate carcinoma. Urol Oncol. 2009;27:525–8.
19. Rischpler C, Maurer T, Schwaiger M, et al. Intense PSMA-expression using (68)Ga-PSMA PET/CT in a paravertebral schwannoma mimicking prostate cancer metastasis. Eur J Nucl Med Mol Imaging. 2016;43:193–4.
20. Lütje S, Sauerwein W, Lauenstein T, et al. In vivo visualization of prostate-specific membrane antigen in adenoid cystic carcinoma of the salivary gland. Clin Nucl Med. 2016;41:476–7.

21. Sager S, Vatankulu B, Uslu L, et al. Incidental detection of follicular thyroid carcinoma in 68Ga-PSMA PET/CT imaging. J Nucl Med Technol. 2016;44:199–200.
22. Verburg FA, Krohn T, Heinzel A, et al. First evidence of PSMA expression in differentiated thyroid cancer using [68Ga]PSMA-HBED-CC PET/CT. Eur J Nucl Med Mol Imaging. 2015;42:1622–3.
23. Taywade SK, Damle NA, Bal C. PSMA expression in papillary thyroid carcinoma: opening a new horizon in management of thyroid cancer? Clin Nucl Med. 2016;41:e263–5.
24. Shetty D, Loh H, Bui C, et al. Elevated 68Ga prostate-specific membrane antigen activity in metastatic non-small cell lung cancer. Clin Nucl Med. 2016;41:414–6.
25. Pyka T, Weirich G, Einspieler I, et al. 68Ga-PSMA-HBED-CC PET for differential diagnosis of suggestive lung lesions in patients with prostate cancer. J Nucl Med. 2016;57:367–71.
26. Sathekge M, Modiselle M, Vorster M, et al. 68Ga-PSMA imaging of metastatic breast cancer. Eur J Nucl Med Mol Imaging. 2015;42:1482–3.
27. Vamadevan S, Shetty D, Le K, Bui C, et al. Prostate-specific membrane antigen (PSMA) avid pancreatic neuroendocrine tumor. Clin Nucl Med. 2016;41:804–6.
28. Sasikumar A, Joy A, Nanabala R, et al. (68)Ga-PSMA PET/CT imaging in primary hepatocellular carcinoma. Eur J Nucl Med Mol Imaging. 2016;43:795–6.
29. Demirci E, Ocak M, Kabasakal L, et al. (68)Ga-PSMA PET/CT imaging of metastatic clear cell renal cell carcinoma. Eur J Nucl Med Mol Imaging. 2014;41:1461–2.
30. Einspieler I, Tauber R, Maurer T, et al. 68Ga prostate-specific membrane antigen uptake in renal cell cancer lymph node metastases. Clin Nucl Med. 2016;41:261–2.
31. Huang YT, Fong W, Thomas P. Rectal carcinoma on 68Ga-PSMA PET/CT. Clin Nucl Med. 2016;41:167–8.
32. Gupta M, Choudhury PS, Gupta G, et al. Metastasis in urothelial carcinoma mimicking prostate cancer metastasis in Ga-68 prostate-specific membrane antigen positron emission tomography-computed tomography in a case of synchronous malignancy. Indian J Nucl Med. 2016;31:222–4.
33. Kanthan GL, Hsiao E, Kneebone A, et al. Desmoid tumor showing intense uptake on 68Ga PSMA-HBED-CC PET/CT. Clin Nucl Med. 2016;41:508–9.
34. Kanthan GL, Coyle L, Kneebone A, et al. Follicular lymphoma showing avid uptake on 68Ga PSMA-HBED-CC PET/CT. Clin Nucl Med. 2016;41:500–1.
35. Rahbar K, Weckesser M, Huss S, et al. Correlation of intraprostatic tumor extent with 68Ga-PSMA distribution in patients with prostate cancer. J Nucl Med. 2016;57:563–7.
36. Kobe C, Maintz D, Fischer T, et al. Prostate-specific membrane antigen PET/CT in splenic sarcoidosis. Clin Nucl Med. 2015;40:897–8.
37. Henninger M, Maurer T, Hacker C, et al. 68Ga-PSMA PET/MR showing intense PSMA uptake in nodular fasciitis mimicking prostate cancer metastasis. Clin Nucl Med. 2016;41:443–4.
38. Noto B, Vrachimis A, Schäfers M, et al. Subacute stroke mimicking cerebral metastasis in 68Ga-PSMA-HBED-CC PET/CT. Clin Nucl Med. 2016;41(10):449–51.
39. Gykiere P, Goethals L, Everaert H. Healing sacral fracture masquerading as metastatic bone disease on a 68Ga-PSMA PET/CT. Clin Nucl Med. 2016;41:346–7.
40. Artigas C, Alexiou J, Garcia C, et al. Paget bone disease demonstrated on (68)Ga-PSMA ligand PET/CT. Eur J Nucl Med Mol Imaging. 2016;43:195–6.
41. Derlin T, Weiberg D, von Klot C, et al. 68 Ga-PSMA I&T PET/CT for assessment of prostate cancer: evaluation of image quality after forced diuresis and delayed imaging. Eur Radiol. 2016;24:4345–53.
42. Chakraborty PS, Tripathi M, Agarwal KK, et al. Metastatic poorly differentiated prostatic carcinoma with neuroendocrine differentiation: negative on 68Ga-PSMA PET/CT. Clin Nucl Med. 2015;40:163–6.

^{18}F-NaF PET/CT Imaging

10

Sharjeel Usmani, Kanhaiyalal Agrawal, Abdulredha Esmail, Fahad Marafi, and Gopinath Gnanasegaran

Contents

10.1 Introduction

Bone scintigraphy is used to help diagnose conditions such as malignancy, inflammation and fracture. It provides functional imaging to visualise bone metabolism which radiograph and CT cannot pick up. Its ability to pick up areas of increased bone turnover may correlate better with sites of active pathology [1]. However, the

S. Usmani (✉)
Department of Nuclear Medicine, Kuwait Cancer Control Center (KCCC), Shuwaikh, Kuwait

K. Agrawal
Department of Nuclear Medicine, All India Institute of Medical Sciences (AIIMS), Bhubaneswar, India

A. Esmail · F. Marafi
Department of Nuclear Medicine, Jaber Al-Ahmad Molecular Imaging Center, Kuwait City, Kuwait

G. Gnanasegaran
Department of Nuclear Medicine, Royal Free NHS Foundation Trust, London, UK

K. Agrawal et al. (eds.), *PET/CT Imaging*, Clinicians' Guides to Radionuclide Hybrid Imaging, https://doi.org/10.1007/978-3-030-75476-1_10

intrinsic anatomic resolution of the technique is limited. Even though the introduction of multi-modality SPECT-CT has improved the sensitivity and specificity of bone scintigraphy, ^{18}F-sodium fluoride (^{18}F-NaF) PET/CT currently offers better image quality and is reported to be superior to conventional ^{99m}Tc-MDP bone scan [2]. ^{18}F-NaF PET/CT is an emerging and promising bone imaging agent for characterisation of osseous lesions. ^{18}F-NaF is an excellent bone-seeking agent owing to high bone uptake due to rapid single-pass extraction, minimal binding to serum proteins and fast clearance from the soft tissues [3]. It is a sensitive tool for detecting skeletal metastases in adults and it surpasses conventional bone scintigraphy (Fig. 10.1) [4]. Encouraging results have also been reported for its use in characterising benign bone and joint conditions [5, 6].

^{18}F-NaF PET/CT improves diagnostic confidence with definitive reports in the majority of the cases with a high inter-rater agreement [7]. This superior diagnostic profile must be attributed to improved signal-to-noise ratio due to better bone accumulation versus soft tissue uptake and the higher spatial resolution [8]. In hybrid imaging, anatomic localisation with CT often improves both the specificity of assessment of the bone lesion and soft tissue uptake (Table 10.1).

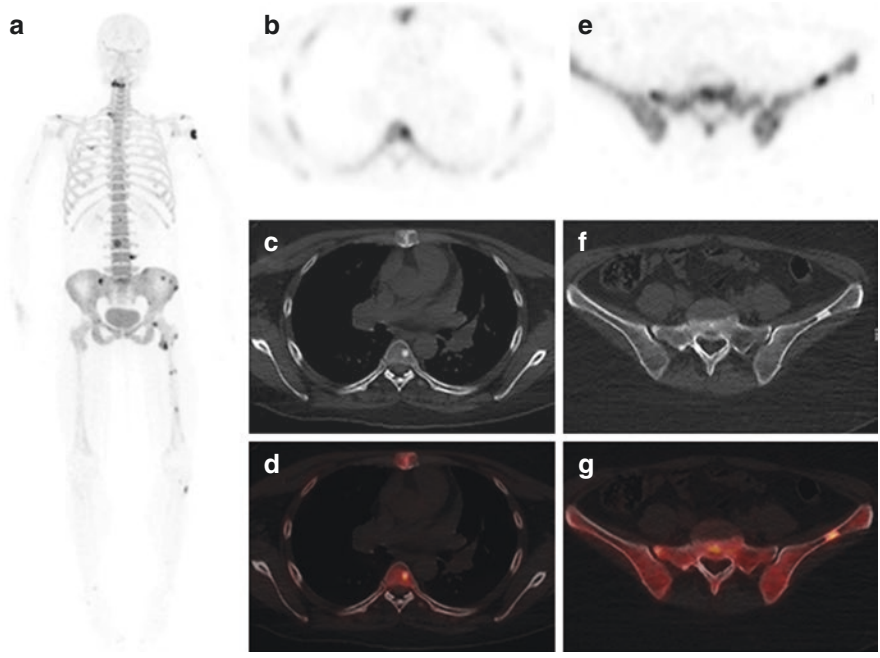

Fig. 10.1 40-year-old female recently diagnosed with breast cancer. ^{18}F-NaF PET/CT anterior MIP image (**a**) shows multifocal increase tracer activity in the left humeral head, left scapula, a few right ribs, C3, D5 and L3 vertebral bodies, left transverse process of L4, pelvic bones, left femur and left proximal fibula. Axial images at D5 level (**b**–**d**) and pelvis (**e**–**g**) show sclerotic lesions with corresponding increased uptake on fused images. Findings are consistent with multiple osteoblastic bone secondaries

Table 10.1 ^{18}F-NaF PET/CT indications

Detection of skeletal metastasis
• Initial staging
• Disease extent
• Response to therapy
Benign bone disease
• Trauma
• Unexplained backpain
• Paget's disease
• Bone viability
• Condylar hyperplasia
• Symptomatic accessory ossicle
• Metabolic bone disease
• Painful prosthesis
• Spondylolysis and spondylolisthesis
• Inflammatory and degenerative arthritis
• Enthesopathies
Pediatric bone disease
• Bone trauma, child abuse
• Back pain
• Langerhans cell histiocytosis
• Osteochondrosis and condylar hyperplasia
Special circumstances
• Obese patients
• End stage renal failure

10.2 Pharmacokinetics and Mechanism of Uptake

^{18}F-NaF bone uptake is related to blood flow and almost all ^{18}F-NaF delivered is retained by bone after a single pass of blood, resulting in an almost 100% first-pass extraction [9]. The bone uptake of ^{18}F-NaF is double that of ^{99m}Tc-MDP [10]. Uptake of ^{18}F-NaF has a similar mechanism compared to ^{99m}Tc-MDP, following chemisorption of fluoride ions onto the surface of hydroxyapatite, they exchange with the hydroxyl (OH^-) ions in the crystal, forming fluoroapatite [11]. It has negligible plasma protein binding, rapid blood and renal clearance and high bone uptake early after injection, which is reflected in high target-to-background ratios (Table 10.2) [3]. Plasma clearance is very rapid. Approximately 50% of the injected ^{18}F-NaF is taken up in bone [12].

10.3 Normal Biodistribution

A normal ^{18}F-NaF PET study demonstrates uniform symmetrical tracer distribution throughout the skeleton (Fig. 10.2). The pattern of physiologic tracer uptake is related to regional blood flow, amount of new bone formation and bone crystal surface area accessible to the tracer. The CT component of PET/CT is performed for attenuation correction and localisation, potentially improves the interpretation (Fig. 10.3). Normal ^{18}F-NaF shows generally a symmetrical tracer uptake except

Table 10.2 Advantages of ^{18}F NaF as a bone tracer

• High and rapid bone uptake
• No protein binding
• Rapid clearance from blood
• High bone to soft tissue background
• Superior image quality of ^{18}F-NaF PET

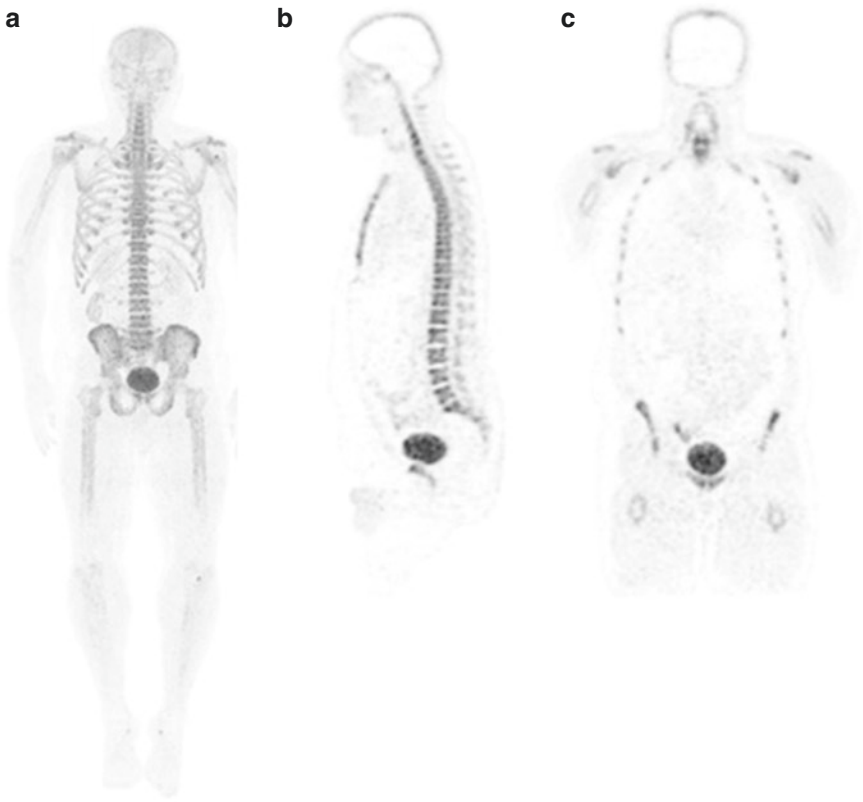

Fig. 10.2 45-year-old male with prostate cancer (**a**) ^{18}F-NaF PET MIP images, (**b**, **c**) coronal and sagittal ^{18}F-NaF PET images shows normal tracer distribution

peri-articular regions that may show variable pattern of tracer uptake (Fig. 10.4). Normal growth causes increased tracer uptake in the epiphyseal plates of children and adolescents (Fig. 10.5). Normal urinary washout is the major route of tracer excretion which leads to kidney, ureters and urinary bladder visualisation if renal function is within the normal limits.

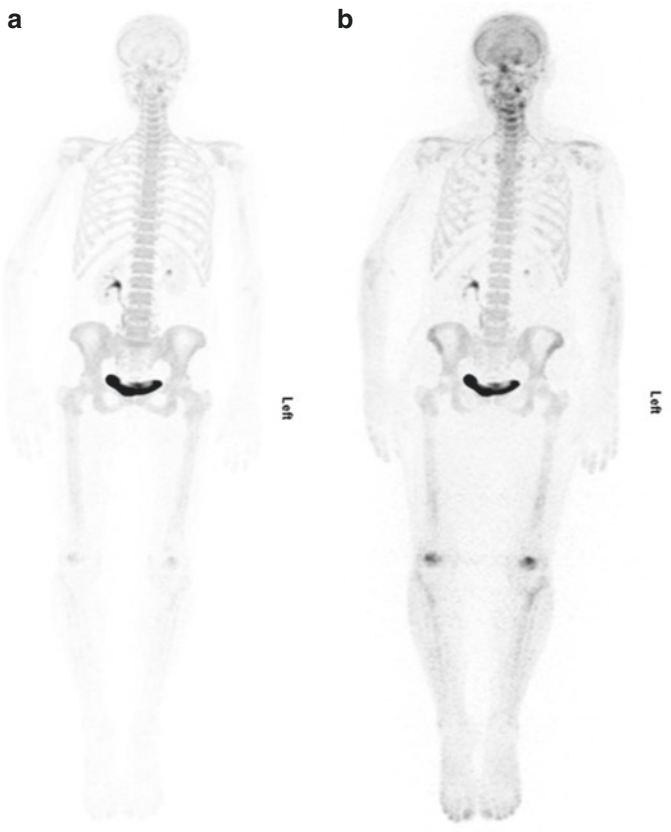

Fig. 10.3 35-year-old male with breast cancer. ^{18}F-NaF PET/CT (**a**) MIP attenuated corrected images, (**b**) MIP non-attenuated corrected images show normal tracer distribution with no abnormal tracer localisation

10.4 Normal Variant and Pitfalls of ^{18}F-NaF PET/CT

As ^{18}F-NaF is highly sensitive, its uptake may be quite prominent in benign findings as well. Reasons of altered bone metabolism may cause increased ^{18}F-NaF uptake which is mainly dependent on regional blood flow and/or new bone formation. The degree of tracer uptake does not differentiate benign from malignant processes. With increasing clinical interest in ^{18}F-NaF PET/CT imaging, it is important to have knowledge of normal variants in ^{18}F-NaF PET/CT imaging. These normal variant may lead to misinterpretations of the images.

Common normal variants increased tracer uptake at the head and neck region include uptake at confluence of sutures, occipital protuberance and hyperostosis frontalis (Fig. 10.6). Diffuse uptake in the calvarium is often seen in post-chemotherapy and in metabolic bone disease patients. Focal increased uptake in the

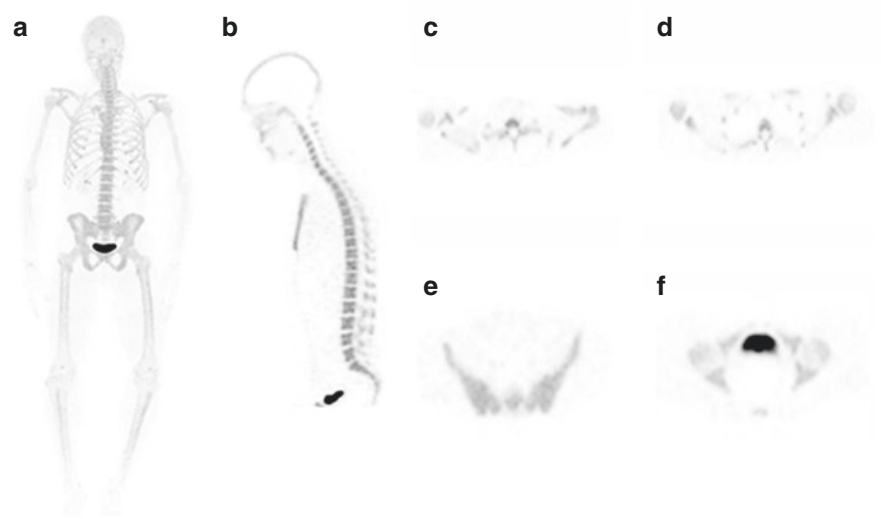

Fig. 10.4 45-year-old male with breast cancer. ^{18}F-NaF PET/CT (**a**) MIP attenuated corrected image, (**b**) sagittal image. Transaxial images acromioclavicular joints (**c**), shoulders (**d**), sacroiliac joints (**e**) and hips (**f**)

mandible is often due to underlying benign dental pathology and increased tracer uptake in the sinuses is frequently due to infection or inflammatory disease. The common normal variant in thoracic region that can mimic pathology includes uptake at manubrio-sternal, xiphisternum and age related variable uptake at acromioclavicular and sternoclavicular joints. The pattern of tracer uptake in the sternum is variable, and it is important to recognise the normal variants as they can mimic pathology (Fig. 10.7). In abdominopelvic region, the common variants are related to kidney, bladder and collecting system (e.g. bladder diverticulum). Other examples are post-partum pelvic diastases and ischiopubic synchondrosis (Fig. 10.8). In the long bones, focal areas of increased tracer uptake are often seen at the sites of repeated stress (e.g. the site of muscles insertions). In the elderly calcification of the arteries is commonly seen on ^{18}F-NaF PET. Common examples of ^{18}F-NaF tracer uptake in normal variants are mentioned in Table 10.3.

10.5 Artifacts on ^{18}F-NaF PET/CT

Artifacts on ^{18}F-NaF PET can be technical or patient related. The technical artifacts include equipment, radiopharmaceutical and image processing related problems.

Equipment-related artifacts may be due to inadequate quality-control procedures and calibration.

Patient related artifacts include radiotracer extravasations, contamination, patient movement and therapy related bone changes (e.g. post-radiotherapy) (Fig. 10.9).

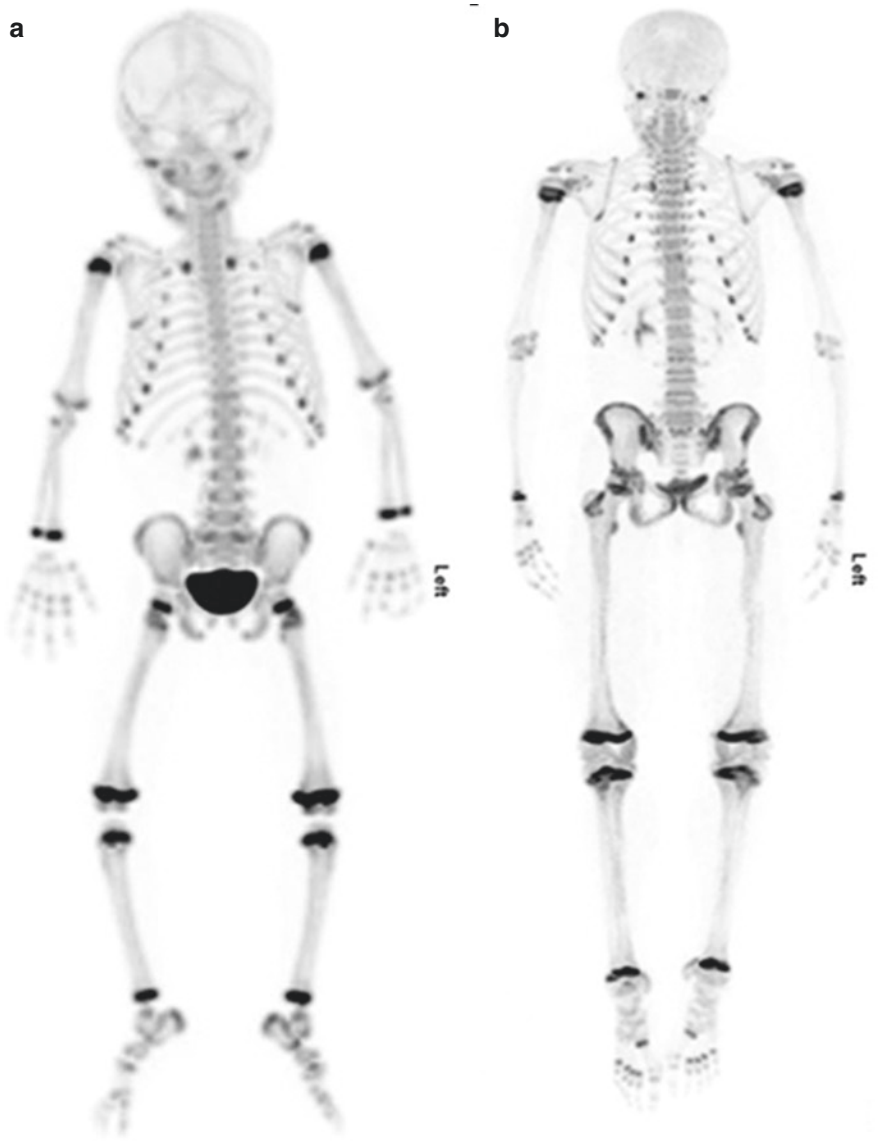

Fig. 10.5 (**a**) Normal ^{18}F-NaF PET MIP image of 3-year-old showing increase uptake at the growing ends of the bone, i.e. costochondral junctions, epiphyseal plates of the upper and lower limbs. Uptake also noted at coronal and sagittal sutures. (**b**) ^{18}F-NaF MIP images of 13-year-old girl complaining of back pain since 2 months. MRI was normal. PET/CT images show symmetrical tracer distribution. Normal increase uptake noted at the growing end plates with no abnormal tracer localization seen

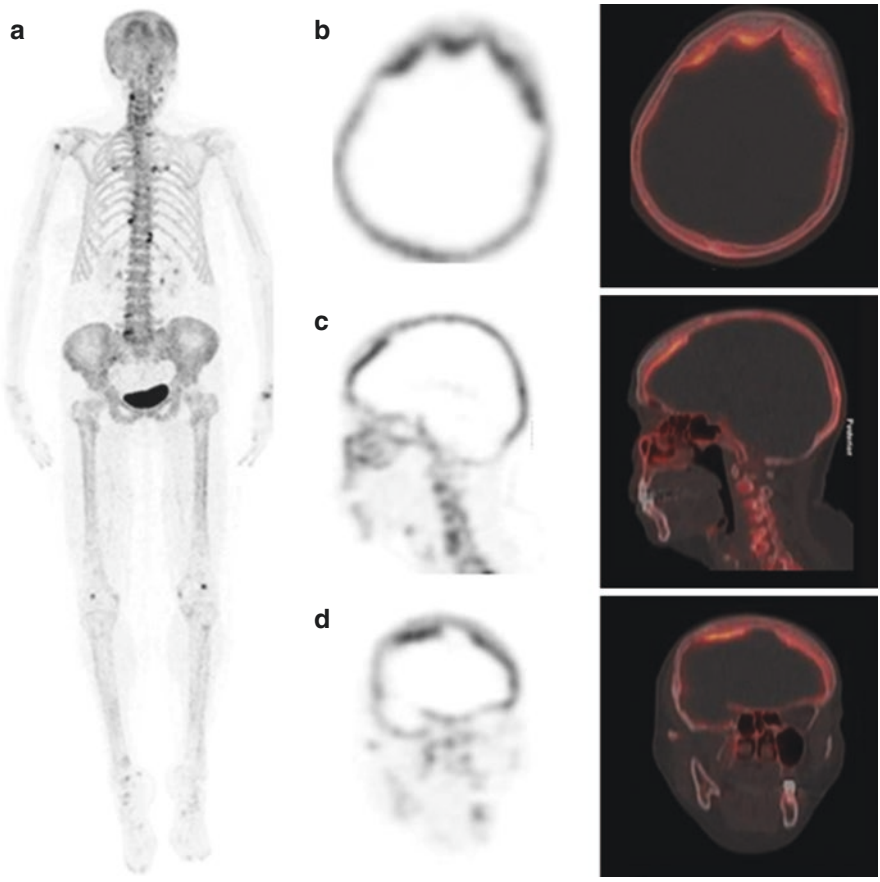

Fig. 10.6 73-year-old female with breast cancer. ^{18}F-NaF-PET/CT (**a**) MIP image, (**b–d**) transaxial, sagittal and coronal images show diffuse increase uptake in the frontal bone. Fused PET/CT images show thickening of the inner side of the frontal bone of the skull with increase tracer uptake suggesting normal variant uptake at hyperostosis frontalis. There is degenerative changes noted at lumbar spine and both knee joints but no evidence of bone secondaries

The CT component of PET/CT can be used for both localisation and for attenuation correction. Several CT related artifacts are mentioned in the literature. Artifacts that are commonly encountered are beam hardening changes, misregistration, CT noise and high attenuation object (Fig. 10.10). The most common ^{18}F-NaF PET/CT artifacts are mentioned in Table 10.4.

10.6 Extra Osseous Uptake of ^{18}F-NaF

^{18}F-NaF is a bone imaging agent but often variable tracer uptake in the soft tissues is observed, such as arterial vasculature, genitourinary tract and occasionally in the gastrointestinal tract (Table 10.5) [13]. The mechanisms of uptake of ^{18}F-NaF in soft

Fig. 10.7 46-year-old female with breast cancer. ^{18}F-NaF-PET/CT (**a**, **b**) MIP anterior and lateral images, (**c**–**e**) sagittal PET, CT and fused PET/CT images show increase tracer uptake at sternal angle suggesting normal variant uptake. There are degenerative changes at right patellofemoral joints. No evidence of bone secondaries

tissue are reported to be similar to those for ^{99m}Tc-MDP bone scan [14]. As bone-seeking agent, ^{18}F-NaF might also localise in extra osseous calcifying lesions [15]. Soft tissue calcifications secondary to tumoral necrosis, vascular, infectious or traumatic process often demonstrate ^{18}F-NaF uptake [16]. Lesions containing dystrophic or microscopic calcification, or calcified visceral metastases can show focal increased uptake of ^{18}F-NaF (Fig. 10.11) [17].

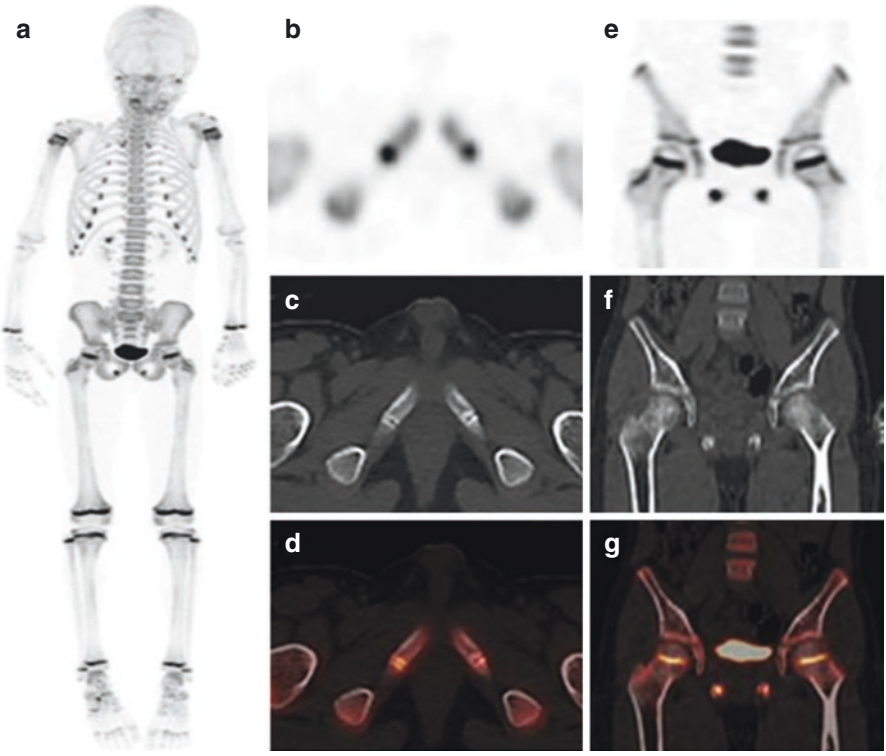

Fig. 10.8 8-year-old boy complaining of back pain. ^{18}F-NaF-PET/CT (**a**) MIP anterior, (**b**–**d**) transaxial PET, CT and fused PET/CT images show increase tracer uptake at bilateral inferior pubic ramus, which is due to normal synchondrosis. Increase uptake is noted at the growing ends of the bone, i.e. epiphyseal plates of the upper and lower limbs (**a**, **e**–**g**)

Table 10.3 Normal variants in ^{18}F-NaF PET/CT

Head and neck	Skull sutures, pterion, occipital protuberance, hyperostosis frontalis, angle of mandible, sinuses (frontal, ethmoidal, sphenoidal and maxillary), and benign calcification in the brain (falx cerebri calcification and calcified choroid)
Thorax	Manubrium sternum/xiphisternum, tip of scapulae, symmetrical uptake at the site of muscle insertion in the ribs
Abdomen and Pelvis	Kidney, bladder, bladder diverticulae, pelvic diastasis and variable uptake at accessory SI joints

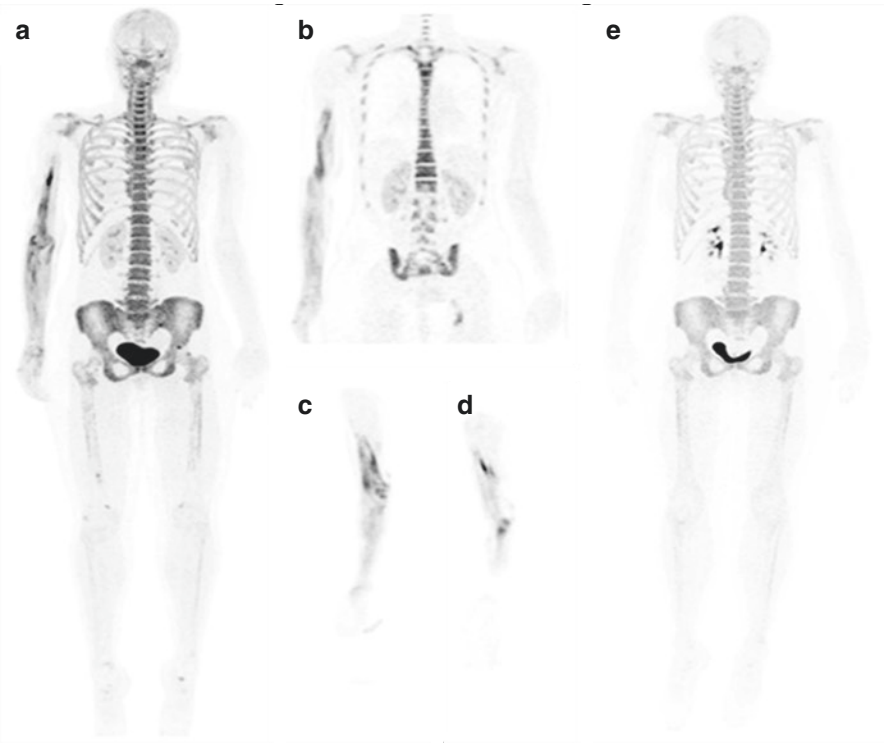

Fig. 10.9 31-year-old female with left breast cancer. ^{18}F-NaF PET/CT (**a**) MIP anterior image shows increase tracer uptake in the right distal humeral shaft with no definite CT abnormality. Injection was given at right antecubital vein. (**b**–**d**) coronal and sagittal PET images show linear increase tracer uptake pattern appears to be activity in the vessels. (**e**) Follow-up study after 1 year shows no abnormal tracer localization in the right humerus

Fig. 10.10 (**a**) 44-year-old female with right breast cancer. ^{18}F-NaF PET/CT MIP image shows photon deficient reconstruction artifact (blue arrow) due to dose infiltration at left hand (red arrow). (**b**) In 59-year-old morbidly obese female with the left breast cancer and BMI 54.9 kg/m^2, ^{18}F-NaF PET/CT MIP image shows photon deficient area in the pelvis due to beam hardening reconstruction artifact

Table 10.4 Common artifacts in ^{18}F-NaF PET/CT

Injection related	Radiotracer extravasations, arterial injection, injection in the central line and catheter
Technical	Insufficient counts, image processing, pharmaceutical related inadequate quality-control procedures and calibration
Attenuation	Belt buckle, medallion, metal jewellery and pace maker
Treatment related	Post-radiotherapy, post-chemotherapy and hormonal therapy
Motion	Respiratory movement, voluntary and involuntary movement
CT related	Beam hardening, streak artefact, high attenuation object (prosthesis), thick CT slices and CT noise
Contamination	Urine contamination

Table 10.5 Common causes of extra osseous^{18}F-NaF uptake

Tissue origin	Condition
Brain	Metastases, meningioma and cerebral infarcts
Cardiac	Metastases, amyloidosis and coronary calcification
Liver	Metastases
Lung	Non-small cell lung carcinoma, metastases and amyloidosis
Lymph node	Metastases, calcified nodes
Ovary	Metastases
Skin	Subcutaneous calcification
Stomach	Hypercalcemia
Thyroid	Thyroid cancer
Vessels	Atherosclerosis
Urinary tract and bladder	Bladder stone and urinary bladder cancer

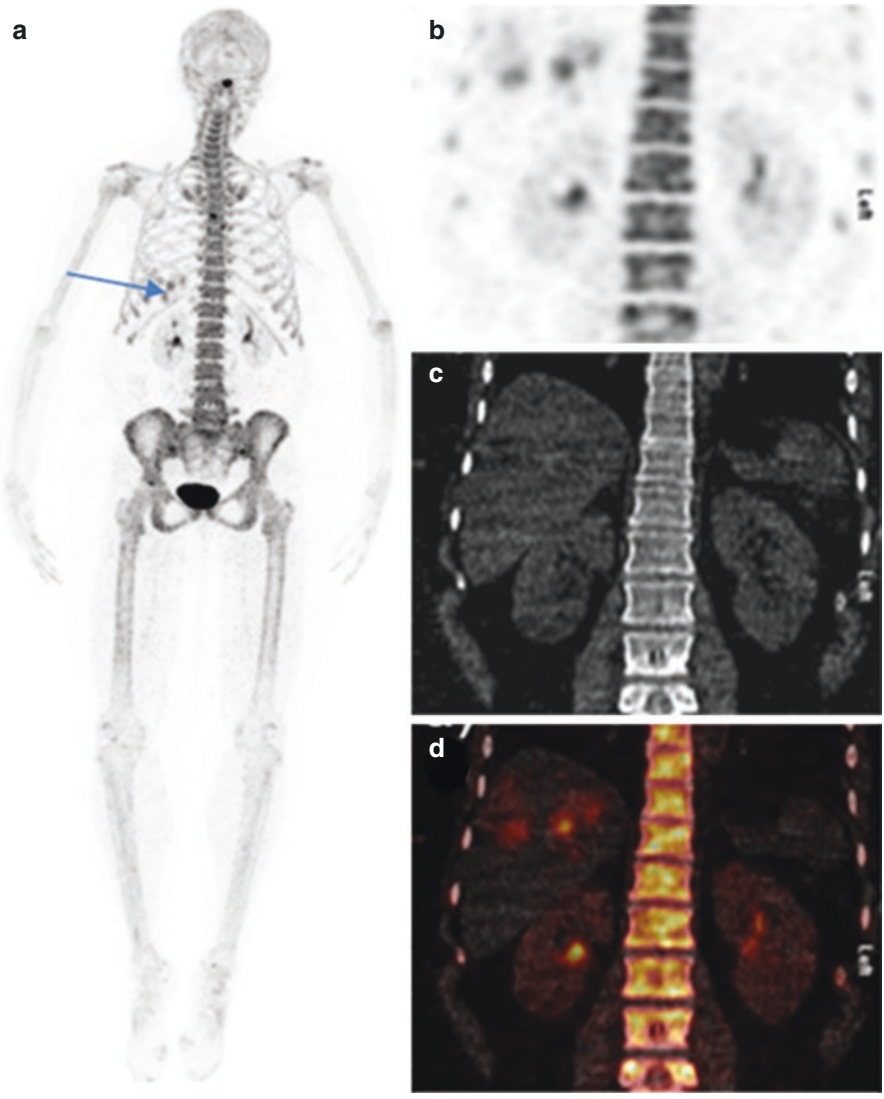

Fig. 10.11 46-year-old female with breast cancer. ^{18}F-NaF PET/CT (**a**) MIP image shows increase tracer uptake in the right hypochondrial region (arrow). (**b**–**d**) Coronal PET, CT and fused PET/CT images show uptake in calcified hepatic lesions at segment VII. Findings are suggestive of liver metastasis

Key Points

- ^{18}F-NaF is an excellent bone-seeking agent owing to high bone uptake due to rapid single-pass extraction, minimal binding to serum proteins and fast clearance from the soft tissues.
- ^{18}F-NaF PET/CT improves diagnostic confidence with definitive reports in the majority of the cases with a high inter-rater agreement.
- ^{18}F-NaF is highly sensitive, its uptake might be quite prominent in benign findings as well.
- Equipment-related artifacts may be due to inadequate quality-control procedures and calibration.
- Patient related artifacts include radiotracer extravasations, contamination, patient movement and therapy related bone changes.

References

1. Even-Sapir E, Metser U, Mishani E, et al. The detection of bone metastases in patients with high-risk prostate cancer: 99mTc-MDP planar bone scintigraphy, single- and multi-field-of-view SPECT, 18F-fluoride PET, and 18F-fluoride PET/CT. J Nucl Med. 2006;47:287–97.
2. Araz M, Aras G, Kucuk ON. The role of 18F-NaF PET/CT in metastatic bone disease. J Bone Oncol. 2015;4:92–7.
3. Czernin J, Satyamurthy N, Schiepers C. Molecular mechanisms of bone 18F-NaF deposition. J Nucl Med. 2010;51:1826–9.
4. Löfgren J, Mortensen J, Rasmussen SH, et al. A prospective study comparing 99mTc-hydroxyethylene-diphosphonate planar bone scintigraphy and whole-body SPECT/CT with 18F-fluoride PET/CT and 18F-fluoride PET/MRI for diagnosing bone metastases. J Nucl Med. 2017;58:1778–85.
5. Laverick S, Bounds G, Wong WL. [18F]-Fluoride positron emission tomography for imaging condylar hyperplasia. Br J Oral Maxillofac Surg. 2009;47:196–9.
6. Drubach LA, Connolly SA, Palmer EL. Skeletal scintigraphy with 18F-NaF PET for the evaluation of bone pain in children. AJR Am J Roentgenol. 2011;197:713–9.
7. Even-Sapir E, Metser U, Flusser G, et al. Assessment of malignant skeletal disease: initial experience with 18F-fluoride PET/CT and comparison between 18F-fluoride PET and 18F-fluoride PET/CT. J Nucl Med. 2004;45:272–8.
8. Grant FD, Fahey FH, Packard AB, et al. Skeletal PET with 18F-fluoride: applying new technology to an old tracer. J Nucl Med. 2008;49:68–78.
9. Frost ML, Blake GM, Cook GJ, et al. Differences in regional bone perfusion and turnover between lumbar spine and distal humerus: 18F-fluoride PET study of treatment-naive and treated postmenopausal women. Bone. 2009;45:942–8.
10. Blake GM, Park-Holohan SJ, Cook GJ, et al. Quantitative studies of bone with the use of 18F-fluoride and 99mTc-methylene diphosphonate. Semin Nucl Med. 2001;31:28–49.
11. Fogelman I. Skeletal uptake of disphosphonate: a review. Eur J Nucl Med Mol Imaging. 1980;5:473–6.
12. Dworkin H, Moon N, Lessard R, et al. A study of the metabolism of fluorine-18 in dogs and its suitability for bone scanning. J Nucl Med. 1966;7:510–20.
13. Derlin T, Tóth Z, Papp L, et al. Correlation of inflammation assessed by 18F-FDG PET, active mineral deposition assessed by18F-fluoride PET, and vascular calcification in atherosclerotic plaque: a dual-tracer PET/CT study. J Nucl Med. 2011;52:1020–7.

14. Gnanasegaran G, Cook G, Adamson K, et al. Patterns, variants, artifacts, and pitfalls in conventional radionuclide bone imaging andSPECT/CT. Semin Nucl Med. 2009;39:380–95.
15. Stewart VL, Herling P, Dalinka MK. Calcification in soft tissues. JAMA. 1983;250:78–81.
16. Hawkins AS, Howard BA. Unusual soft tissue uptake of F-18 sodium fluoride in three patients undergoing F-18 NaF PET/CT bone scans for prostate cancer. Nucl Med Mol Imaging. 2017;51:274–6.
17. Agrawal K, Bhattacharya A, Harisankar CN, Abrar ML, Dhaliwal LK. Mittal BR.F-18 fluoride uptake in calcified extraosseous metastases from ovarian papillary serous adenocarcinoma. Clin Nucl Med. 2012;37(1):22–3.